EFFECTS OF CLAY MINERALS ON THE PETROPHYSICAL PROPERTIES OF SANDSTONE RESERVOIRS FROM THE OFFSHORE PLETMOS BASIN, SOUTH AFRICA

UNIVERSITY *of the*
WESTERN CAPE

BY

KIRK CHARLES JACOBS (3241057)

Submitted in fulfillment of the requirements for the Degree of

Magister Scientae in Applied Geology

Supervisor: Prof. T. K. Chatterjee

Co-– Supervisor: Dr. M. Opuwari

Department of Earth Sciences
University of the Western Cape, Cape Town, South Africa

December 2019

DECLARATION

I declare that my research work titled, "**EFFECTS OF CLAY MINERALS ON THE PETROPHYSICAL PROPERTIES OF SANDSTONE RESERVOIRS FROM THE OFFSHORE PLETMOS BASIN, SOUTH AFRICA"** is my own work, that it has not been submitted before for any degree or examination in any other university, and that all the sources I have used or quoted have been indicated and acknowledged by means of complete references.

Kirk Charles Jacobs **December 2019**

Signed_____

DEDICATION

This project is dedicated to

The

ALMIGHTY GOD

For

I can do all things through Jesus Christ who strengthens me

ACKNOWLEDGEMENT

I would like to give the creator of my faith the Lord Jesus Christ, all the praise, glory and honour. It is only through His grace and mercy that has sustained me through the trials that was encountered throughout this journey.

It would not have been possible to have written this thesis without the support of my principal supervisor, Prof. T.K. Chatterjee, for his guidance and unsurpassed knowledge of the petroleum field as well as my co-supervisor Dr. M. Opuwari's knowledge in the field of petrophysics.

I am particularly grateful to my parents Mr and Mrs Jacobs for the role played in developing my academic career and to allow myself to pursue my dream. Thank you for the values that they have instilled in me, their prayers and unequivocal support in all of my endeavours, my mere expression of saying thank you is only a small token of my appreciation for you. To my brother Ehren, thank you for your encouragement and continuous believe in me.

The contribution from the Petroleum Agency of South Africa (PASA) for providing the data that was used in this thesis and their assistance. To UCT, thank you providing the facilities for me to do my QEMSCAN analysis and IThemba Labs for my XRD analysis.

To my fellow postgraduate students and in particular Mr. N. Dominick and Mr. Y. Hendricks of the Department of Earth Science at the University of the Western Cape, thank you for the time we have worked together on a daily basis and the experiences we have drawn from one another.

ABSTRACT

With the latest advancements in the Pletmos Basin it is imperative to understand and study how sandstone reservoirs are affected by clay minerals. Clay minerals are an influential component in sandstone reservoirs worldwide and thus have an impact on the reservoir quality and petrophysical properties. The present research was aimed at assessing the effects of clay minerals on the petrophysical properties of sandstone reservoirs from the Offshore Pletmos Basin. This was done by integrating geological (wireline logs and core analysis), geochemical (XRD and pore water chemistry) and petrographical (QEMSCAN and thin section petrography) analysis to highlight the effects of clay minerals on the intrinsic properties (porosity, permeability and fluid saturation) on reservoirs encountered within the two wells (Ga- Q1 and Ga – S1).

The results highlight pervasive quartz cementation as well as the presence of clay minerals: Glauconite (Illite group), Kaolinite (Kaolinite group), Clinochlore (Chlorite group) as the dominant clay minerals and Calcite as the dominant cement in both well Ga – Q1 and well Ga – S1. The most abundant clay mineral in both wells is Glauconite. This clay mineral had a more profound effect on the petrophysical parameters compared to the other clay minerals. The clay minerals occur as pore–filling Kaolinite and pore–bridging Glauconite and pore–lining Clinochlore. As a result, the clay minerals affected the pore connectivity (permeability) more than the pore spaces (porosity). This is confirmed by the petrophysical analysis where both wells have extremely low permeability and good porosity values. The study concludes that the presence of Glauconite, Kaolinite, Clinochlore and Calcite in both wells (Ga-Q1 and Ga-S1) had an adverse effect on the permeability more compared to the porosity in sandstone reservoirs. Due to the high volume of clay and high clay mineral content in well Ga-Q1, the petrophysical parameters were more adversely affected compared to well Ga-S1. As a result, we see better petrophysical properties (porosity and permeability) in the sandstone reservoir from well Ga-S1 due to intense bioturbation. The reservoir quality of well Ga-S1 is much better compared to well Ga – Q1 because water saturation averages at 42% and gas saturation averages at 58%, has decent porosity averages at 12% but low permeability ranges of 0, 1 – 4mD.

KEYWORDS: **Clay minerals, Porosity, Permeability, Sandstone reservoirs, Pletmos Basin**

TABLE OF CONTENTS

LIST OF FIGURES

LIST OF TABLES

CHAPTER ONE

1.1 Introduction

The petrophysical properties viz. porosity, permeability and fluid saturation are fundamental components of any reservoir. Understanding what and how these parameters are affected by different clay minerals are crucial when evaluating any reservoir. This research is focused on assessing how different clay minerals affect the petrophysical properties of sandstone reservoirs in the Pletmos Basin, South Africa. Clay minerals are found in all sandstone reservoirs and as a result it is imperative to understand how each clay mineral group directly affects the petrophysical properties.

Clay minerals are referred to as hydrous aluminum phyllosilicates. Four different types of authigenic clay minerals are recognized and each group has their own distinctive properties (Bjorkum and Nadeau, 1997). The four groups of clay minerals are: Kaolinite group, Chlorite group, Illite group and Smectite group. The distinctive property that characterize each group is as follows: the Kaolinite group clay minerals are characterized by their 'pore – filling' nature; the Chlorite group clay minerals are characterized by their 'pore – lining' nature; the Illite group clay minerals are characterized by their 'pore – bridging' nature and lastly the Smectite group clay minerals are characterized by their 'swelling' nature (Ellis and Singer, 2007). The intrinsic properties of clay minerals could have an effect on petrophysical parameters such as porosity and permeability of sandstone reservoirs. The occurrence and distribution of specific clay minerals could also affect the pore geometry; as a result, this will determine whether the open spaces in the rocks are connected or not (Wilson and Pittman, 1997). Worthington (2008) used a petrophysical model to demonstrate how clay mineralogy affects sandstone reservoirs. The model used by Worthington (2008) explains that before porosity can be evaluated, the four porosity logs (neutron, density and sonic logs) must be calibrated for clay mineral effects.

The significance of clay minerals in sandstone reservoirs cannot be denied or ignored. The role and effects that clay minerals have on hydrocarbon production has to be thoroughly studied and understood in order to accurately evaluate the reservoir potential.

Thesis Outline:

Chapter One: Introduction, Aims and Objectives

Chapter Two: Literature Review

Chapter Three: Regional Geology of the Pletmos Basin

Chapter Four: Methodology

Chapter Five: Petrophysical Analysis and Core Analysis

Chapter Six: Petrography and Geochemical analysis

Chapter Seven: Discussions and Conclusion

1.2. Aims and Objectives

The aim of the present research was to assess the effects of clay minerals on the petrophysical properties of sandstone reservoirs in the offshore Pletmos Basin, South Africa.

The study was done by integrating, examining and interpreting the results derived from core analysis wireline well logs study, thin section petrography and geochemical analysis. The incorporation of all above mentioned analyses provided a clear indication and better understanding on how the clay minerals affects the petrophysical properties of reservoir zones. The petrophysical parameters (porosity, permeability and fluid saturation) were calculated from the Interactive Petrophysics (IP) software program. Industry accepted mathematical formulae were used to calculate the petrophysical property.

Objectives:

- Identify reservoir zones from each of the selected wells.
- Identify and construct lithofacies succession from the studied core samples.
- Determine the depositional environment(s) of the identified lithofacies from the Core analysis and gamma ray log shapes.
- Calculate the petrophysical parameters (volume of clay, porosity, permeability and fluid saturation) of the reservoir zones.
- To identify the clay minerals present within the reservoir zones.
- To quantify the clay minerals, present in the reservoir zones.

1.3. Scope of work

The scope of the work is outlined below:

- Delineation of reservoir zones using Interactive Petrophysics software.
- Basic petrophysical properties are calculated using Interactive Petrophysics software program.
- Thin section petrographic analysis was done to understand the basic mineralogical composition of samples.
- The QEMSCAN petrographical study was used to quantify the clay minerals present in each sample.
- Quantification of clay minerals gives a better understanding on the effects of these on reservoir quality.
- Analysis of interstitial pore waters of the reservoir sands to know the influence of Ec and pH.
- X-ray diffraction (XRD) analysis was done to infer semi – qualitative mineralogical composition of the reservoir zone.

1.4. Location of the study area

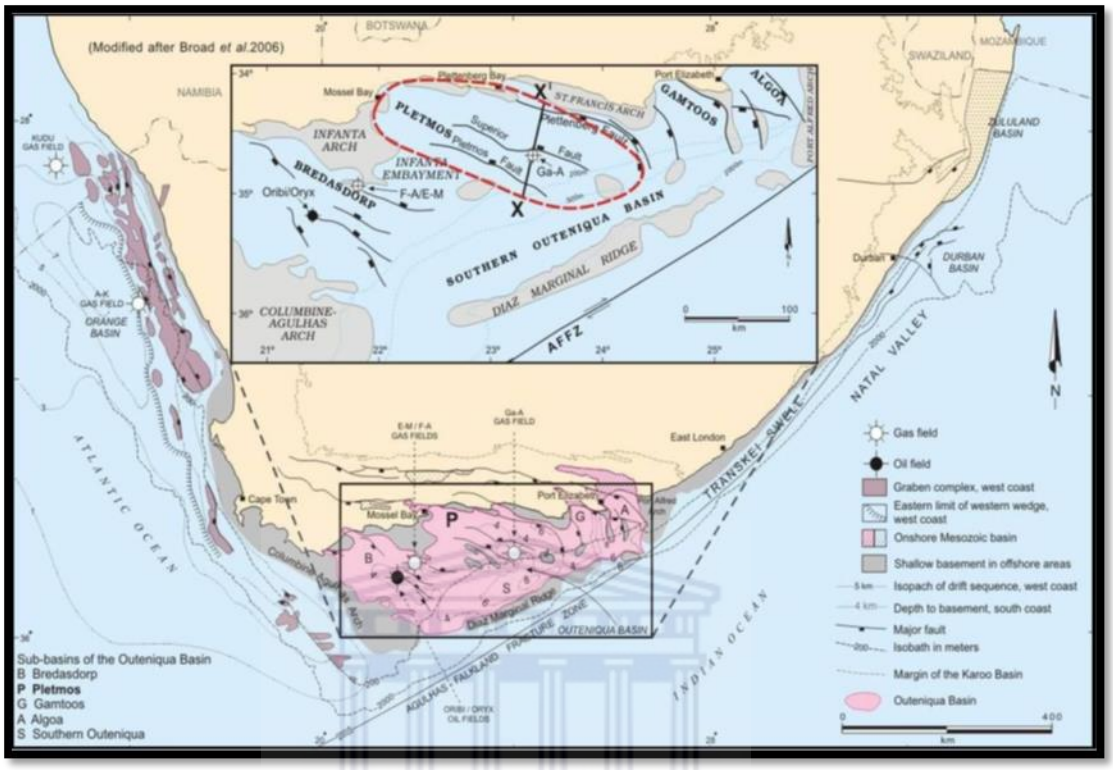

Figure 1.4.1: Location of the Outeniqua Basin as well as displaying a section location of the Pletmos Basin (Broad et al., 2006).

The study area is located in offshore Pletmos Basin (Figure 1.4.1) which is a sub-basin within a larger offshore Outeniqua Basin (Table 1.0 and Table 1.1). This basin together with the Bredasdrop, Gamtoos and Algoa basins forms the Outeniqua Basin. Together these sub–basins form part of a group of divergent basins located along the southern region of the African Plate in the Indian Ocean.

The Pletmos Basin is located approximately 90km SSE of George, a town located in South Africa. It is situated between the Infanta Arch to the South West and the St Francis Arch to the North East. The Pletmos Basin is orientated in south-easterly direction and about 200 km long and 150 km wide and covers an area of about 20 000 $km^{2.}$

Table 1.0: Names and locations of wells studied

Wells	Total Depth (m)	Kelly bushing to sea level (m)	Coordinates
Ga –S1	3700	25	Latitude: 34° 50' 01, 26" S Longitude: 23° 45' 20, 73" E
Ga– Q1	3249	26	Latitude: 34° 37' 10, 00" S Longitude: 23° 46' 53,60" E

Table 1.1 List of samples taken from respective wells

Well Ga – S1 Sample depths (m)	Well Ga – Q1 Sample Depths (m)
3028.88m	2330m
3030.45m	2334m
3033.65m	2337m
3036.90m	2339m
3039.82m	2344.30m
3044.50m	2347.27m

1.5. Exploration activity in the Pletmos Basin

In 1968, the first offshore well was drilled by the Superior Oil Company. An oil and condensate discovery (Lower Cretaceous, syn – rift shallow marine sandstones) from well Ga – A1, Block 11a (Figure 1.5.1) was also made by the Superior Oil Company and is located in the Pletmos Basin (PASA, 2013). The syn rift shallow marine sandstones from Well Ga-A1 produced mostly gas at commercial rates of 22MMscfd (Roux, 1997). A total of 38 wildcat wells have been drilled throughout the Pletmos Basin and the Infanta embayment (Figure 1.5.1) the targets were the synrift structures (Roux, 1997). Sandstones at depths of 1565m -2500m has good porosities of up to 25% and averaged in the region of 11% to 18%, permeability values ranges between 10 and 100mD (Roux, 1997).

The two wells, Ga–Q1 and Ga–Q2, that were drilled south of well Ga–A1 (Southern Pletmos Basin) (figure 1.4.1) encountered gas saturated sandstones within the synrift succession. In the adjacent Bredasdrop sub-basin (Block 9) (figure 1.5.1) has been subjected to more drilling and

seismic activity during 1980's. As a result, in the Bredasdrop Basin a number of commercial oil and gas fields have been discovered (PASA, 2013).

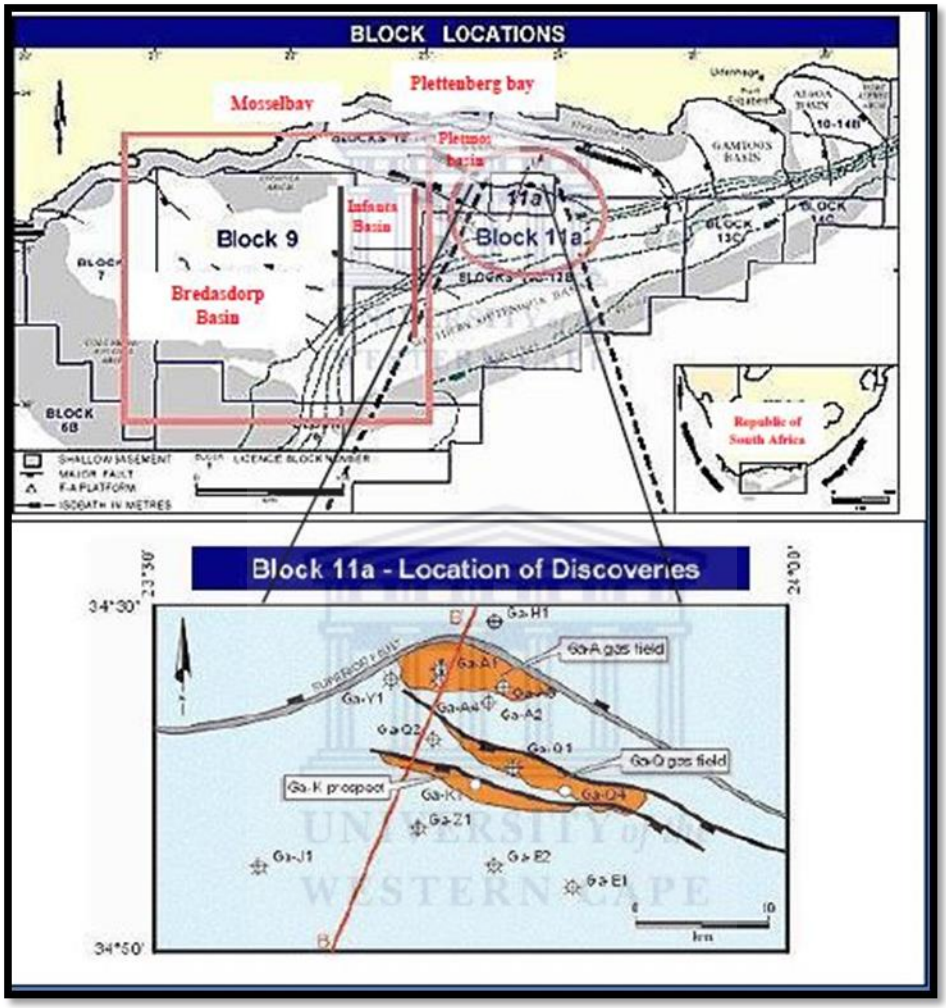

Figure 1.5.1.: Block location of the sub-basins in the Outeniqua Basin (Top) and Location of discoveries in the Pletmos Basin (bottom), modified after (Roux, 1997).

CHAPTER TWO: Literature Review

2.1. Clays and Clay Minerals

Clay minerals have the distinctive property of having particle sizes of less than 4 nm (Wentworth, 1922). Clay minerals can be classified based on their chemical composition, that being an assorted group of hydrous aluminosilicates. Four different groups of clay minerals exist namely: The Kaolinite group, the Chlorite group, the Illite group and Smectite–Montmorillonite group. In this chapter the distinctive properties of each clay mineral group will highlight their effects on reservoir properties**.**

2.1.1. Kaolinite Group

Kaolin, is also referred to as China Clay, is soft white clay. It is naturally a white, soft powder primarily consisting of the mineral Kaolinite. The mineral Kaolinite was discovered (1867) and named after a hill in China called Kao–ling from which it was mined. Kaolinite consists of a group of minerals with a general formula of $Al_2 Si_2 O_5 (OH)_4$. The Kaolinite group consists of polymorphs (Grim, 1950). The Kaolinite group has a simple crystal structure; we see a silicate sheet (Si_2O_5) bonded to an aluminum hydroxide layer ($Al_2 (OH_4)$) also known as the gibbsite layer. The members that make up the Kaolinite group are: Dickite, Nacrite and Kaolinite (Ruiz and Cruz, 1994). The Kaolinite group generally occurs in the shape of a booklet and vermicules consisting of pseudo–hexagonal crystals that grow at the expense of feldspars and micas.

Authigenic clay minerals have severe effects on the reservoir as they are formed due to rock-fluid interactions. The most common clay minerals in sandstone reservoirs are Kaolinites and Illites (Beaufort et al., 1998). The dominant clay mineral found in crustal rocks where fluid flow has occurred is Dickite and Nacrite (Kaolinite group) (Parnell et al., 2000). The formation of Kaolinite can occur in two ways: from acidic meteoric fluids in a weathering environment (Estoule – Choux, 1983), aluminium rich basinal fluids or from the dissolution of feldspars (MacLuagling et al., 1994). Hydrothermal fluids interaction with rocks has also been identified as a significant process in the formation of Kaolinite (Schroeder and Hayes, 1968). Thus, the general consensus is that Kaolinite is formed due to the hydrothermal alteration of micas and

feldspars. The hydrothermal alteration process occurs below 120° and as a result is not prone to shrinking or swelling regardless of their water content.

The precipitation of Kaolinite affects the porosity and permeability values. This is occurs when coalification acidizes the depositional environment. The reduction in porosity and permeability values occur due to dissolution of feldspars and micas and meteoric flushing (Bjorlykke, 1983). Ehrenberg, (1991) demonstrated the significant role of acidic environment in the formation of Kaolinte. He observed Kaolinite formation at the top and bottom of the Garn Formation Shelf (Norwegian Continental) sandstones. Grim (1951), noted that Kaolinte is not abundant in ancient sediments compared to sediment of younger age. Therefore, this meant that the Kaolinte clay mineral must have altered into another clay mineral. The usage of SEM and XRD can identify and separate allogenic Kolinite from authigenic Kaolinite. Detrital Kaolinte is poorly crystallized and is fine grained when observing under the thin section microscope and SEM (Hancock and Taylor, 1978).

2.1.2. Chlorite Group

The hydrothermal alteration of metamorphic rocks rich in ferromagnesian minerals results in the formation of the Chlorite clay mineral group (Bailey, 1988). Fe-Mg- rich minerals such as biotite, garnet, pyroxene and amphibole are crucial in the formation of the chlorite group clay minerals. The Chlorite group forms in an alkaline environment (pH values above 7) with high iron content (Berger et al., 2009). They are characterized based on the dominant metal. The Chlorite group members are: Pennantite (Mn – rich), Nimite (Ni – rich), Clinochlore (Mg – rich) and Chamosite (Fe – rich) (Bayliss, 1975). The formula of chlorite group is given as $(Mg,Fe)_3(Si,Al)_4O_{10}(OH)_2 \cdot (Mg,Fe)_3(OH)_6$. The crystal structure is characterized by have a hydroxide sheet surrounded by three divalent cations. Chlorite group minerals are trioctahedral.

The chlorite group are considered pore – lining minerals. This means that the clay mineral precipitate and line the pores in reservoirs. The formation of early authigenic chlorites has always preserved pore spaces from pervasive quartz cementation. The origin of the Chlorite group minerals is complex. It is controlled by the source, pore water chemistry, early clay minerals and opening and sealing of pore spaces (Huang et al., 2004). As a result, Chlorites does not affect the porosity in a negative way but does negatively affect the permeability to a point.

The chlorite group minerals are also considered a non – expansive clay mineral. Chlorites are responsible for anomalous porosity and permeability values (Sun et al., 2008), specifically in the deep sandstone reservoirs (Bloch et al., 2002).

2.1.3. Illite Group

The Illite group clay minerals are characterized by their non – expanding nature. The Illite group has a dioctahedral crystal structure. The general formula of Illite group is $(K,H)Al_2(Si,Al)_4O_{10}(OH)_2$-$xH_2O$, where x represents the amount of water that this group could contain This clay mineral group is structurally very similar to muscovite. It consists of a central octahedral sheet with two inward–pointing silica tetragonal sheets (Pevear, 1999). The main difference between illite and muscovite is that on average illite has more silica, iron and magnesium and water with less aluminum and potassium interlayer. The Illite group has an iron rich member called Glauconite. In argillaceous rocks Illites are the dominant clay mineral where they formed due to the weathering of primarily feldspars and the alteration of other clay minerals. Neutral to alkaline pore fluid conditions and high concentrations of potassium and aluminum in general support the formation of illite. In marine environments Glauconite forms authigenically and occurs as pallets. Illite clay minerals need to be studied because of their pore-bridging nature. The occurrence of illite in reservoirs severely affects the permeability of potential reservoirs. It has been observed in the Permian Rotiliegendes (North Sea) that illite replaces kaolinite (Lanson et al., 2002). The presence of Illite in the Rotiliegendes sandstones does not affect the porosity but negatively affects the permeability.

2.1.4. Smectite/Montmorillonite Group

The general formula of the Smectite group is $(Ca,Na,H)(Al,Mg,Fe,Zn)_2(Si,Al)_4O_{10}(OH)_2$-$xH_2O$ where x represents the amount of water that members of this group could contain. The group consists of minerals like vermiculite, talc, montmorillonite, nontronite and sauconite. The crystal structure of the Smectite group is either trioctahedral or dioctahedral and consists of silicate layers sandwiching a gibbsite or brucite layer (Guven, 1988). This results in a stacking sequence (s-g-s layers) with variable amount of water molecule in between s-g-s layers. Smectite group clay minerals are consider expanding clay minerals. The clay minerals of the smectite group

forms in alkaline conditions when volcanic ash is chemically altered (Bilbey et al., 1974; Owen et al., 1989). When smectite comes into contact with fresh water, this has damaging effects on reservoirs. (Guven, 1988) This is due to smectites larger surface area. A large surface area of a clay mineral tends to always promote a reduction in permeability values in reservoirs. Poor quality reservoirs always tend to have a reasonable amount of smectite present. Due to the smectite group minerals accommodating variable amounts of water molecules, this results in smectites 'swelling' which in turn reduces porosity and permeability values of reservoirs.

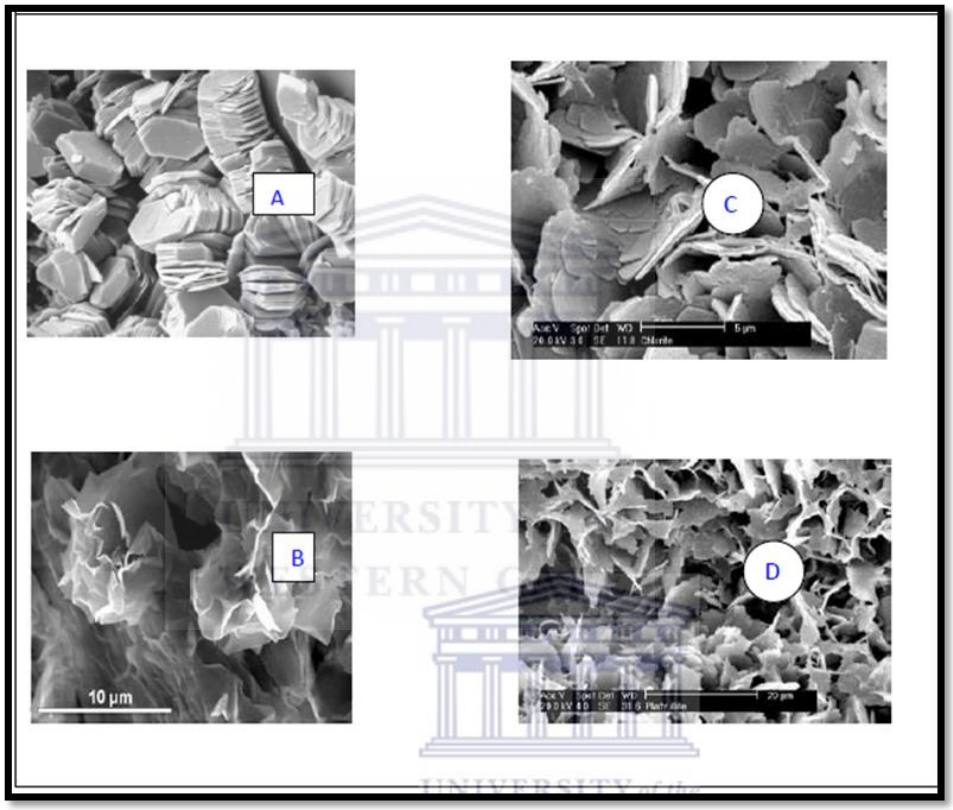

Figure 2.1.1: SEM images showing the different authigenic clay minerals from different basins (A) from Hirschau. South East, Germany idiomorphic platelets of Kaolinite (B)A rose-like texture seen in the mineral Montmorillonite, from Miocene age Arkose, Madrid Basin, Spain (C) the clinochlore (Mg – rich) mineral in Rotliegendes Sandstones, Northern Germany and (D) Platey Illite from the Rotliegendes Sandstones, Northern Germany, modified after (Samakinde, 2013).

2.2. Core Description

Cores are long cylindrical-shaped samples of subsurface rocks. They are retrieved using a long core barrel and cut using a special coring bit. The core barrels vary from 9m to 17m (Reifenstuhl, 2002). The study of conventional cores is a fundamental component for understanding subsurface rocks as it provides a true reflection of the rocks. The basic information that can be derived from the studies of conventional cores are: location of core (longitude and latitude), depth and core length. A detailed core analysis provides information on: the rock type, colour, texture, grain size, sorting, facies, sedimentary structures, fossils, chemical composition, compaction and hydrocarbon occurrence. Therefore, valuable information can be derived from the analysis of conventional cores and that's why it is crucial to study. A general understanding of the reservoir's behavior can be obtained from integrated studies of petrographic thin sections with megascopic studies of core and interpretations. Sampling of cores provides accurate information but damage can be done if test procedures, sampling and handling are done incorrectly (Sinclair and Duguid, 1990). Cores can be damaged by plugging or partial disintegration of formation which results in increased petrophysical values (Hurst, 1987). Procedures such as drying of samples can lead to water content being lost in clay samples. It is common to integrated core analysis with other petrographic methods such as SEM or XRD for a qualitative purpose. A common discrepancy is that different laboratories will use different procedures and methods for core analysis. For example, a laboratory measuring porosity using humidity – controlled dried core plugs are always lower than oven-dried core plugs.

Figure 2.2.1: Showing the layout of Cores (MN drill core library, http://www.hutchk12.org/geo/mngeo/page19.html , 02/04/2019)

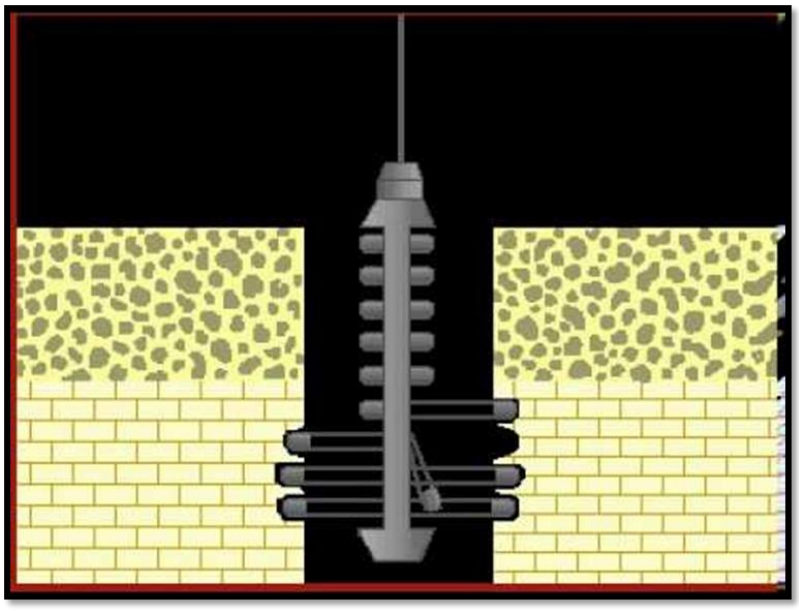

Figure 2.2.2: Percussion Sidewall – Coring Scheme, (SWC sidewall coring, www.youtube.com, 02/04/2019)

2.3. Depositional Environment

Each depositional environment is unique and therefore possesses its own unique processes, physical, chemical and biological processes that allow specific sediments to be deposited. Each depositional environment can be closely linked with the abundance and occurrence of clay minerals. Shammari et al., (2011) studied the depositional environments of sandstones found in Unayzah, Saudi Arabia and concluded that clay coatings were present in all observed depositional environments. By observing all depositional environments Kaolinite is the most dominant clay cement apart from aeolian settings and is most abundant in mature quartzose and subarkosic sandstones. In quartzose/subarkosic sandstones that were deposited in an aeolian and fluvial setting abundant Illite will be found (Kupecz et al., 1997). In deep marine depositional environments Smectite is common. However, volcanic ash deposited in a non-marine environment (fresh water) will alter to Kaolinite, whereas when volcanic ash is deposited in a marine environment it will alter to Smectite (Bohor and Triplehorn, 1993). Glauconite is found in marine environments that are characterized by alkaline waters.

2.4. Petrophysical Properties

Petrophysical properties are the fundamental components of reservoirs. The Interactive Petrophysics software program was used to analyze wireline logs in detail to determine the petrophysical properties of reservoir intervals.

2.4.1. Porosity

Porosity can be simply defined as the volume of the void spaces that contain fluids to the total volume of the rock. The pore spaces reflect the ability of the rock to hold fluids in it. It is generally represented as a percentage (%). Porosity can be calculated using two methods: 1) direct measurement from core samples 2) using wireline logs to calculate porosity. Interconnected pore spaces are regarded as the effective porosity as it allows the flow of fluids. Total porosity includes all pore spaces (isolated and interconnected) (Levorsen, 1967). Defined by many authors (Juhasz, 1990 and Clavier et al., 1984), Effective Porosity = Total porosity – volume of isolated pore spaces.

Porosity can be considered primary or secondary. Primary porosity forms upon deposition. Secondary porosity forms after initial deposition and is a result of dissolution of unstable grains caused by compaction. The porosity of a particular rock is dependent on factors such as, rock type, arrangement of grain and matrix. Information with regards to porosity can be derived from neutron, density and sonic logs. A combination of the three logs gives a good indication of the porosity values and type of rock

$$Fe= fT- vD\phi_T= (\rho_{ma} - \rho)/ (\rho_{ma} - (\rho_{hc}\cdot(1-S_{xo})+\rho_{mf}\cdot S_{xo}))$$

The grain density is r_{ma}, the density log measurement is r, in-situ hydrocarbon density is r_{hc} (from pressure data or sampling), the mud filtrate density is r_{mf} (from correlation charts normally) and the invaded zone water saturation is S_{xo}.

.

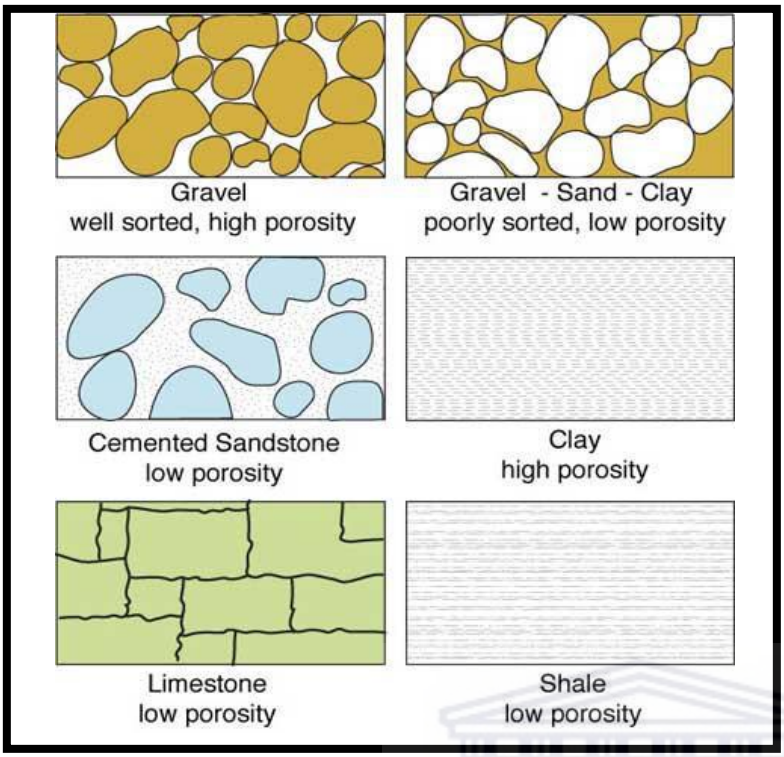

Figure 2.4.1: Porosity identification in various types of rocks (**http://www.amiadini.com/NewsletterArchive/110128-NL143/envEnl-143.html)**

2.4.2. Permeability

Permeability is a measure of the rocks ability to allow fluids (water, oil and gas) to flow through it. A high permeability means that the rock allows the fluid to flow easily. The permeability of rock depends upon the pressure gradient as well as the porosity of the rock unit. Permeability is is expressed in millidarcys (mD).

Permeability is an important component in reservoir studies because it expresses fluid flow rates. There are two methods used to calculate the permeability from wireline logs: Interactive Petrophysics software and Carman-Kozeny equation (1968). Hydraulic conductivity and intrinsic permeability are the two measures of permeability. Hydraulic conductivity is dependent of the properties of the fluid while intrinsic permeability is related to the fluid in the reservoir. In a reservoir the size of the grains and the sorting of the grains have major implications on the permeability (Beard and Weyl, 1973). Rocks that are well sorted with coarse grains tend to have

larger pore spaces which results in good permeability values, while poorly sorted rocks experience a significant reduction in permeability. Clay minerals also have an significant affect on the permeability and it is dependent on their distinctive properties (Stalder, 1973). Pore – filling clay minerals affect the permeability more than pore – lining clay minerals (Pallat et al., 1984). However, if a reservoir has a significant amount of chlorite and illite, it will significantly affect the permeability of that reservoir.

Darcy's equation defines permeability:

$K = Q \mu / A (\Delta P/L)$,

K = Permeability (Darcy)
Q = Flow per unit time (cm/s)
μ=Viscosity of flowing medium (cp)
A = Cross section of rock (cm^2)
L = Length of rock (cm)
ΔP = Change in pressure (psi)

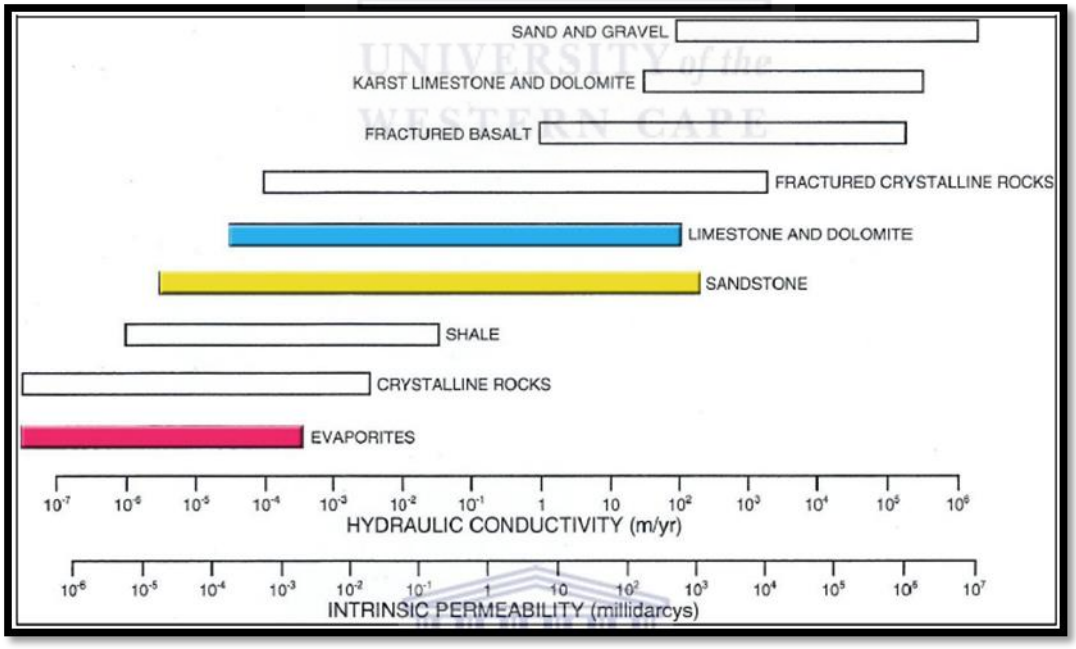

Figure 2.4.2: The permeability ranges of different rocks (Garven, 1986)

2.4.3. Fluid Saturation

When studying potential hydrocarbon reservoirs, petroleum geologist wants to know what fluids occur in that reservoir as well as the volumes of that fluid. The calculation of fluid saturation is a crucial tool in petroleum reservoirs. Fluid saturation can be simply seen as the ratio of water/hydrocarbons volume to pore volume in a reservoir. For example, this means that out of 100% of the pore volume, water occupies 30% and hydrocarbons occupy 70%.

In a reservoir, the hydrocarbons will always occur above water due to their respective density differences. Migration of hydrocarbons into pore spaces will displaces connate water downward. In reservoirs it is very important to know the position of the hydrocarbon-water contact. Knowledge of this contact will allow geoscientist to plan production techniques. This will ensure efficient and effective recovery of hydrocarbons.

Archie (1942) formulated a resistivity index (RI) that linked fluid saturation to electrical conductivity/resistivity of the formation. The resistivity index (RI) was the ratio of true resistivity of formation rock (Rt) to the resistivity of the same rock filled with water (Ro). RI= Rt/Ro

CHAPTER THREE

3.1. Geological setting

The Pletmos Basin forms part of the larger basin called the Outeniqua Basin. Offshore rift and post rift basins north of the Algulhas Falkland Fracture Zone forms part of the Outeniqua Basin. (AFFZ) (Figure 3.2.1). The Outeniqua Basin is made up of four syn-rift basins the basins are: the Bredasdrop Basin, the Pletmos Basin, the Gamtoos Basin and Algoa Basin. The Bredasdrop and Pletmos basins are located in the western region of the Outeniqua Basin and the Gamtoos and Algoa are situated to the east of the Outeniqua Basin. The Outeniqua Basin is constrained by basement highs to the east, the St Francis Arch, and in the west by the Algulhas Columbine Arch (Brown et al., 1995).

3.2. Paleogeography

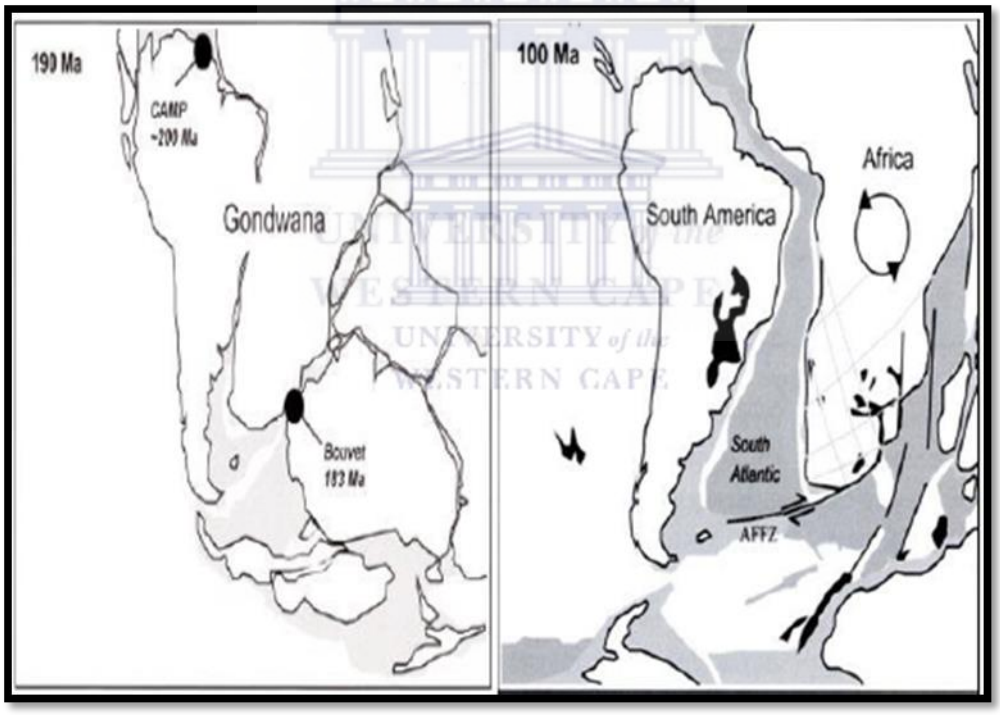

Figure 3.2.1: A diagram showing where the breakup of Gondwana initiated 190 -100 Ma ago (Scotese, 2002) and (De wit et al., 2001).

Research conducted by Dingle, et al. (1983) where he looked at magnetic survey anomalies, suggested that rifting between the Antarctic and Africa plates started to the west of Madagascar. This was when Southern Gondwana (figure 3.2.1.) started to break up between 143 Ma and 133 Ma years ago. Around 127 Ma ago south western Gondwana began to break up into the South American and African plates along the AFFZ (Larsen and Ladd, 1973) (figure 3.2.1).

During the Valanginian, the rifting phase came to an end (Figure 3.3.3.). The end of the rifting phase was accompanied by extensive erosion of a drift onset unconformity and regional uplift (126 Ma). During this period the initial formation of the post rift Pletmos Basin occurred as a result of a combination of various Algulhas rift basins. During the early Aptian (around 112 Ma), movement of the Falkland plateau westwards ended, this resulted in a third episode of post rift basement erosion and uplift (Brown et al., 1995)**.**

3.3. Depositional setting

The Pletmos Basin covers an area of about 18000 km^2 and consists of post rift, syn rift I and II Cretaceous sediments (PASA, 2010). The basin is bordered to south west by the Infanta Embayment and to the north east by the St Francis Arch (figures 3.3.1. and 3.3.2). The Pletmos Basin is a NW-SE trending basin that can be divided into five segments: Northern, North Eastern, Plettenberg, Southern and South Eastern segments (Brown et al., 1995). The Pletmos, Superior and Plettenberg faults confine the five sub basins.

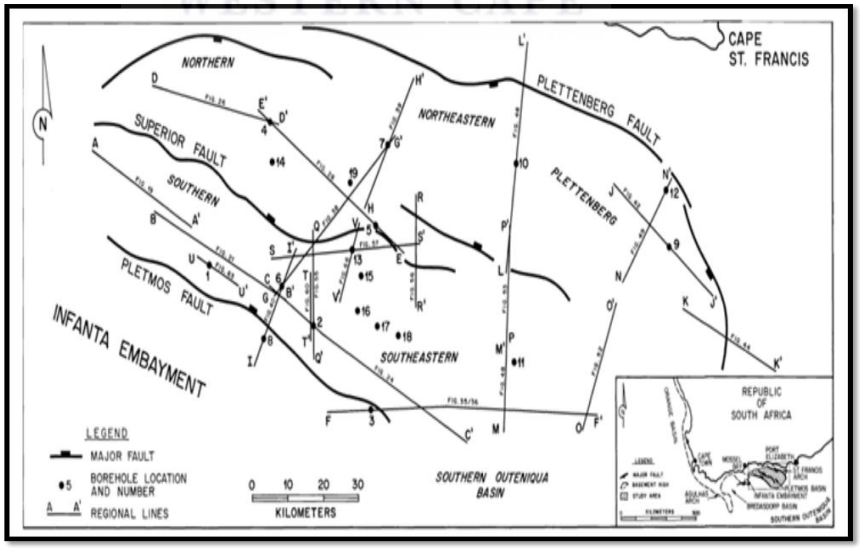

Figure 3.3.1: Map of the Pletmos Basin and its sub-basins with its major bounding faults (Brown et al., 1995).

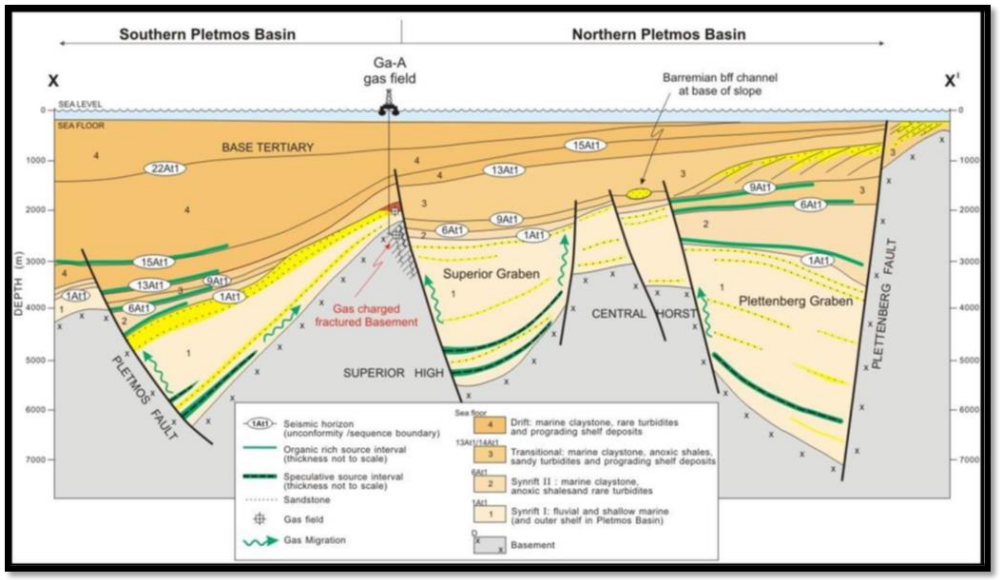

Figure 3.3.2: Schematic geological cross section of the Pletmos sub-basin, illustrating the structural styles present as well as the stratigraphic subdivision (Roux and Davids, 2010*).*

The synrift 1 phase during Cretaceous period seen throughout the Pletmos Basin was influenced by siliciclastic depositional systems. According to Brown et al. (1995), second order tectonic episodes (variations in sediment supply rates, accommodation and subsidence rates and increasing open marine activities) resulted in a change of depositional system. Three distinctive depositional systems can be observed in the Pletmos Basin. The depositional systems vary from: fan deltaic systems (126-117.5 Ma), river to tide dominated embayment systems (1175-112 Ma) and open marine wave and river dominated systems (112-68 Ma) (Brown et al., 1995). The basin-wide uniformities D, 1Atl and 13Atl delineates the onset of rift transitional to early drift and late drift phases of sedimentation seen in Pletmos Basin (figures 3.3.2 and 3.3.3.). North of the Superior fault (figure 3.3.2.) and north of the Pletmos fault is where thick sediment accumulations of interval D to 1Atl are found. Interval D to 1Atl consists of inner to outer shelf sandstones with non- marine green and red beds (McMillan et al., 1997).

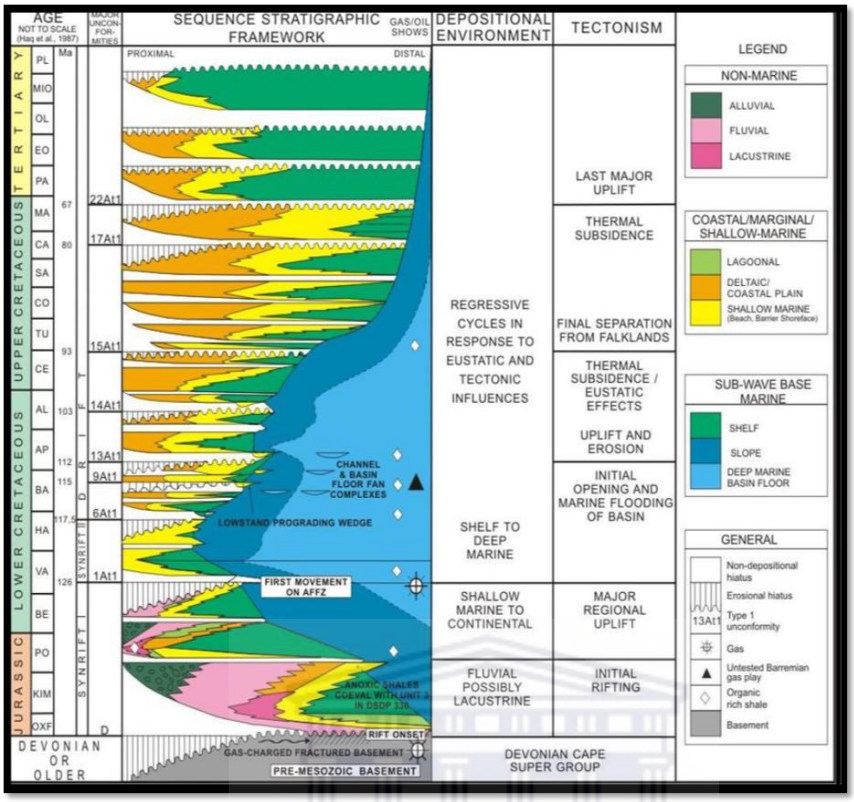

Figure 3.3.3: Generalised stratigraphic chart of the Pletmos basin (PASA, 2010).

3.4. Structural controls and sediment input

According to McMillan, et al. (1997) an extensional stress orientated regime between horizon D and 1Atl (Kimmeridgian to Late Valanginian) (figure 3.3.3.) led to the development of horst and graben system as well as accumulation of thick packages of sediment. The three faults in the Pletmos Basin enforce significant structural controls on the basin. Upper Jurassic and Lower Cretaceous synrift 1 reservoirs have structural closures while post rift sediments required the development of stratigraphic trap plays (Brown et al., 1995)

3.5. Basement controls

The pre – Mesozoic basement has only been penetrated by a few wells in the Pletmos Basin but only on basement highs. The pre – Mesozoic consists of Ordovician – Silurian quartzites (McMillan, et al., 1997).

3.6. Stratigraphic controls

Stratigraphic controls are influenced by the deposition of the lowstand reservoirs. Marine transgressive shales are considered as seals (Brown et al., 1995). Unfavorable diagenetic damage within the lowstand tracts to porosity, permeability, textural and grain constraints lead to poor migration of hydrocarbons (Brown et al., 1995).

3.6.1. Facies

According to McMillan, (2003), the Bredasdrop Basin and Pletmos Basin have a distinct similarity in depositional sequence. Horizon D to 1Atl (Kimmeridgian to Late Valanginian) graben fill succession, consists primarily of marine shelf (figure 3.3.3) grey claystones and glauconitic sandstones with red fluvial claystones.

CHAPTER FOUR

4.1. Materials and Methods

The present chapter discusses the various materials, methods and techniques used in the study. The flow chart below illustrates the procedure utilized to achieve the desired aims, objectives and results from the analyses used in this study. The software program IP (interactive Petrophysics) was used in this study. The core samples were collected from the Petroleum Agency of South Africa (PASA), Cape Town and used for geochemical and petrographical analyses. Digital wireline logs and geological well completion reports of the two wells (Ga–Q1 and Ga–S1) were also collected from PASA. Materials received from PASA are listed below:

1. Core samples from selected depth intervals (Table 1.1).
2. Wireline log data (Gamma ray, neutron, density, resistivity and sonic)
3. Geological well completion reports of the well Ga–Q1 and Ga–S1)

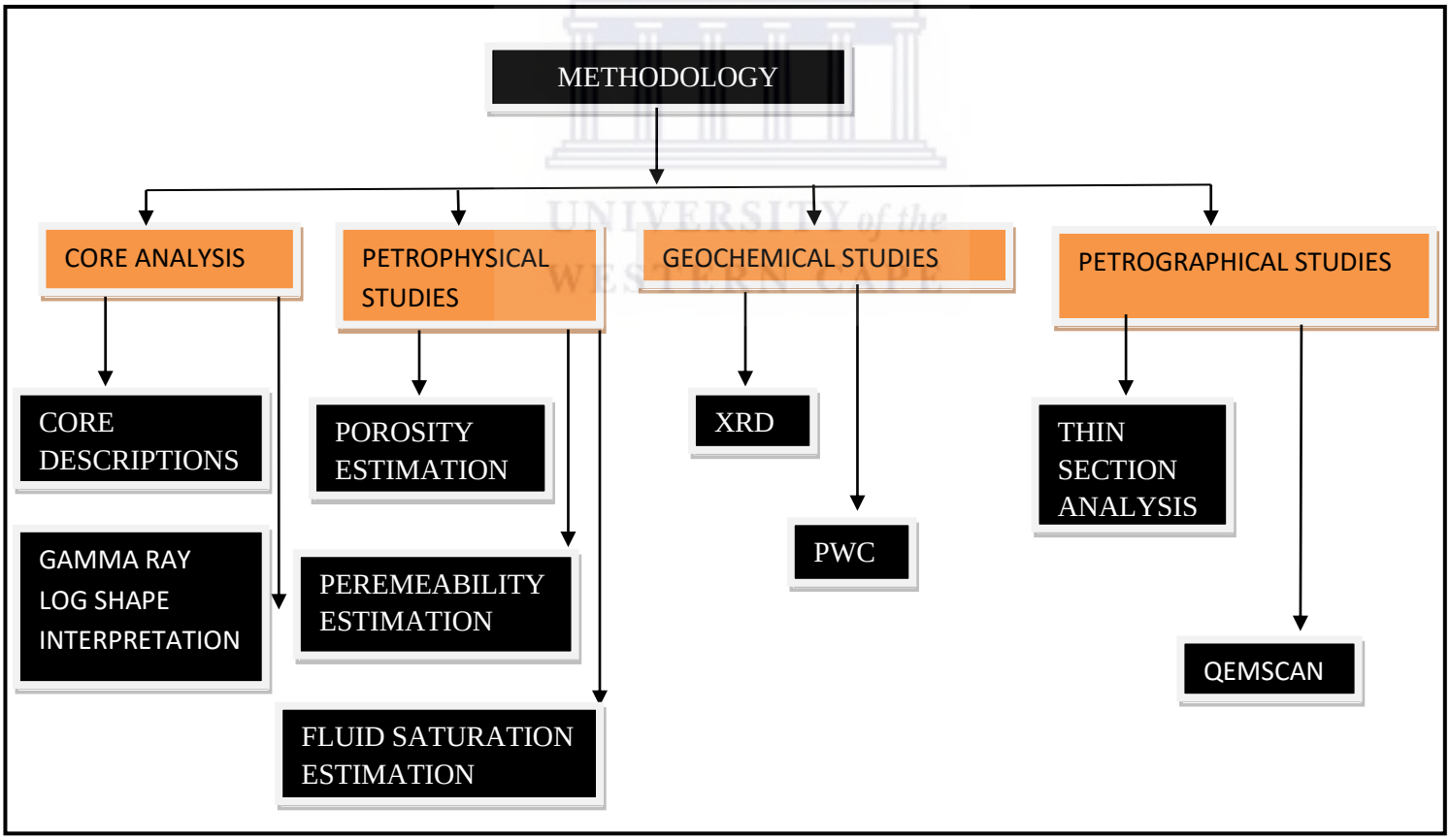

Figure 4.1.1: Methodology framework

A Petrophysical evaluation was conducted on well Ga – Q1 and well Ga – S1 using the Interactive Petrophysics software program. Core samples were taken from the two wells. The samples were used to do core (lithofacies description), geochemical (XRD and PWC) and petrographical (thin section and QEMSCAN) analysis. The sampling depths were determined based on: length and availability of core and the number of facies identified from core analysis. Gamma ray log shapes were interpreted and used to confirm depositional environments.

The XRD analysis was a semi – qualitative/quantitative study of the minerals. Detailed petrographic analysis was carried out on all thin sections. Properties like texture, grain size and shape; mineral identification as well porosity estimation was conducted. The QEMSCAN technique, which is a quantitative and qualitative method, was used to quantify clay minerals, identify minerals as well as illustration the spatial distribution of identified minerals. Pore water chemistry was conducted on samples to determine the pH and Ec of pore waters.

4.2. Wireline logs

In 1927 Marcel and Conrad Schlumberger became the first to apply geophysical logging to a borehole in France. The aim of the method was to measure the electrical properties of the subsurface rocks within the borehole (Schlumberger, 1972). Since then, geophysical logging has become a fundamental tool in the petroleum industry. It is an important tool used by geologists to gather information on subsurface rock succession. The information that can be gathered around the borehole from geophysical logging is: the composition and physical properties. Wireline logging is done by embedding a sonde in a drill string (LWD)-Logging while drilling a well. Wireline logs can measure radioactive and electrical properties of the encountered borehole rocks with depth and is done before landing of casing. Wireline logs can measure parameters such as: resistivity, radioactivity (natural gamma radiation), travel time and density and the parameters correspond with a depth. Wireline logs can be classified as follows:

4.3. Methods of wireline logs usage

For the present research four wireline logs were used to calculate the petrophysical parameters of the reservoirs. The four wireline logs are: Gamma ray log, resistivity, neutron log and density log.

4.3.1. Gamma Ray log

The gamma ray log is used to measure the natural radioactivity of the rocks. The gamma ray log measures the K, Th and U component found in sedimentary rocks. This helps to distinguish rock types as it is accepted that the radioactive elements are found in clays and shales. The gamma ray log is useful to correlate sand bodies and detect reservoir zones. The standard unit of measurement for the gamma ray log is American Petroleum Institute (API). Generally, gamma ray values of less than 45 API highlights clean sand. A gamma ray value of above 75 API indicates a shale body while an API value of between 45 and 75 API indicates a shaly sand body. The different API values indicate the radiation intensity of the formation. The API scale is normally 0 -150 API. When the gamma ray curve deflects to the left it represents sandstone. Sandstone intervals are usually coloured with yellow. When the gamma ray deflects to the right it represents a shale unit. The shale units are represented by the colour green (Figure 4.3.2).

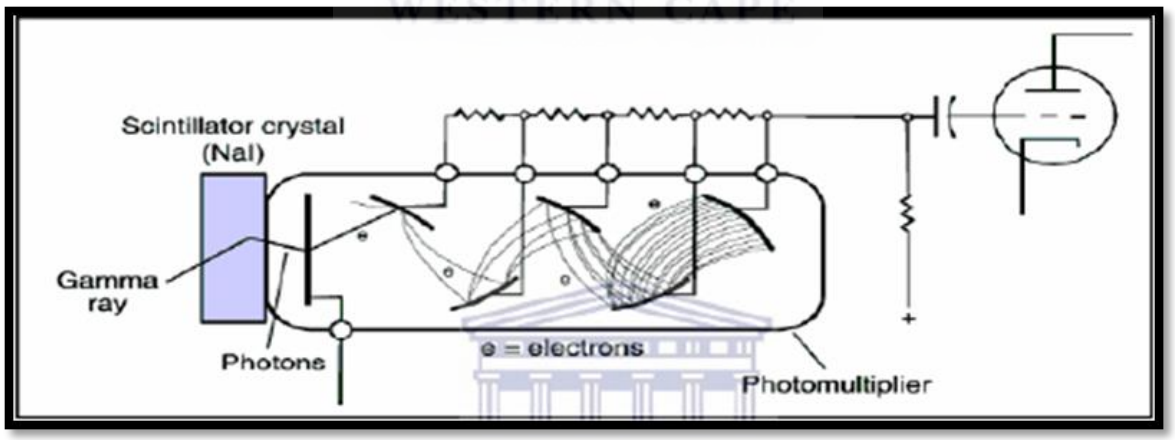

Figure 4.3.1: Gamma ray tool (after Serra, 1984).

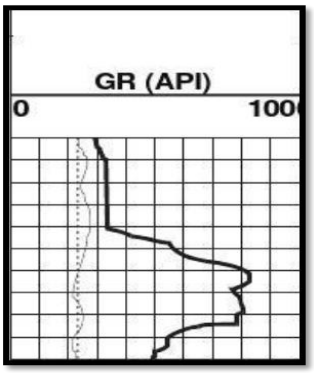

Figure 4.3.2: Typical Gamma ray log response to lithology. Schlumberger, (1972).

4.3.2. Resistivity log

The resistivity log measures and characterizes the electrical conductivity of the rock formation. Resistivity is a fundamental component as it represents how strongly the rock opposes the flow of current. Resistivity logs use electrical conductors to eliminate the resistance of the contact leads. The resistivity log is run to the boreholes that have conductive mud filtrate. Electrical properties of the formation depend on pore structure, geometry and water saturation. The resistivity log plays a crucial role in formation evaluation. The various resistivity logs are mentioned below:

4.3.2.1 Induction logs

This resistivity log makes use of a high frequency electromagnetic transmitter to induce current into an undisturbed formation (formation distant from borehole) and measure the conductivity.

4.3.2.2. Laterolog

This a resistivity log applied in undisturbed formations. The log can identify over – pressure and determine fluid saturations. The log essentially monitors drops in potential differences between the electrode and tool. A drop in potential difference signifies changes of resistivity in the formation**.**

4.3.2.3. Micro – Resistivity log

This tool measures the resistivity of the flushed zone and the invaded zone. This tool does not reflect the true resistivity of the formation.

4.3.3. Neutron log

When geological formations are bombarded with a radioactive source (electronic neutron generator), which is always neutrons, the neutron log will measure the concentration of hydrogen ions in the formation. Fast emitted neutrons emitted from radioactive sources will interact with atoms of similar atomic mass, which are usually hydrogen atoms. Hydrogen atoms are always prominent as they occur in water and hydrocarbons. Due the collisions, the fast-moving neutrons will slow down and start to disperse energy. As the neutrons continuously slow down they are absorbed into the nuclei of heavier atoms. Due to this absorption they become unstable; gamma rays are emitted after they lose energy. The emitted gamma rays are recorded by a detector. The detector which positioned at a predetermined position from the source can measure: concentration of epithermal neutrons, concentration of thermal neutrons or gamma rays emitted as a result of the absorption.

The type of neutron logs that are run in boreholes:

4.3.3.1. Sidewall Neutron Porosity log

This tool is crucial in measuring the porosity of a reservoir section. This tool can be run in an open hole or cased hole. However, casing and cement has to be taken into consideration and corrections have to be made (Krygowski, 2003).

4.3.3.2. Compensated Neutron log

This tool is used in both open and cased holes and detects thermal neutrons. It has two detector spacing's and is sensitive to slow neutrons (Figure 4.3.3).

Apart from porosity identification, this neutron log can also determine lithological properties when it is combined with the gamma ray log and when combined with density logs it can detect gas bearing zones.

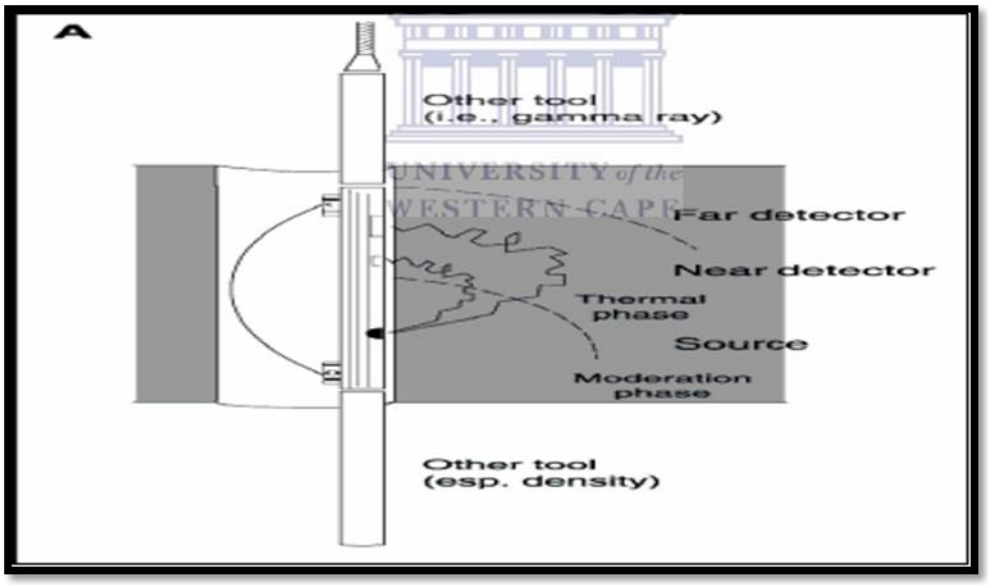

Figure 4.3.3: Illustration of compensated neutron log (after Rider, 1996)

4.3.4. Density log

Density logging is another application of gamma ray in gathering data about subsurface formations. Density logging tools rely on gamma-gamma scattering or on photoelectric (PE) absorption. As a result, the density logging tool measures the amount of gamma rays scattered back. A typical radioactive source is Cesium – 137 that emits gamma rays of 0.66 MeV into the surrounding formations. At these high energy levels, Compton scattering is observed. Compton scattering is the interaction/collision of fast-moving particles with electrons in the formation. After every collision the gamma ray suffers an energy loss to the electron and then it continues with diminished energy. As a result, the scattered gamma rays will reach a detector and will be counted. These values reflect the formation density while the amount of Compton scattering is proportional to the electron density of the formation.

4.3.4.1. Formation Bulk Density

Formation bulk density is the overall density of the rock and that encompasses pores spaces, fluids trapped in pores spaces as well as the matrix. As a result, the density log measures the density of the formation. Each rock type has specific density range, (Rider, 1996). See table 4.0 below.

Table 4.0: the average density values of various rock types

Lithology	**Density Values** (g/cm^3)
Limestone	2.71
Sandstone	2.65
Dolomite	2.87 (reading in zero porosity)
Anhydrite	2.98
Salt	2.03
Shale	2.2 – 2.7
Coal	1.5+

4.4. Petrophysical properties

The interpretation of various wireline log suites will be used to calculate the petrophysical parameters (volume of clay, porosity, permeability and fluid saturation). Interactive Petrophysics (IP) software program will be used to accurately calculate the petrophysical parameters

4.4.1. Porosity

The density log is used to determine the porosity because it is highly accurate and has minimal borehole effect

Porosity= Pma-Pb /Pma-Pf

An indication of gas bearing zones can be achieved by using a neutron-density log combination. Log. Porosity from neutron log is thus calculated with the density log, where:

$[0.5*(\Phi d2+\Phi cnl2)]^{0.5}$

Φd = Porosity reading from density log.

Φcnl= Porosity reading from neutron log

For gas bearing reservoirs while for non-gas bearing reservoirs;

Total porosity= Density porosity + Neutron porosity /2.

Effective porosity is given as [Total porosity *(1-Vsh)] provided Vsh is calculated by the Steiber method.

4.4.2. Permeability

Permeability values would be derived by using Coates formula and is measured in milliDarcies.

K = GΦeff 4 [ΦT - (Φeff * Swir)/Φeff * Swir

The Coates formulae for calculating permeability works well in shaly -sandy formation

Φeff = Effective porosity

ΦT= Total porosity

Swir =Irreducible water saturation

4.4.3. Volume of shale

This is the measure of clay content present in the reservoir interval. The Steiber method was used to calculate volume of shale

Using the Steiber equation (1970), Vsh (volume of shale) is calculated as:

Vsh = IGR/3-(2IGR)

4.4.4. Fluid saturation

Resistivity logs can be used to calculate the fluid saturation of hydrocarbon bearing reservoir intervals. To ensure accurate calculation of fluid saturation values, the combination of deep and shallow resistivity logs are used

$Sw= [F*(Rw /Rt)]^{0.5}$

Where $F=a/Porosity^m$, Rw = Resistivity of water, Rt = True resistivity of the formation

The hydrocarbon saturation would be calculated as $S_{hc}= 1 - S_w$

Bulk volume of water (Vb) = Sw*Porosity

S_{irr}= Vb/ effective porosity/ $(1-Vsh^2)$.S_{irr} implies the minimum attainable amount of water that can be displaced from the reservoir due to hydrocarbon migration.

When $S_w=S_{irr}$……. Hydrocarbon bearing intervals

$S_w>S_{irr}$…….. Hydrocarbon production likely

$S_w<S_{irr}$…… Erroneous estimation

4.5. Wireline log loading

Well logs were obtained from PASA and were formatted in LAS (Log ASCII Standard) files. The LAS files were uploaded onto the Interactive Petrophysics program. The wireline logs that were used: Gamma ray log, Resistivity, Density and Neutron. These logs were calibrated and used to calculate petrophysical parameters for wells Q1 and S1.

4.6. Core description

Materials needed for core descriptions are:

- Hand lens
- Log sheet
- Sample bags
- Digital camera
- Water
- Measuring tape

The core of well Ga-Q1 and well Ga- S1 were laid out at PASA core laboratory. The cores from both wells were 18m in length. The core logging process was done by analyzing the cores from bottom and finishing up at the top of the core. Detailed core descriptions were done with reference to the depth. The information obtained was: rock type, texture, grain size, colour, sedimentary structures. All information obtained from core analysis was to identify lithofacies in each core and photos of the core and important sedimentary structures were taken.

4.7. Thin section analysis

Thin section petrography involves the study of rock slide section under microscope. The information that is derived from thin section petrography is: mineralogy, texture (grain size, sorting, packing and porosity estimation). Rock samples were cut to about 5mm and thinned to about 40 microns and mounted upon a thin section slide. Thereafter, the thin sections were impregnated with an epoxy to prevent material loss and then polished. Thin section analysis is an important technique as cements could be identified. Clay mineral is difficult to study under the microscope (only Glauconite could be easily identified). Thin section results were compared

with information of QEMSCAN and XRD to confirm mineral identification. The spatial distribution of minerals plays an influential role in affecting the petrophysical properties.

4.8. X – Ray diffraction

XRD analysis of milled samples was conducted at Ithemba Labs x – ray facility, Cape Town and used a Bruker D8 Advanced diffractometer. The main objective for using the XRD method was to identify the clay minerals present within each sample. The XRD procedure was as follows. First samples had to be milled to a fine powder and then put into separate containers. Thereafter, the samples were analyzed at Ithemba Labs. The XRD method works as follows:

Electromagnetic radiation (X-rays) generated from photon energies (around 100ev to 1000 Kev) penetrates deep into the sample to reveal the bulk X-ray structure. The experiment set up includes a divergence slit of 3 degrees on the primary and secondary side. Samples prepared for XRD analysis were measured from a 2-theta starting point of 10 degrees to 2– theta stop of 85 degrees with step a stop time 0.3s and a step size of 0.02 degrees

4.9. Quantitative Evaluation of Minerals by Scanning Electron Microscope (QEMSCAN)

QEMSCAN is the top of the range automated mineral analyzer. It is an analytical tool which provides rapid, reproducible and statistically reliable quantitative information on minerals. The purpose of the (QEMSCAN) was to quantify the identified minerals but more specifically the clay minerals present. The QEMSCAN 650F uses a field emission gun –scanning electron microscope (FEG – SEM) from FEI together with a high-resolution BSE (Back scattered electron), a Bruker energy Dispersive Spectrometers (EDS) and a Spectral Analysis Engine (SAE) to analyze mineral phases. The aim for using the QEMSCAN was to identify the clay minerals present, quantify the identified clay minerals present and generate a particle map illustrating the distribution of the minerals in a sample. Samples (thin sections) were prepared by carbon coating each sample before being analyzed by the QEMSCAN. Each sample was analyzed for about 6 to 8 hours. The result thereof was the identification and quantification of the clay minerals as well as a low–resolution digital map generated by the field scan measurement

technique together with the Bulk Mineralogical Analysis (BMA) which give the statistically information of the minerals identified.

4.10. Pore water chemistry

Pore water chemistry is the measurement of the concentration of hydrogen ions - acidity/alkalinity (pH) and electroconductivity (Ec) of the pore fluids. The Eckert method (1998) was used. The procedure to determine the pH and Ec, was to first crush core rock samples and then weigh 5 grams thereof. The crushed samples were dissolved with 50 ml of ultra water in a beaker. The solution in the beaker was spun in a centrifuge machine for 20min and allowed to settle for 20min. The solution was then poured through 50-micron filter paper and a clear solution was captured. The solution was then analyzed using a pH meter probe to determine the pH and Ec of the solution.

CHAPTER FIVE

5. Introduction: Core and Petrophysical Analysis

In this Chapter two key aspects are analyzed and interpreted: Petrophysics and Core analysis. The description of cores together with interpreting the gamma ray log curve response derived from the IP program resulted in the identification and interpretation of the depositional environments. The petrophysical parameters of the reservoir zones are calculated using the Interactive software program (IP).

5.1. Petrophysical Analysis of wireline logs

The wireline logs used for this work are: 1) the gamma ray log 2) the sonic log 3) resistivity (shallow and deep) logs 4) neutron logs and 5) density logs. Interpretation of these wireline logs is crucial to accurately calculate the petrophysical properties. The combination of shallow and deep resistivity logs was used to calculate fluid saturation values. A combination of density and neutron logs were used to calculate porosity values. A linear regression formula obtained from on Interactive Petrophysics was used to calculate permeability values. The conventional core data (from PASA reports) of some petrophysical properties and the calculated petrophysical parameters derived from the Interactive Petrophysics software program from the two wells were compared and correlates in a near perfect manner.

Petrophysical analysis was conducted on two wells: Ga- Q1 and Ga- S1. The cored data (porosity, permeability and water saturation) that was obtained from the conventional core analysis (PASA reports) was used to calibrate the calculated porosity and permeability logs. The volume of clay for each cored interval was established and used to classify the type of reservoir. The following volume of clay parameters was used: less than 10% = sandy reservoir, 10% - 35% = shaly/sand reservoir and lastly, more than 35% = shaly reservoir.

5.1.1. Petrophysical Analysis of Well Ga – Q1

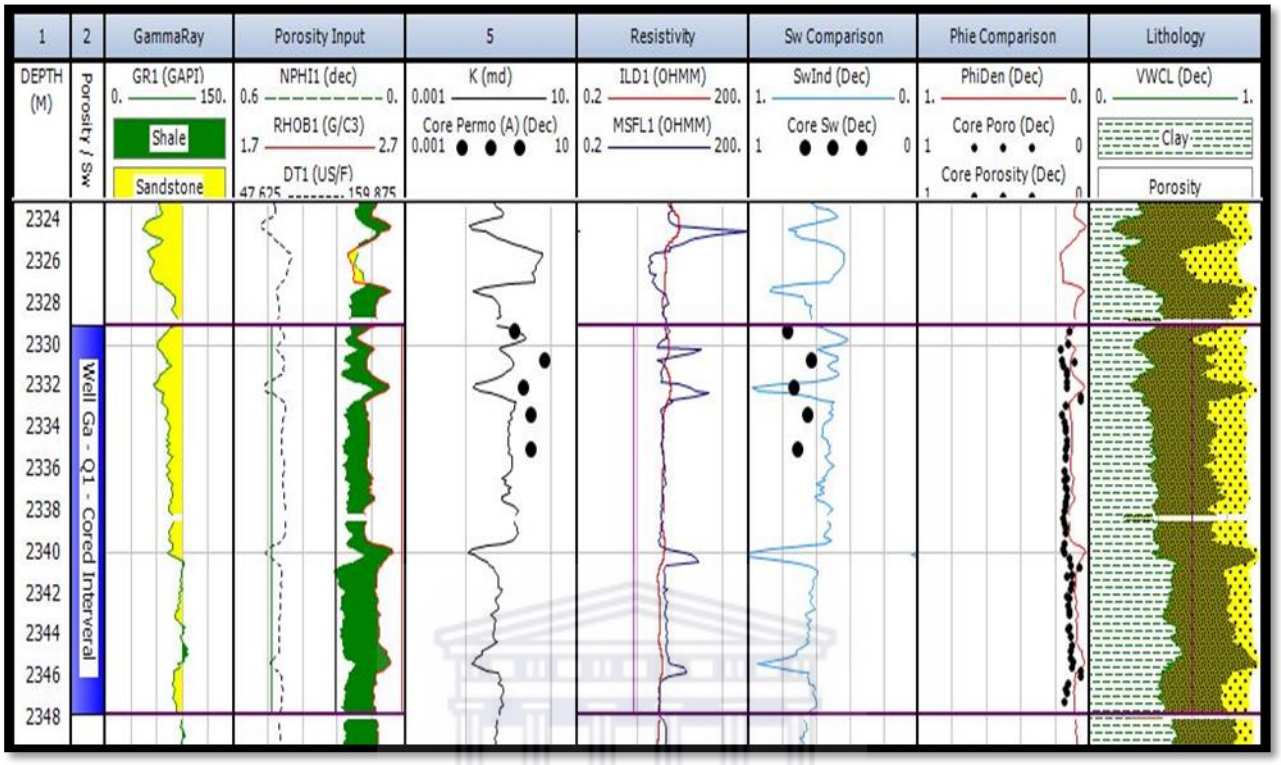

Figure 5.1.1.1: Logs suites interpreted for well Ga –Q1

In well Ga-Q1, cored interval of 18m is analyzed and it ranges from 2329m to 2347m. In track 3 (GR log), the gamma ray log differentiates between sand and shale intervals. In order to differentiate between the sand and shale, a gamma ray log baseline had to be established. This was established by generating a GR histogram (Figure 5.1.1.2) and checking the average API value for the well. The baseline of 90 API was set for well Ga- Q1.

Looking more into detail the following petrophysical parameters were calculated using Interactive Petrophysics: track 5 permeability values (K), track 7 fluid saturation value (S_w), track 8 porosity values and track 9 volume of clay.

The volume of clay content for the cored interval was used to establish the type of reservoir. The average volume of clay calculated for the cored interval is 40% making the cored interval of well Ga- Q1 a Shaly reservoir. Furthermore, the average GR reading for the cored interval is 78 API (Minimum GR reading of 57 API and a maximum GR reading of 96 API) and the GR (mode) is 74 API. The API readings together with the gamma ray log (track 3) confirm the shaly nature of

the reservoir. In track 5, the average calculated permeability (K) was 0.2 mD. The permeability from the top of the core to the base ranges from 0.1 mD to 2,5 mD. The average calculated porosity (Track 8) was 9% and by analyzing the core from top to base the porosity ranges from 5% - 17%. The calculated fluid saturation (Track 7) was 80% water saturated.

Table 5.1.1: Petrophysical parameters of the cored interval (2329m – 2347m) derived from IP

Well	Avg. VCl (%)	Reservoir type	Avg. Porosity (%)	Avg. Permeability (mD)	Avg. Fluid Saturation (%)	GR(Avg. of core) – API	GR(min. of core) – API	GR(max. of core) - API
Ga – Q1	40	Shaly	9	0.2	80 (S_w)	78	57	96

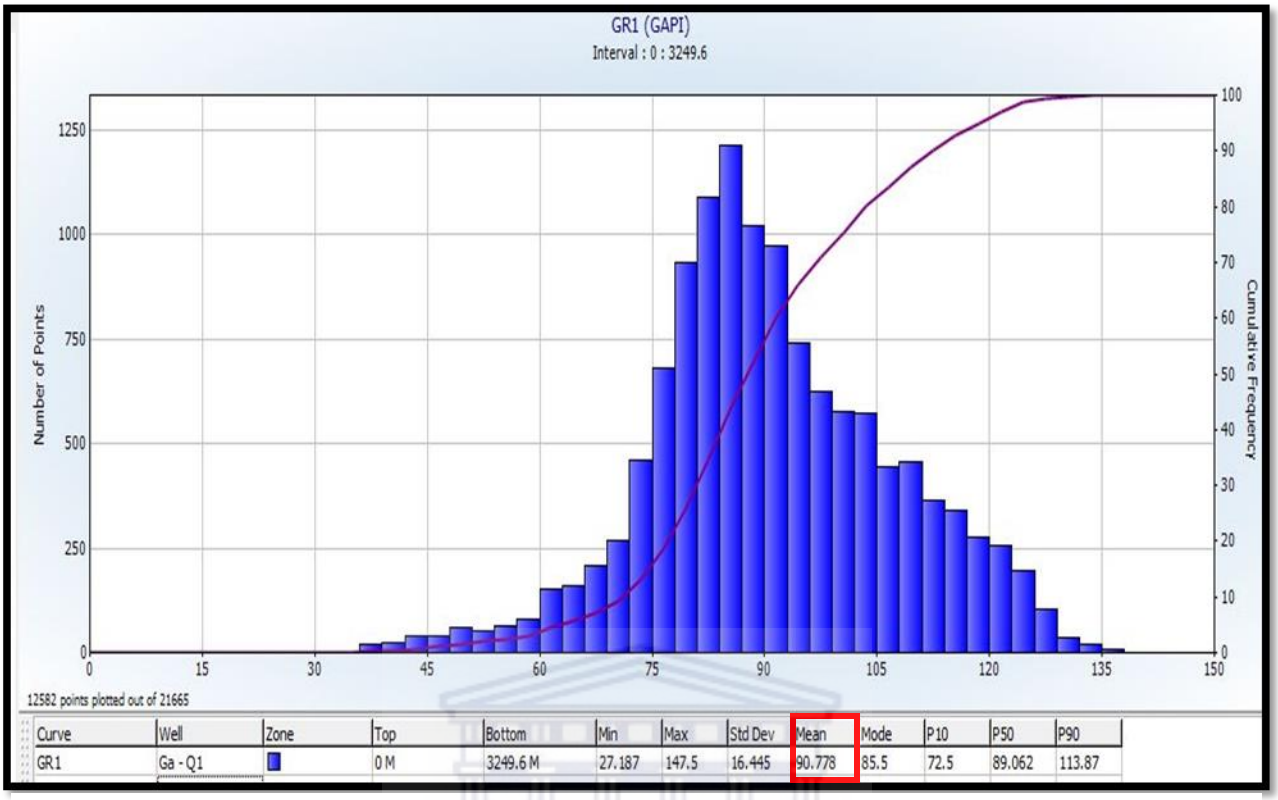

Figure 5.3.1.2: Gamma ray histogram of well Ga – Q1, used to set the GR log baseline for the well

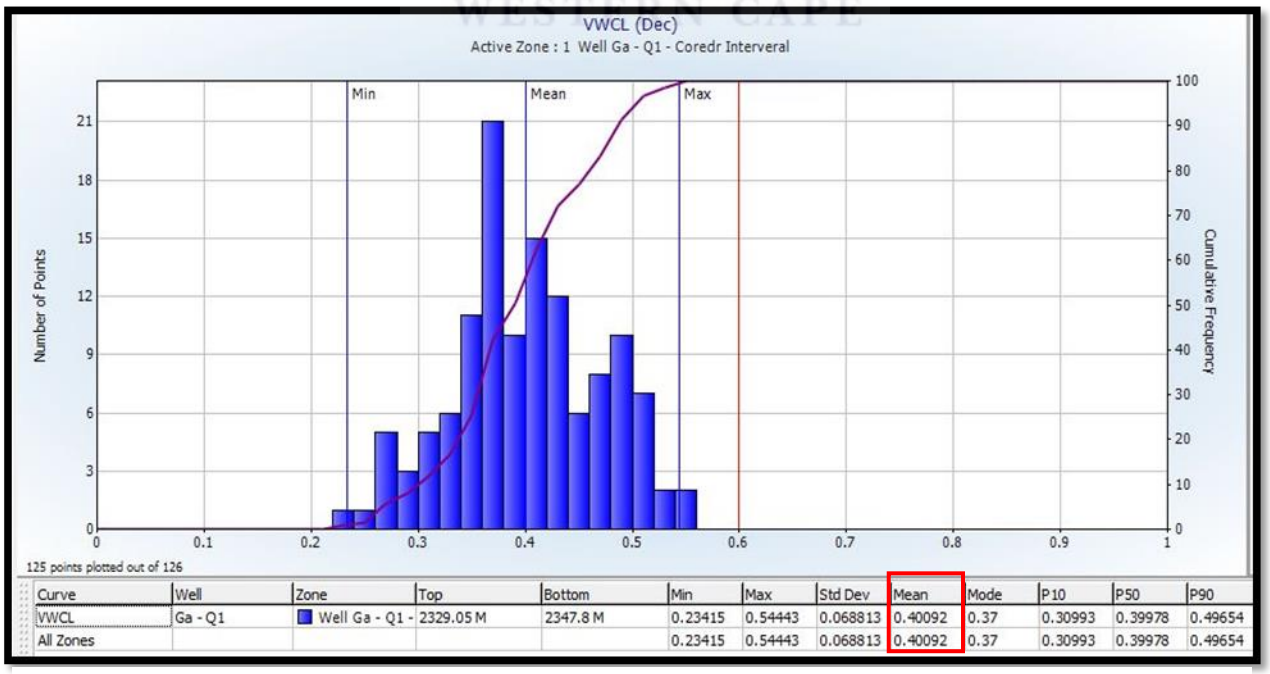

Figure 5.1.1.3: Volume of clay histogram used to classify the reservoir from the cored interval of well Ga-Q1

5.1.2. Petrophysical Analysis of Well Ga-S1

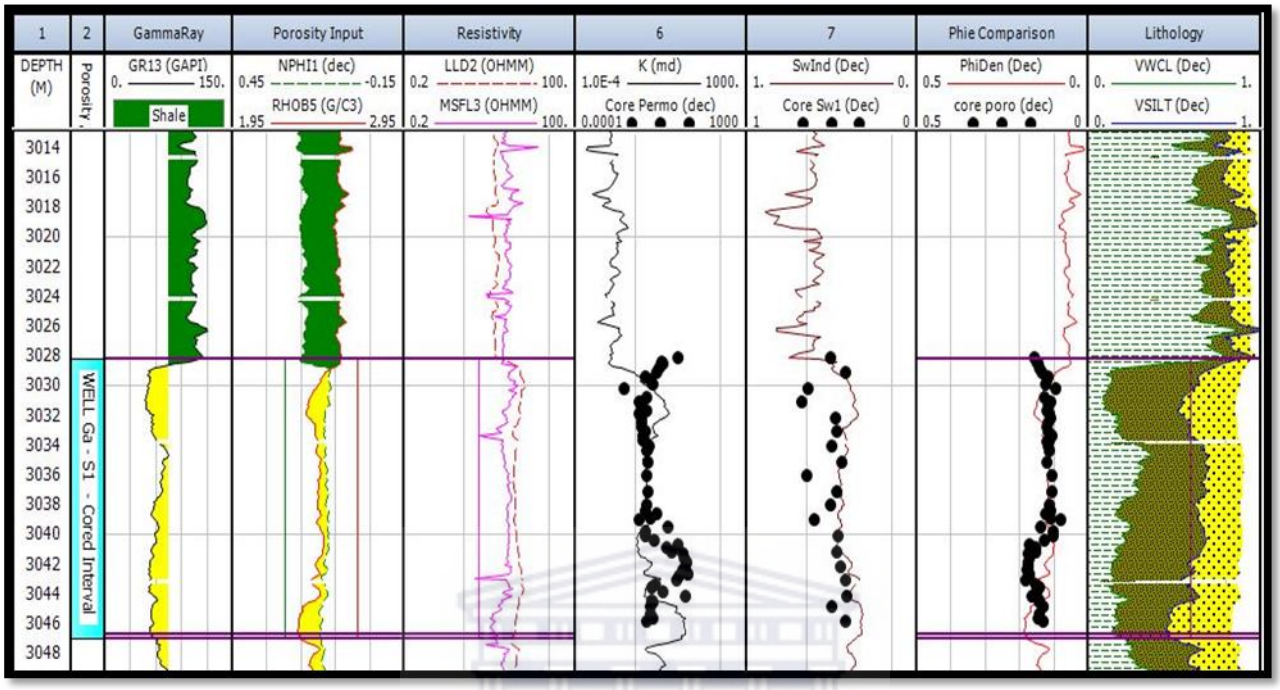

Figure 5.1.2.1: Log suite interpreted for well Ga – S1

In well Ga–S1 one cored interval of 18m was analyzed and ranging of 3028m to 3046m. In track 3 (GR log), a gamma ray baseline had to be established to differentiate sand and shale bodies for the well. A GR histogram (See figure 5.1.2.3) was generated to calculate the API average for the well. A baseline of 85 API was set for well Ga – S1.

Looking more into detail the following petrophysical parameters were calculated using Interactive Petrophysics: track 6 permeability values (K), track 7 water saturation value (S_w), track 8 porosity values and track 9 volume of clay.

The volume of clay content for the cored interval was used to establish the type of reservoir. The average volume of clay calculated for the cored interval is 21% making the cored interval of well Ga – S1 a shaly/sand reservoir. Furthermore, the average GR reading for the cored interval is 59 API (Minimum GR reading of 48 API and a maximum GR reading of 117 API) and the GR (mode) is 56 API. The API readings together with the gamma ray log (track 3) confirm the sandy nature of the reservoir. In track 6, the average calculated permeability (K) was 0.3 mD and

ranges from 0.1 mD to 4 mD. The average calculated porosity (Track 8) was 12% and ranges from 8% to 18%. The calculated fluid saturation (Track 7) was 42% water saturated.

Table 5.1.2: Petrophysical parameters of core interval (3028m – 3046m) derived from IP

Well	Avg. VCl (%)	Reservoir type	Avg. Porosity (%)	Avg. Permeability (mD)	Avg. Fluid Saturation (%)	GR(Avg. of core) – API	GR(min. of core) – API	GR(max. of core) – API
Ga – S1	21	Shaly/sand	12	0.3	42 (S_w)	59	48	117

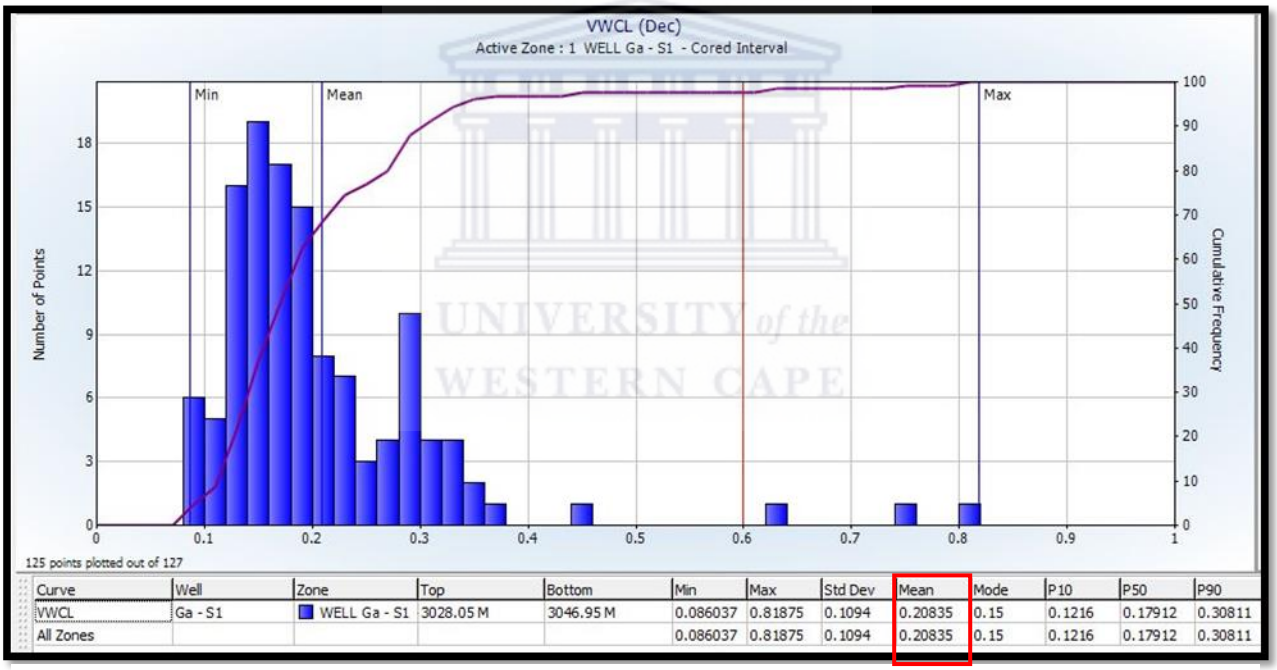

Figure 5.1.2.2: Volume of clay histogram of the cored interval from well Ga - S1, used to classify the cored reservoir interval.

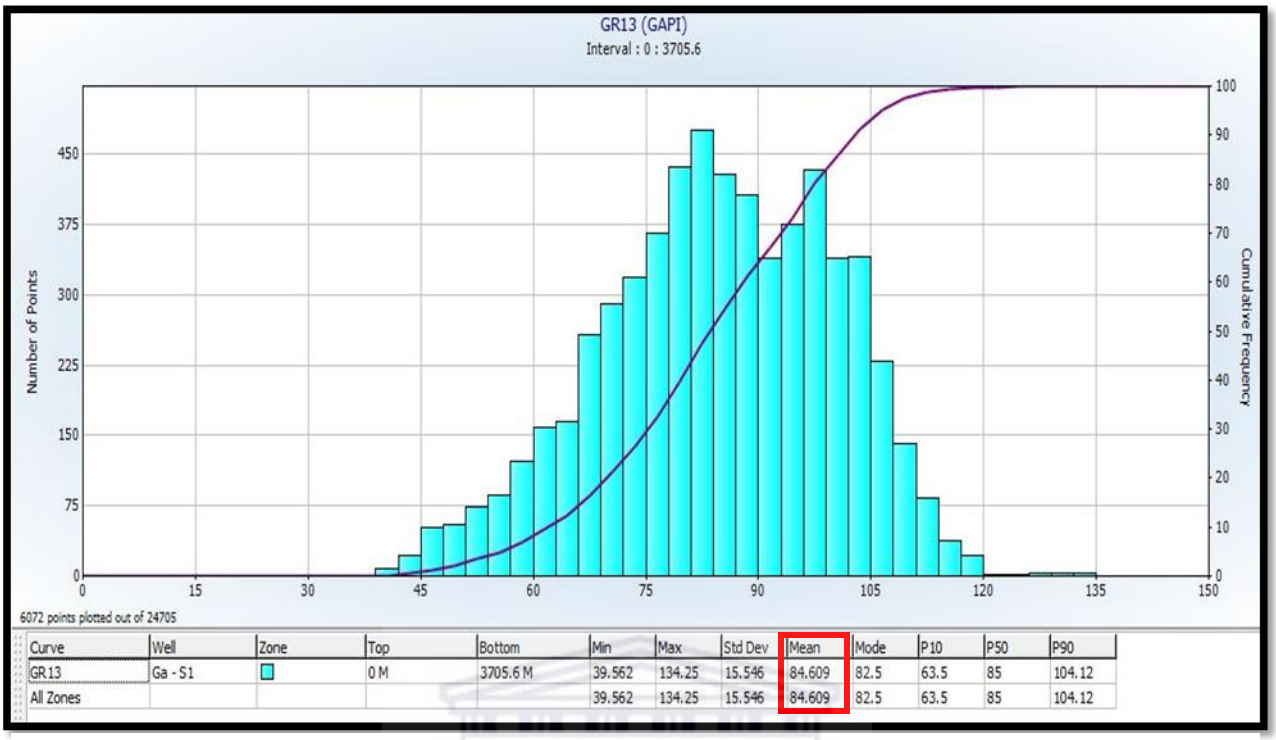

Curve	Well	Zone	Top	Bottom	Min	Max	Std Dev	Mean	Mode	P10	P50	P90
GR13	Ga - S1		0 M	3705.6 M	39.562	134.25	15.546	84.609	82.5	63.5	85	104.12
All Zones					39.562	134.25	15.546	84.609	82.5	63.5	85	104.12

Figure 5.1.2.3: Gamma ray log histogram used to set the baseline for well Ga - S1.

5.2. Core Analysis

The most important information derived from core analysis is the Lithological and lithofacies identification.

Two cores were obtained from the two wells Ga-Q1 and Ga-S1. The total lengths of the cores are: well Ga-Q1 = 18m and well Ga-S1 = 18m. An approach used by Nieto (1998) was used to identify different facies. Nieto's approach identified facies based on the rock type, colour, grain size, mineralogy and sedimentary features. Variation in grain size was used to differentiate between the different groups of facies. Based on the approached used by Nieto (1998), two different facies were identified from the cored intervals. Facies A is identified in well Ga- Q1 and Facies B is identified in well Ga-S1.

5.2.1. Conventional core analysis

The measurement of porosity, permeability and fluid saturations (water, oil and gas) are included in the conventional core analysis. These three parameters are fundamental components to understand the dynamics of the reservoir. The measured parameters provide information about whether the reservoir rocks pore spaces contain fluids (porosity), whether the fluids in the pore spaces are filled with hydrocarbons and could these hydrocarbons be produced (permeability)? This analysis focuses on analyzing and interpreting a predetermined area of interest (e.g. a cored interval). The analysis is performed on lithologies such as sandstones, shaly sands and carbonates. As mentioned above the analysis was conducted on well Ga-Q1 and well Ga- S1. All the conventional core analysis results presented in this study were obtained from the conventional core analysis and core description reports provided by PASA

5.2.1.1. Well Ga-Q1 Cored interval

Core 1 was cut at a depth between 2329m and 2347m and 100% of the core was retrieved. Core 1 was cut to evaluate a drilling break and gas show. Core 1 consisted of predominantly coarsening upward shallow marine sandstones (argillaceous) with minor amounts of siltstone and claystone. Core permeability values ranged between 0.21 mD and 2.51 mD, Core porosity values ranged from 5% to 15% and water saturation values ranged between 63% and 77% (PASA report). The conventional core analysis included grain density, gas expansion (helium) porosity, air (Ka) and liquid (KL) permeability) and fluid saturation (water, oil and gas).

The table (Appendix A) represents the results obtained from the conventional core analysis of well Ga – Q1 and was used to calibrate wireline log data.

5.2.1.2. Well Ga-S1 Cored interval;

In well Ga- S1, three cores were cut below horizon 13At1 in order to evaluate good drilling breaks and gas shows. For this study Core 1 was used to conduct the study. It was cut at a depth between 3028m and 3046m (100% of core 1 was retrieved). Core 1 consisted of extensively bioturbated inner shelf sandstones. Core porosity values ranges between 8% - 18%, core permeability values ranged between 0.1 mD and 4 mD and water saturation values ranged between 41% and 68% (PASA report).

The table (Appendix B) represents the results obtained from the conventional core analysis of well Ga- S1 and was used to calibrate wireline data.

5.3. Lithofacies Descriptions

5.3.1. Lithofacies description of Well Ga- Q1

Within well Ga - Q1, one facie (Facie A) was identified within the 18m cored interval. Facie A is characterized by a coarsening upward sequence. The base of the core is characterized by siltstone and gradually coarsens to the top of the core to a fine – grained to medium- grained sandstone. Facies A consists of laminated mud, silt and fine-grained sand which are rippled and burrowed. Petrography ranges from glauconitic protoquartzite to feldspathic sand. The cored interval is greyish in colour and can be classified as glauconitic sandstones. The sedimentary features present are asymmetrical current ripples (ripple lamination) preserved only in the sandy sections as well as low angle planar cross bedding. Burrowing is intense, which results in the disruption of bedding in silty sections. The type of burrowing that occurs within the cored interval is vertical burrowing. Heterolithic lamination is also observed in the cored interval. The heterolithic lamination is sand-dominant. Sand – dominated heterolithic lamination is also known as flaser bedding and is a distinctive feature of the inter-tidal deposits. Rippled sand that migrate over a muddy substrate result in the formation of flaser bedding. Facies A can be interpreted as being coarsening upward tidal bar unit deposited in the inter – tidal zone of the Tidal flat environment.

A) Illustrates a 10cm thick medium grained sandstone with low angle (15 deg.) planar cross bedding at 2330, 74m B) At 2330m (top of section), we find flaser bedding – incomplete mud laminae trapped in ripple troughs during periods of low water and the bottom, we see asymmetrical ripplies (amplitude 5mm and wave length 5cm) C) illustrates the vertical burrowing (12cm long) seen in the silty sections at 2346m

Figure 5.3.1.1: Images of the core interval from PASA, indicating Facie A and specific sedimentary features identified from well Ga – Q1.

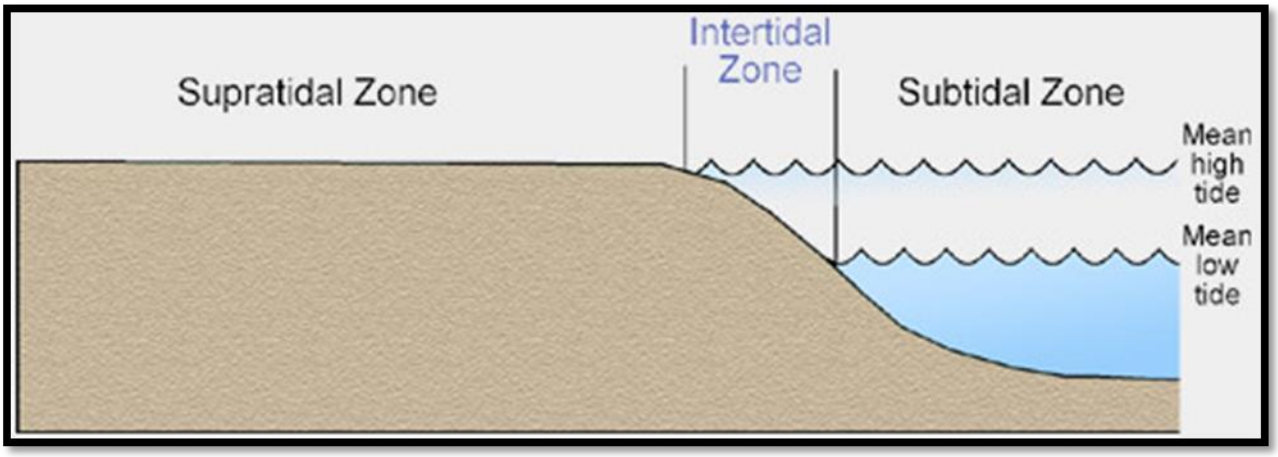

Figure 5.3.1.2: Simple generalized illustration of the sub environment found within the Tidal flat environment

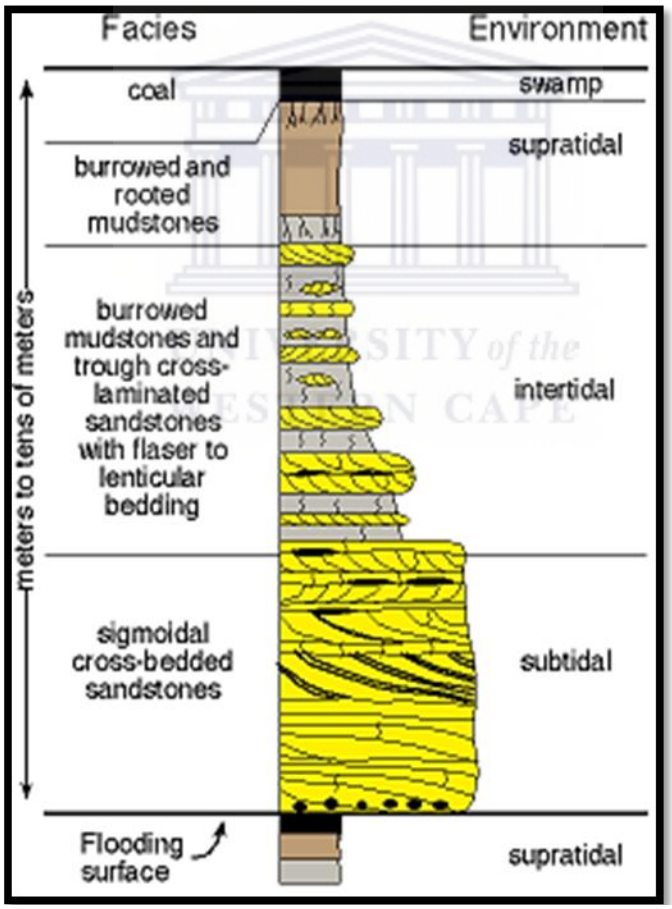

Figure 5.3.1.3: Illustration of a sedimentary profile and sedimentary features of the Tidal flat environment

5.3.2. Lithofacies description of Well Ga- S1

Within well Ga- S1, one distinctive facie (Facie B) was identified within the 18m cored interval. The cored interval could be described as having a siltstone base and coarsening upward where we found a fine grained sandstone top of core. The majority of the core is viewed to be fine grained sandstone with a section near the top of the cored considered as medium grained sandstone.

Facies B consists of very fine to fine grained sandstones and occasionally medium grained sandstones. The sandstone is glauconitic and slightly carbonaceous to carbonaceous. Facies B is intensely bioturbated. As a result, the bioturbation has obscured any original sedimentary features. The abundance of trace fossils, *Helminthoida* and *Ophiomorpha nodosa* are found (PASA report). These trace fossils only occur in the lower shoreface to transitional zone (Balseley, 1988). Therefore, Facies B can be interpreted to be deposited in the Lower shoreface zone of the Beach environment.

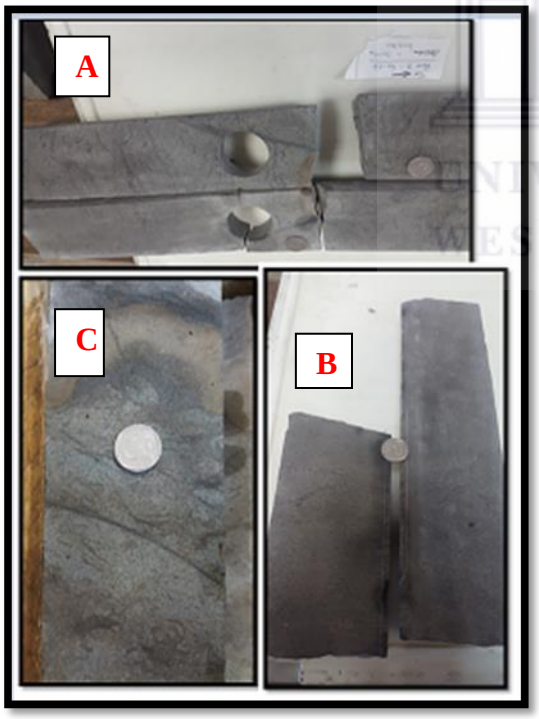

A) At 2328, 3m, illustrates a fine grained sandstone that has been intensely bioturbated and this common throughout core interval B) At 3030, 3m, we seen the extend of the bioturbation that has destroyed primary sedimentary feature through the majority of the cored interval C) At 3039m, illustrates an extremely glauconitic fine grained sandstone that is intensely bioturbated. The brown horizontal section at the top is remnants of burrowing.

Figure 5.3.2.1: Images of the core interval taken from PASA, indicating Facie B and the specific sedimentary features identified from well Ga –S1.

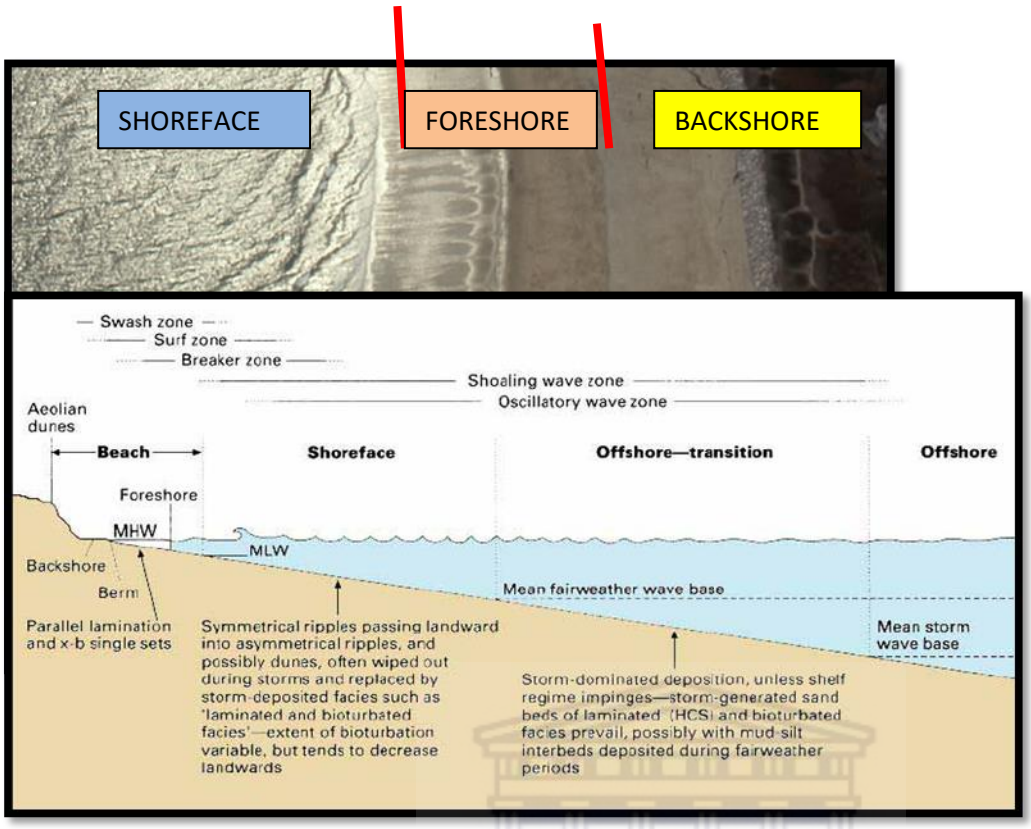

Figure 5.3.2.2: (A) An aerial photograph of the sub zones of the beach environment (B) Illustration of the sub environments of a clastic marine shelf.

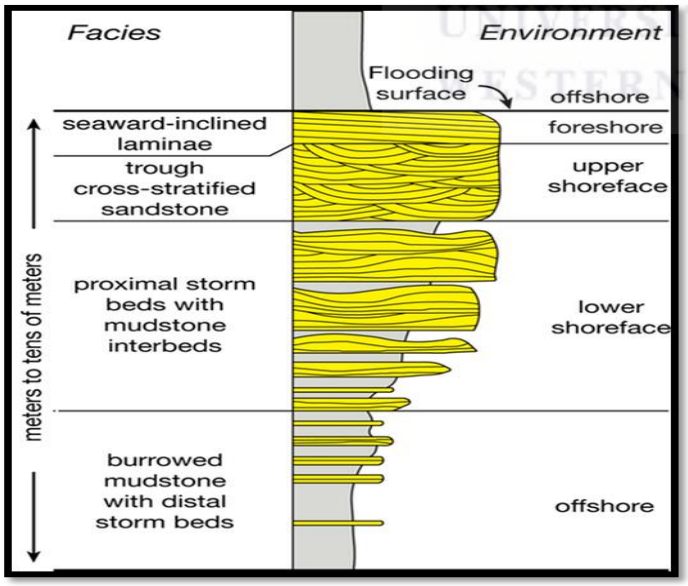

Figure 5.3.2.3: A sedimentary profile illustrating the sedimentary features of the Beach environment.

5.4 Gamma Ray Log Response

The gamma ray log shapes are frequently used for interpreting sedimentary cycles and depositional environments. The five log shapes are described as (Figure 5.4.1.1):

1. Bell Shape – upwards increasing trend in gamma counts (sharp base and fines upwards)
2. Funnel Shape – upward decreasing trend in gamma counts (coarsen upwards and sharp contact on top)
3. Box Shape – car/Cylindrical – relatively consistent gamma readings (sharp contact top and base)
4. Bow/Hour glass – systematic increase and decrease of gamma counts
5. Irregular- no systematic change in gamma readings

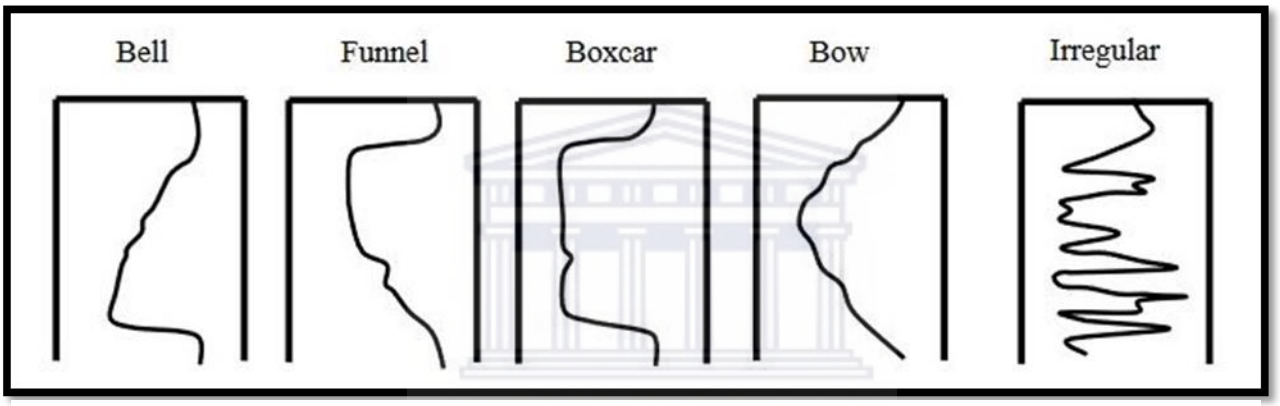

Figure 5.4.1.1: Idealized gamma ray shapes used to characterize depositional facies. Each log shape is associated with a specific depositional environment, (modified after Rider, 1993).

The gamma ray log response for both well Ga – Q1 and well Ga – S1 were analyzed in order to accurately classify the depositional environments of the two studied wells. The gamma ray logs that were used see figure 5.4.1.2 (well Ga –Q1) and 5.4.2.1 (well Ga –S1).

5.4.1. Well Ga – Q1

Three gamma ray log shapes are identified from the cored interval: A) Cylindrical/Box B) irregular and C) Bow/Hour glass (figure 5.4.1.2 and Table 5.4.1.1).

Table 5.4.1.1: The identified GR log shapes from core interval Ga - Q1 – 2329m to 2347m - (from top to base).

Depth (m)	**GR log pattern/shape**	**Symbol**
2329 - 2333	Bow/Hour glass	C
2333 - 2340	Box/Cylindrical	A
2340 - 2346	Irregular	B
2346 - 2347	Box/Cylindrical	A

Analyzing from the base to top of the cored interval we find from at a depth of 2347m to 2346m a Cylindrical/Box – shaped GR response (shape A). At a depth between 2346m to 2340m we find an Irregular – shaped GR response (shape B). At a depth between 2341m to 2334m we find Box – shaped GR response again (shape A). At the top of the cored interval (2334m to 2329m) we find a Bow – shaped GR response (GR shape C).

A correlation (top to base) between the identified lithofacies and GR shapes can be made. The flaser bedding (the sand-dominant heterolithic lamination) observed at the top of the cored interval can be correlated with the bow – shape (**GR shape C**) seen from the GR log. The flaser bedding observed in the intertidal zone is the product of high and low tides and hence the bow shaped (systematic increase and decrease in sea level) GR log response.

The box/cylindrical shaped GR response (**GR shape A**) can be related to the relatively uniform and fine grained sand sediment observed from the cores. The sedimentary features such as current ripples (ripple lamination) and cross bedding are characteristic of the intertidal zone (deeper sections thereof).

The irregular shaped GR response (**GR shape B**) can be related to the influx of silty/muddy sediment observed from the cores. The irregular shape also be interpreted as having no systematic change in gamma ray counts and this can be seen from the cores. The irregular shaped gamma response can also be attributed to a drop in sea level (progradation) and shift from a intertidal zone to a supratidal zone.

The GR shapes identified from the gamma ray log match the facie description and therefore confirm the shallow marine depositional environment or tidal flat environment (intertidal zone) inferred from the core analysis. The GR shapes also confirm the cored interval is coarsening

upward which means that this tidal flat environment experienced a transgression (relative sea level rise).

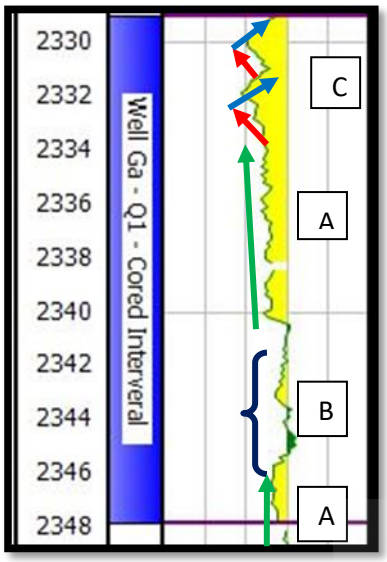

Figure 5.4.1.2: Gamma ray log response use to classify the shape of log and determine the environment of the cored interval from well Ga - Q1

Table 5.4.1.2: Gamma Ray log response the cored interval from well Ga - Q1

Zone	**Core Interval (m)**	**Facies**	**Log Pattern (s)**	**Depositional environment**	**Gamma Ray (API units)**
Well Ga– Q1	2329 to 2347	A	Cylindrical/Box and Bow/Hour glass	Inter-tidal zone	57 – 96

5.4.2. Well Ga – S1

Two gamma ray log shapes can be identified from analyzing the GR log of the cored interval. The two identified shapes are A) Box/Cylindrical and B) Bell (figure 5.4.2.1 and table 5.4.2.1).

Table 5.4.2.1: The identified GR log shapes from cored interval Ga - S1 - 3028 to 3046 - (from top to base)

Depth (m)	**GR log pattern/shapes**	**Symbol**
3028 – 3034	Box/Cylindrical	A
3034 – 3042	Bell	B
3042 – 3046	Box/Cylindrical	A

Analyzing from base to the top of the cored interval we find from a depth of 3046m to 3042m a Box – shape GR response (GR shape A), from a depth of 3042m to 3034m we find a Bell – shaped GR (GR shape B) response and from a depth of 3034m to 3028m we find again at the top of the cored interval a Box – shaped GR response (GR shape A).

A correlation between the GR shapes and facie descriptions can be made. The overall nature of the cored interval resembles a cored interval of little variation. The GR log reflects this uniform grain size nature of the cored interval. The box/cylindrical GR response (**GR shape A**) seen at the base and top reflects the little grain variation seen from the core. The bell-shaped GR (**GR shape B**) seen in the middle of the gamma ray log correlates perfectly with observations made from the core analysis – a slight fining upward sequence. As a whole (from base to top) the environment experiences a sea level increase that correlates with the bell shaped GR response and there culminates in a sea level drop and hence the GR count drop and effectively establishing a box/cylindrical GR shape at the top.

The GR shapes identified from the gamma ray log confirms the environment identified from the core analysis.

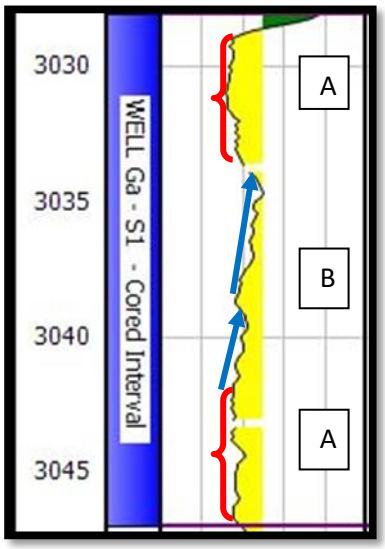

Figure 5.4.2.1: Gamma ray log response used to classify the shape of the gamma ray log and use to determine the environment of the cored interval from well Ga - S1

Table 5.4.2.2: Gamma ray log response of the cored interval from well Ga - S1

Zone	**Core depth (m)**	**Facies**	**Log Pattern (s)**	**Depositional Environment**	**Gamma ray (API units)**
Well Ga – S1	3028 to 3046	B	Cylindrical/Box and Bell	Lower Shoreface zone	48 – 117

5.5. Summary of Core and Petrophysical Analysis

Summary of core analysis

Two cored intervals were studied one from well Ga-Q1 and the other one from well Ga–S1. One facies per well was identified and described. Well Ga-Q1 had Facies A and well Ga-S1 had Facies B. Facies A was interpreted to be deposited in the inter– tidal zone of the Tidal environment. Facie B was deposited in the lower shoreface zone of the Beach environment. The cored interval of well Ga-Q1 (Facie A) reflects a coarsening upward succession and the cored interval of well Ga-S1 (Facie B) reflects slight grain variations. The gamma ray response of the two wells confirms the grain trends observed from core analysis.

Summary of petrophysical analysis

Comparing well Ga-Q1 to well Ga-S1, it is evident that well Ga-Q1 has higher clay content compared to well Ga-S1. The wells were classified based on their volume of clay values. Well Ga–Q1 had a volume of clay volume of 40% making it a shaly reservoir and well Ga–S1 had a volume of clay value of 21% making it a shaly/sand reservoir. The higher clay content of well Ga–Q1 is a key component of tidal flat environments compared to well Ga–S1 which has a lot less clay content due to little sediment variation this is a key component of beach environments. As a result, the clay content and type of sediment is reflected by the average gamma ray readings calculated for the cored interval of well Ga-Q1 is 78 API compared to 59 API of well Ga-S1. Well Ga–Q1, has a average porosity of 9% and a range of 5% to 17%, an average permeability of 0.2 mD and a range of 0.1 to 2.5 mD. The average water saturation is 61%. Well Ga-S1, has an average porosity of 12%, a range of 8% to 18%, an average permeability of 0.3 mD, and a range of 0.1 mD to 4 mD. And a calculated average water saturation of 42%. It is evident that the reservoir quality of well Ga – S1 is good as compared to well Ga – Q1. However, it must be highlighted that both reservoirs has extremely poor permeability values.

CHAPTER SIX

6. Petrography and Geochemistry

Chapter six addresses the petrography and geochemical analysis from wells Ga – Q1 and Ga – S1. The objective for doing petrographical studies was to identify the most abundant minerals in the core samples, understand the crystal habits and shapes as well as analyze distribution patterns of identified clay minerals. Thin section analysis provides information about the textural maturity of the sediments, while X – Ray Diffraction analysis justifies observations made on thin sections by identifying the type of clay minerals present in rock samples. Quantitative Evaluation of Minerals by Scanning Electron Microscope (QEMSCAN) gives quantitative information with regards to the minerals present. It also illustrates how the different identified minerals are distributed within the sample. Geochemical analyses are focused on confirming the observations from the petrographic studies. The analysis of the pore water provides information on the pH and electrical conductivity of pore waters.

6.1. Petrography analysis

Thin section petrographic studies were carried out on selected slides from the two wells Ga-Q1 and Ga-S1 respectively. The important observations made out from the petrographic studies were integrated with QEMSCAN, XRD and core analysis results. Microscopic observation of rock samples was carried out under plain polarized light and crossed [polarized light, this helps in the identification minerals, types of sorting, presence of authigenic cements and nature of pore spaces.

6.1.1. Petrographic study of well Ga – Q1

Six thin section slides were examined and the following results were obtained. The slides were taken from depth interval: 2330m, 2334m, 2337m, 2339m, 2343.3m and 2347.3m depths. The mineralogical compositions of the thin sections are found to be almost the same without any significant variations. Most of the mineral grains are sub-angular to sub-rounded in shape. The mineral grains are surrounded by a matrix of Calcite cement. The degree of sorting for the six samples can be classified as moderately sorted, yet compacted. The degree of compaction

suggests that the permeability factors are negatively affected and not the porosity. This is further confirmed by the low calculated permeability values carried out using the IP software program.

The most abundant mineral across all the samples is quartz. Another notable mineral found in most of the thin sections is Glauconite. Glauconite is typically green in colour under plain polarized light (PPL) as seen in sample1 (Figure 6.1.1 (A)) at a depth of 2230m. The presence of Glauconite is often attributed to mica alteration in shallow marine settings under reducing depositional conditions (Odm and Matter, 1981). The presence of Glauconite is further confirmed by the QEMSCAN analysis of the samples. Information derived for XRD analysis indicates that Calcite is prominent in the well; this is also confirmed by the QEMSCAN data. The presence of Calcite in the well confirms that sands were deposited under shallow marine conditions. Calcite is abundant in shallow marine settings because its precipitation takes place a few centimeters below the sediment-water interface (Bjorlykke, 1984). The above statement is also supported by the presence of Pyrite in the samples and further confirmed by SEM studies. The formation of Pyrite takes places in marine set up under reducing / anoxic depositional environment (Sauer et al., 1992).

Well Ga -Q1

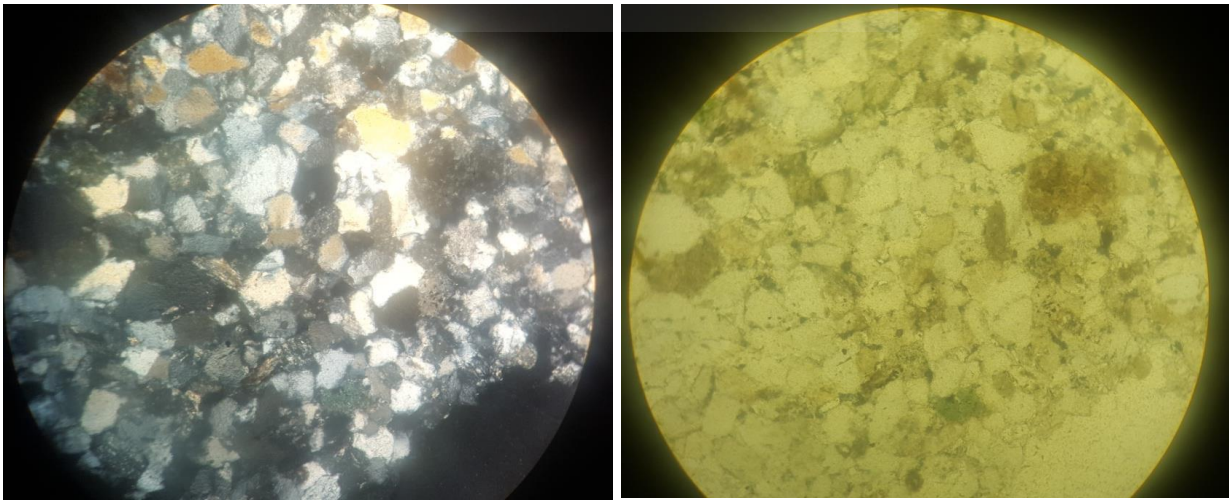

Figure 6.1.1.(A): Thin Section image of sample 1 in cross polar (left) and plain polar (right)

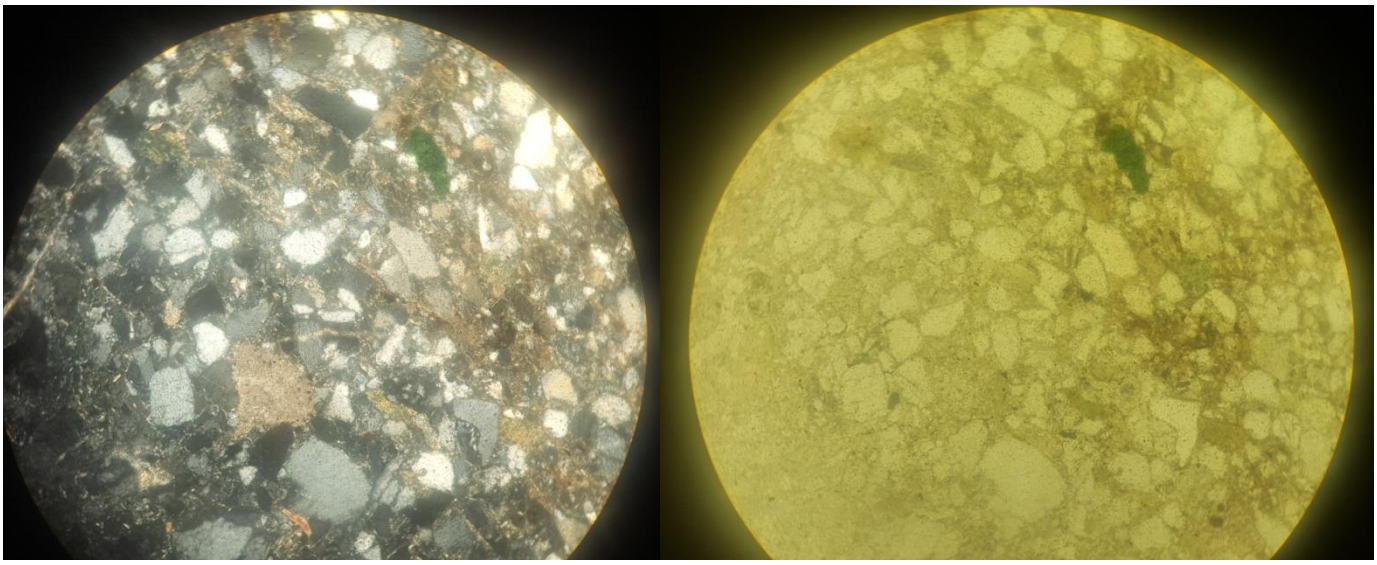

Figure 6.1.1.(B): Thin section image of sample 2 in cross polar (left) and plain polar (right)

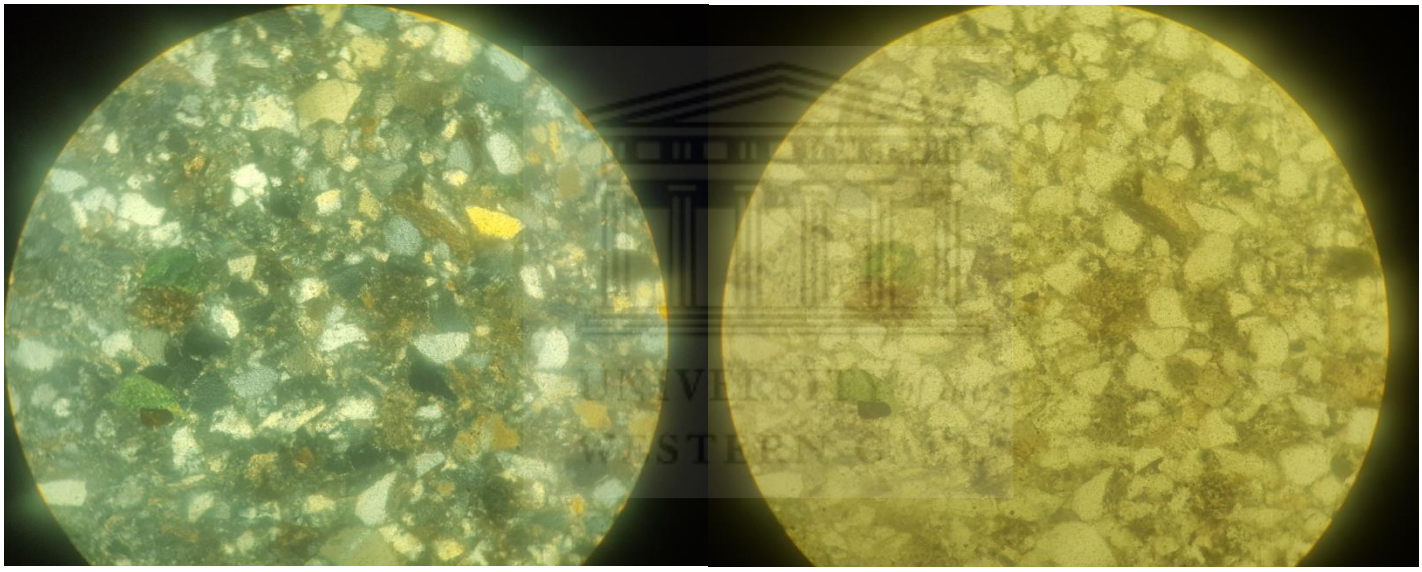

Figure 6.1.1.(C): Thin section image of sample 3 in cross polar (left) and Plain polar (right)

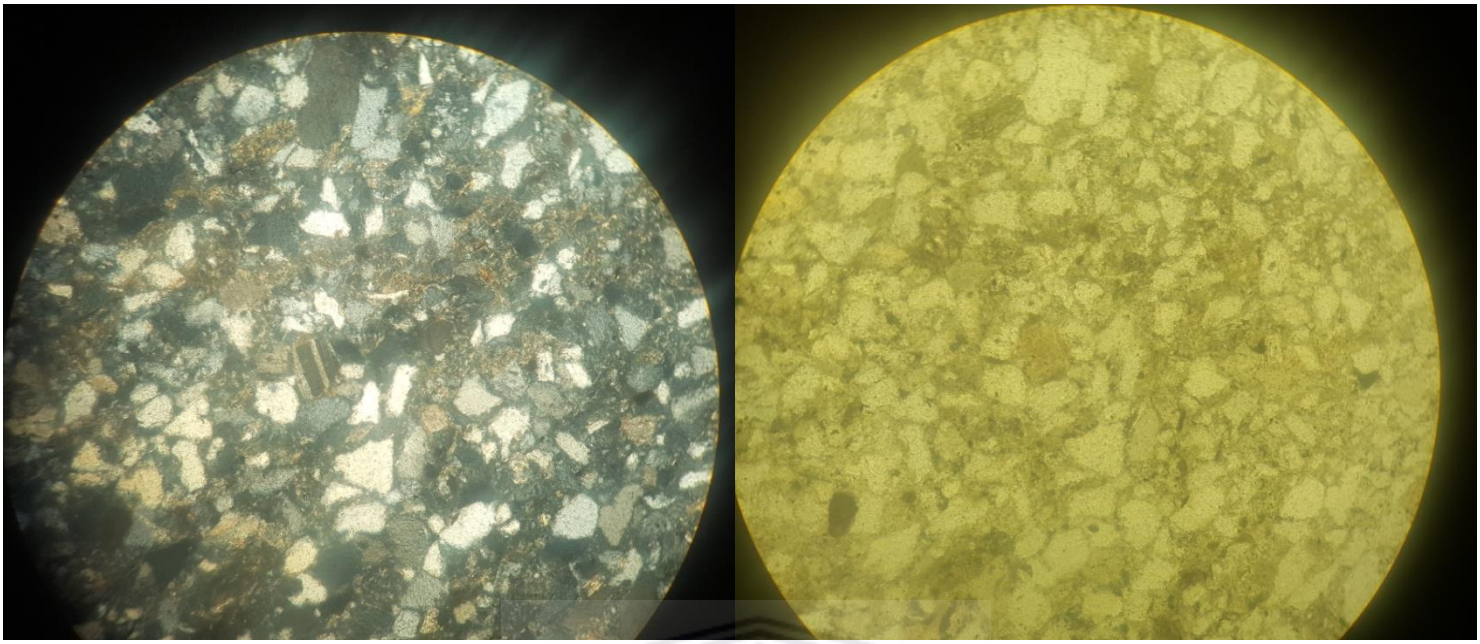

Figure 6.1.1.(D): Thin section image of sample 4 in cross polar (left) and plain polar (right)

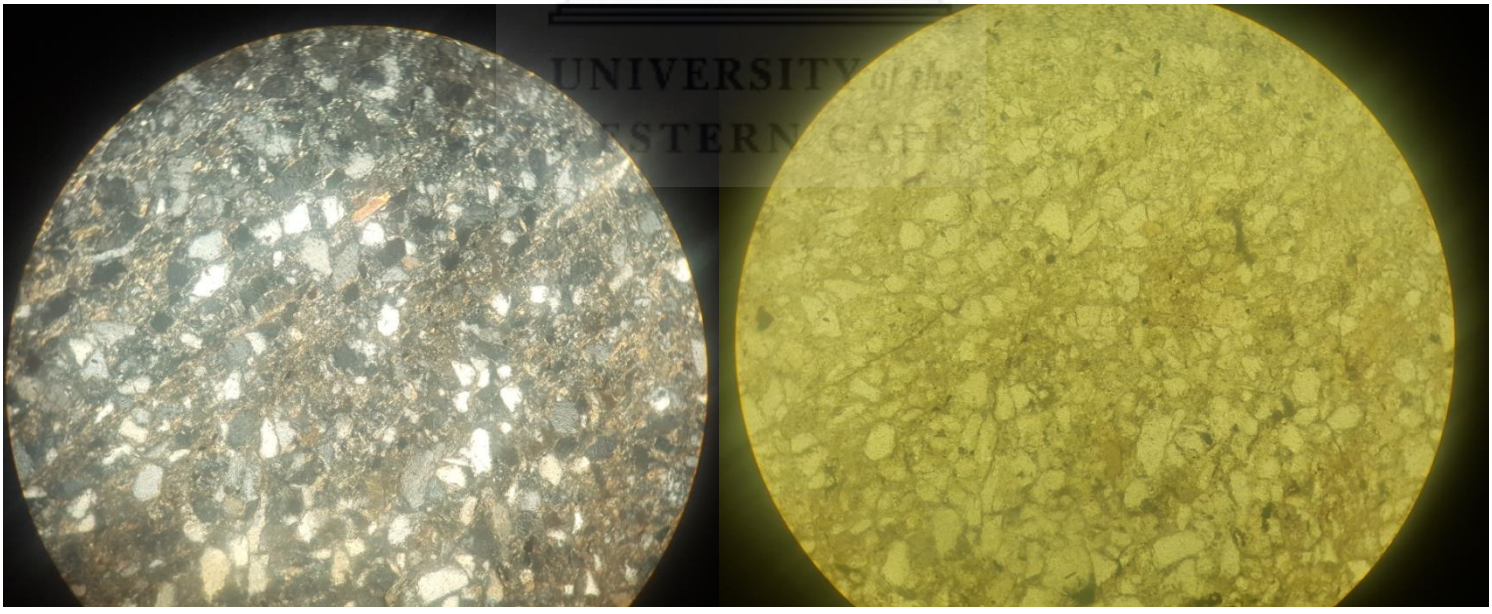

Figure 6.1.1.(E): Thin section image of sample 5 in cross polar (left) and plain polar (right)

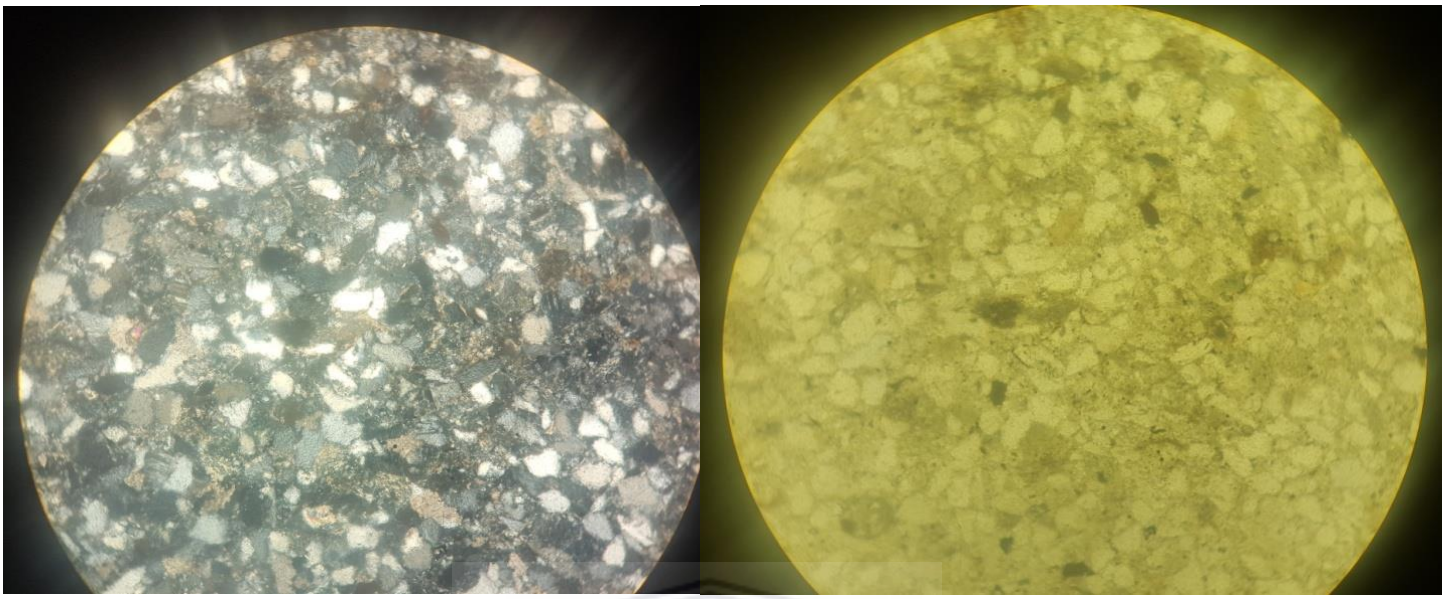

Figure 6.1.1.(F): Thin section images of sample 6 in cross polar (left) and plain polar (right)

6.1.2. Petrographic study of well Ga- S1

In well Ga-S1, six thin section slides from depth interval: 3028.88m, 3030.45m, 3033.65m, 3036.9m, 3039.82m and 3044.5m were studied. The mineralogical compositions of the thin sections show strong similarity. The grain shapes are sub-angular to sub-rounded. The degree of sorting of the samples are observed to be moderately sorted and are fairly compacted. The samples from the well Ga-S1 are comprises mostly of mineral grains and the intergranular spaces are filled by matrix of calcite cement.

Quartz is the most abundant mineral in all the samples of this well and are mostly present as sub-angular to sub-rounded grains. Plagioclase feldspar are also common (figure 6.1.2; A) and are identified by the distinctive lamellar twinning under crossed polarized light. Other significant minerals observed are Glauconite and Calcite. Calcite occurs as the dominant cement. The presence of Glauconite is confirmed by QEMSCAN data and can be seen in Figures 6.1.2 (A – F). Glauconite appears as typical green in colour under PPL. The mineral Glauconite usually forms as a product of mica alteration under reducing depositional conditions in shallow marine

settings (Odm and Matter, 1981). Presence of Calcite is confirmed by XRD and QEMSCAN data. The presence of the Calcite cement confirms that the sand body was deposited in shallow marine conditions. The mineral Pyrite is also observed in the samples. The presence of Pyrite is due to the fact that it also forms in marine environments under reducing conditions.

Well Ga – S1

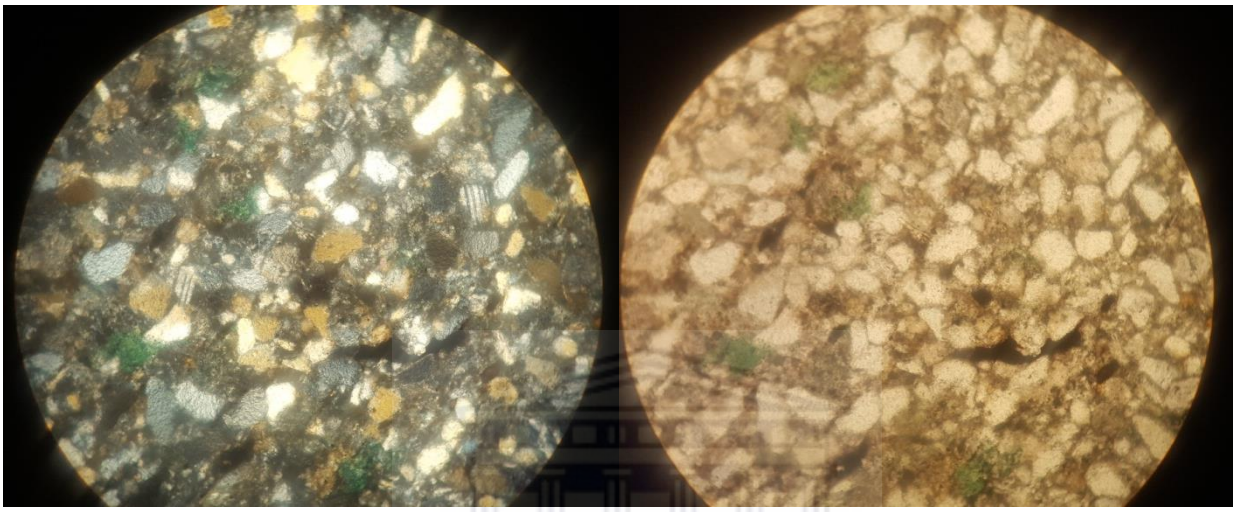

Figure 6.1.2.(A): Thin section images of sample 1 in cross polar (left) and plain polar (right)

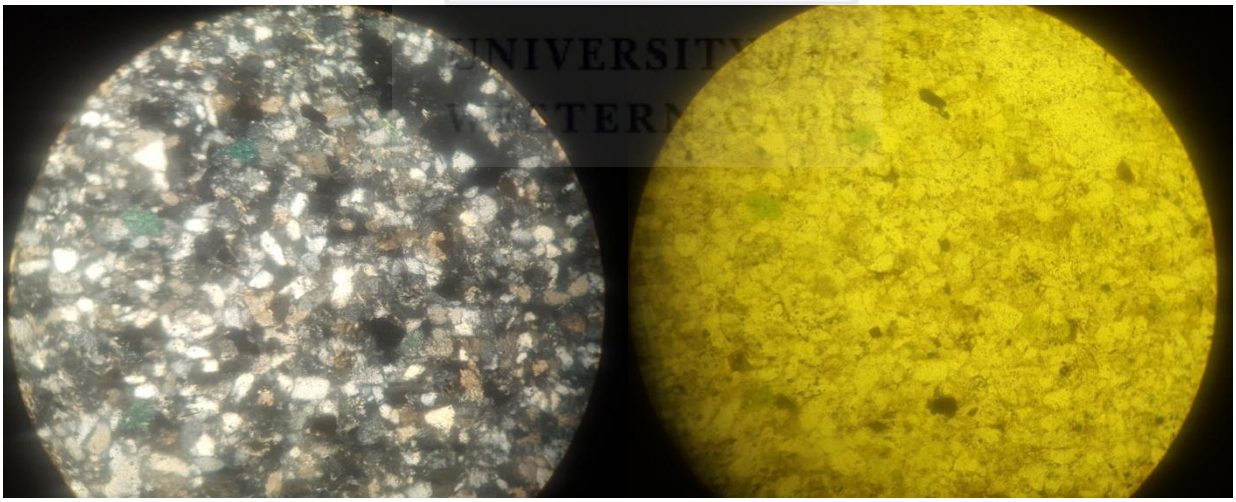

Figure 6.1.2.(B): Thin section images of sample 2 in cross polar (left) and plain polar (right)

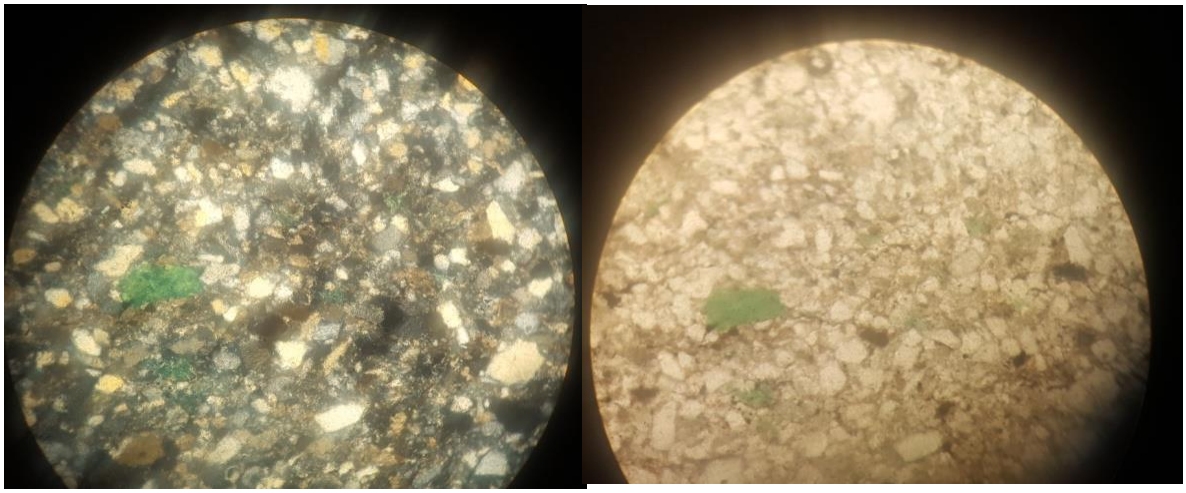

6.1.2.(C): Thin section images of sample 3 in cross polar (left) and plain polar (right)

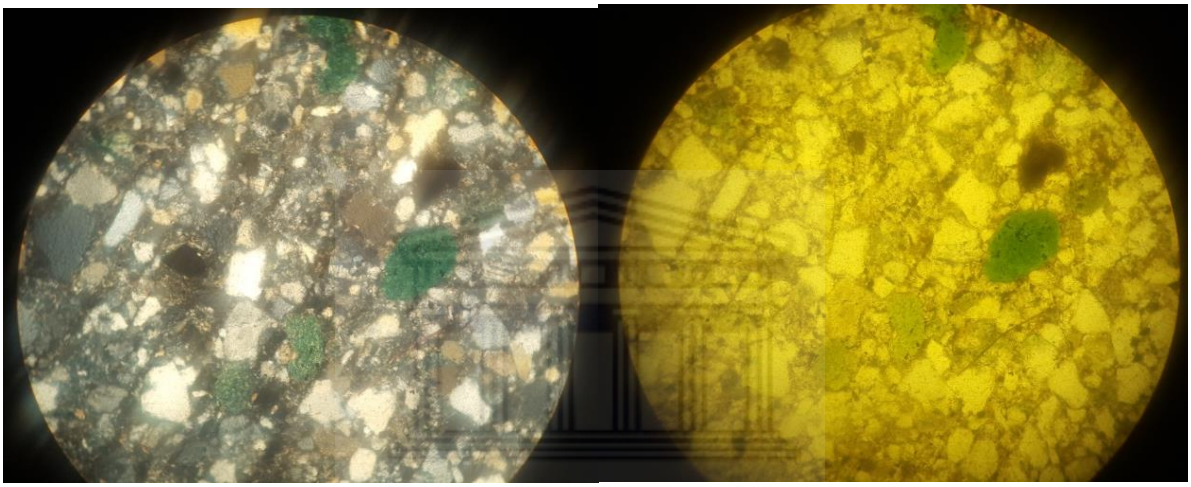

6.1.2.(D): Thin section images of sample 4 in cross polar (left) and plain polar (right)

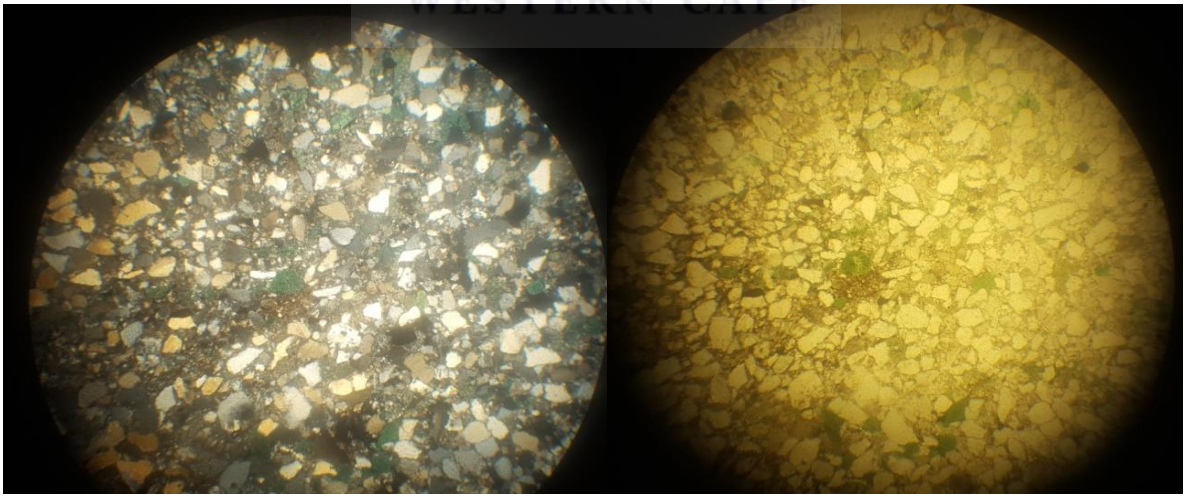

Figure 6.1.2.(E): Thin section images of sample 5 in cross polar (left) and plain polar (right)

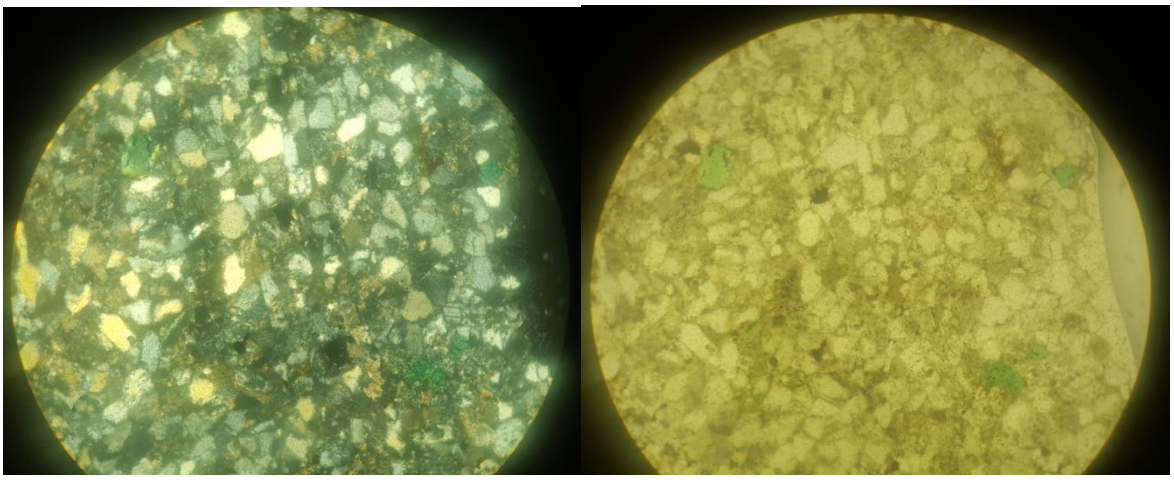

Figure 6.1.2.(F): Thin section images of Sample 6 in cross polar (left) and plain polar (right)

6.1.3. Summary of petrographic analysis

Observations from the petrographic thin sections from the two wells Ga -Q1 and Ga- S1 reflect a very high degree of similarity. The mineralogical composition, the grain shape, the compaction, the degree of sorting, matrix and type of cement remains consistent throughout all the thin sections in both the well samples were observed. The high degree of similarity could be due to the fact the observed thin sections were deposited in similar environments and conditions.

The dominant mineral observed in the thin sections is quartz. Some of the quartz grains appear strained. The straining of quartz grains is indicative of high temperature and pressure situations. The presence of Glauconite is seen throughout in all the thin sections. The significance of Glauconite confirms the suggestion that the two wells in question were deposited in a shallow marine environment. The presence of Pyrite and Calcite is confirmed by XRD and QEMSCAN. The fact that pyrite and calcite is found within the wells gives more proof that it was deposited in a shallow marine setting.

6.2. Quantitative Evaluation of Minerals by Scanning Electron Microscope (QEMSCAN)

A total of six samples were subjected to the QEMSCAN analysis, three samples (sample 1, 2 and 6) from well Ga -Q1 and three samples (sample 1, 4 and 5) from well Ga- S1. The purpose of the QEMSCAN analysis was to quantify the clay minerals identified in the samples. The clay

minerals observed include Kaolinite, Glauconite and minor amounts of Clinochlore. The six samples from the two different wells were analyzed and a field map of the thin sections was produced to illustrate the distribution of the minerals present per sample. Quantifying the clay minerals per sample was crucial as one could see how the amounts of the different clay minerals changed. The change of clay mineral concentration per sample can be referred back to the petrophysical parameters calculated and see how the change in clay content affected the properties.

6.2.1. QEMSCAN interpretations of well Ga – Q1

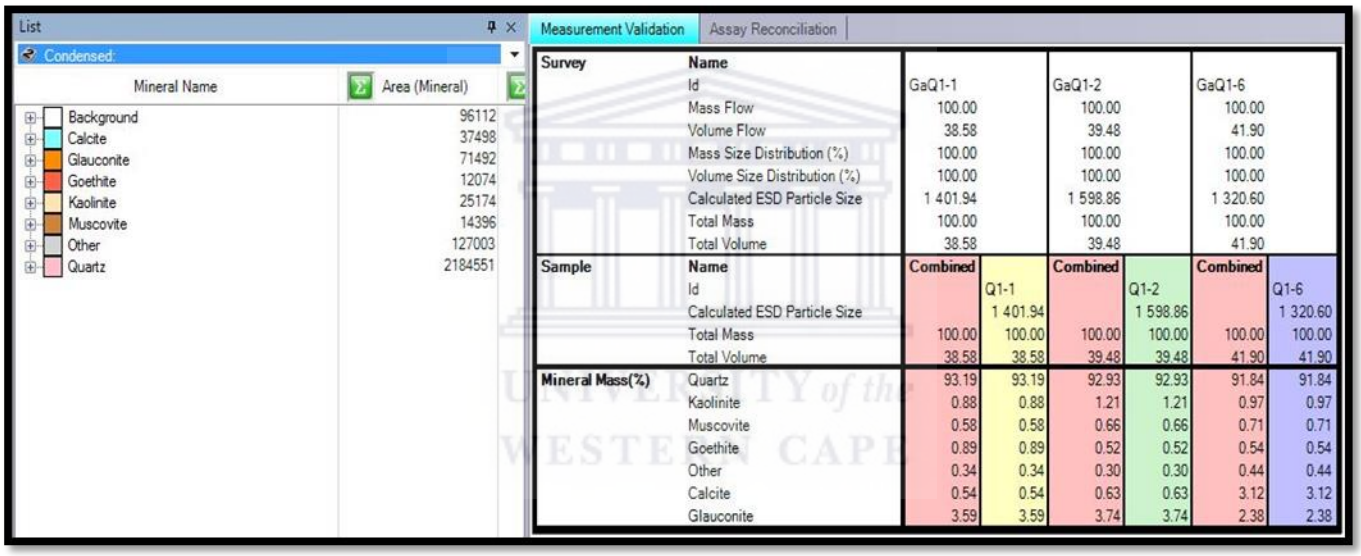

Survey	Name					
	Id	GaQ1-1		GaQ1-2		GaQ1-6
	Mass Flow	100.00		100.00		100.00
	Volume Flow	38.58		39.48		41.90
	Mass Size Distribution (%)	100.00		100.00		100.00
	Volume Size Distribution (%)	100.00		100.00		100.00
	Calculated ESD Particle Size	1 401.94		1 598.86		1 320.60
	Total Mass	100.00		100.00		100.00
	Total Volume	38.58		39.48		41.90
Sample	**Name**	**Combined**		**Combined**		**Combined**
	Id		Q1-1		Q1-2	Q1-6
	Calculated ESD Particle Size		1 401.94		1 598.86	1 320.60
	Total Mass	100.00	100.00	100.00	100.00	100.00
	Total Volume	38.58	38.58	39.48	39.48	41.90
Mineral Mass(%)	Quartz	93.19	93.19	92.93	92.93	91.84
	Kaolinite	0.88	0.88	1.21	1.21	0.97
	Muscovite	0.58	0.58	0.66	0.66	0.71
	Goethite	0.89	0.89	0.52	0.52	0.54
	Other	0.34	0.34	0.30	0.30	0.44
	Calcite	0.54	0.54	0.63	0.63	3.12
	Glauconite	3.59	3.59	3.74	3.74	2.38

Figure 6.2.1.1: QEMSCAN results displaying the identified quantities of the clay minerals for well Ga- Q1

Three samples of well Ga- Q1 were analyzed and a field image was generated (figure 6.2.1.2). The depths of the samples are as follows: sample 1 (2330m), sample 2 (2334m) and sample 6 (2347.3m). The identification and the quantification of the clay minerals found in the samples are summarized under a table (figure 6.2.1.1). All three samples of well Ga- Q1 are represented by the same clay minerals namely, Kaolinite, Glauconite and minor amounts of Clinochlore. Figure 6.2.1.1 doesn't display the Clinochlore mineral because the concentrations are too small to be noticed. The most abundant clay mineral is Glauconite followed by Kaolinite. The Glauconite

mineral is consistently abundant in all of the samples analyzed. Kaolinite is also found consistently in all the samples analyzed however, the concentrations are much less than Glauconite. Calcite was identified as cement by analyzing the thin sections under the microscope. QEMSCAN identified Calcite in all samples analyzed.

In Sample 1 (figure 6.2.1.1) Quartz is the dominant mineral (93. 19%), Glauconite makes up 3. 59%, Kaolinite (0. 88%) and Calcite (0. 54%). Sample 2, the make-up of the sample is similar. Quartz is the dominant mineral (92. 93%), Glauconite (3. 74%), Kaolinite (1. 21%) and Calcite (0. 63%). Sample 6 is made up like this, Quartz dominant again (91. 84%), Glauconite (2. 38%), Kaolinite (0. 97%) and Calcite (3. 12%).

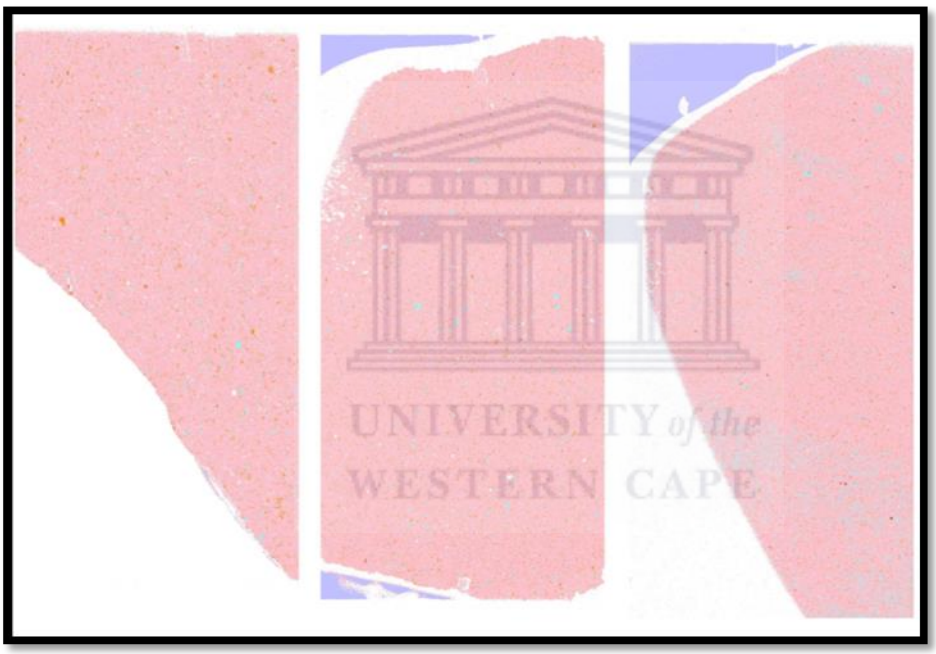

Figure 6.2.1.2: QEMSCAN image of sample 1, sample 2 and sample 6 (Left to Right) from well Ga – Q1

6.2.2. QEMSCAN interpretations of well Ga-S1

List

Condensed

Mineral Name	Area (Mineral)
Background	99434
Calcite	14060
Glauconite	44738
Goethite	12134
Kaolinite	14065
Muscovite	8003
Other	521402
Quartz	1422048

Measurement Validation | Assay Reconciliation

Survey	**Name**	GaS1-1		GaS1-4		GaS1-5
	Id					
	Mass Flow	100.00		100.00		100.00
	Volume Flow	54.35		44.71		42.64
	Mass Size Distribution (%)	100.00		100.00		100.00
	Volume Size Distribution (%)	100.00		100.00		100.00
	Calculated ESD Particle Size	1 394.22		1 147.41		995.92
	Total Mass	100.00		100.00		100.00
	Total Volume	54.35		44.71		42.64
Sample	**Name**	**Combined**	S1-1	**Combined**	S1-4	**Combined** S1-5
	Id					
	Calculated ESD Particle Size		1 394.22		1 147.41	995.92
	Total Mass	100.00	100.00	100.00	100.00	100.00 100.00
	Total Volume	54.35	54.35	44.71	44.71	42.64 42.64
Mineral Mass(%)	Quartz	90.18	90.18	93.95	93.95	79.63 79.63
	Kaolinite	0.82	0.82	1.16	1.16	0.70 0.70
	Muscovite	0.46	0.46	0.75	0.75	0.46 0.46
	Goethite	0.68	0.68	0.74	0.74	1.24 1.24
	Other	4.62	4.62	0.65	0.65	13.85 13.85
	Calcite	0.14	0.14	0.55	0.55	0.81 0.81
	Glauconite	3.09	3.09	2.21	2.21	3.30 3.30

Figure 6.2.2.1: QEMSCAN results displaying the identified quantities of the clay minerals for well Ga -S1

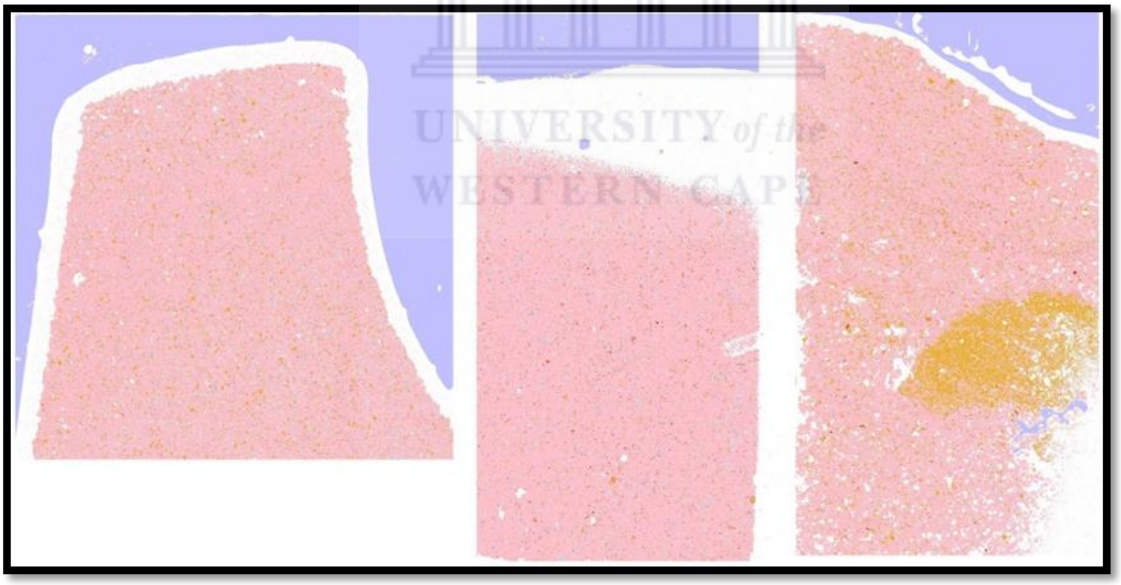

Figure 6.2.2.2: QEMSCAN images of sample 1, sample 4 and sample 5 (left to right) from well Ga = S1

Three samples of well Ga- S1 were analyzed and a field image was generated (figure 6.2.2.2). The depth of the samples is as follows: sample 1 (3028.88m), sample 4 (3036.9m) and sample 5 (3039.82m). The identification and the quantification of the clay minerals found in the samples

were placed under table (figure 6.2.2.1). The most abundant clay mineral identify by the QEMSCAN is Glauconite followed by Kaolinite. Glauconite and Kaolinite appear in all the samples analyzed. Calcite which is identified as cement under the microscope occurs in all samples analyzed.

In sample 1 (figure 6.2.2.1), Quartz is the dominant mineral (90. 18%), Glauconite (3. 09%), Kaolinite (0. 82%) and Calcite (0. 14%). In sample 4, Quartz dominates again (93. 95%), Glauconite (2. 21%), Kaolinite (1. 16%) and Calcite (0. 55%). Sample 5 is made as follows, Quartz (79. 63%), Glauconite (3. 30%), Kaolinite (0. 70%) and Calcite (0. 81%).

6.2.3. Summary of QEMSCAN interpretations

All the QEMSCAN samples that were analyzed reflected a homogeneous nature. This means that the samples reflected a high degree of mineral similarity. This is also confirmed by thin section analysis as well as XRD analysis. Both thin section and XRD data confirm the homogeneous nature observed in the QEMSCAN data. The clay minerals, Glauconite and Kaolinite, confirm findings observed in thin sections. A general trend appears for all samples subjected to QEMSCAN analysis and that is that the Glauconite clay mineral concentrations are more in every sample than Kaolinite. This could mean that the Glauconite mineral may have a greater influence on the petrophysics than Kaolinite.

6.3. X – Ray Diffraction interpretation (XRD)

XRD technique was used to identify minerals present in rock samples. The XRD technique is widely used in the phase identification of minerals, their compositional analysis and their nano-scale structures. The core samples taken from wells Ga-Q1 and Ga-S1 were analyzed at ITHEMBA labs, Cape Town for qualitative identification of authigenic cements present within the sandstone units of the Pletmos Basin.

6.3.1. XRD interpretation of well Ga-Q1

The XRD results obtained from the six core samples of well Ga- Q1 show a distinctive similarity in mineral composition. The dominant mineral in the studied samples is Quartz. The clay minerals are Kaolinite and Clinochlore. The iron rich Illite also known as Glauconite is not detected by XRD but is observed under the microscope. Other minerals identified by the XRD

are Albite, Muscovite and Cristobalite. The mineral Calcite is also present probably as cement as identified through thin section petrography.

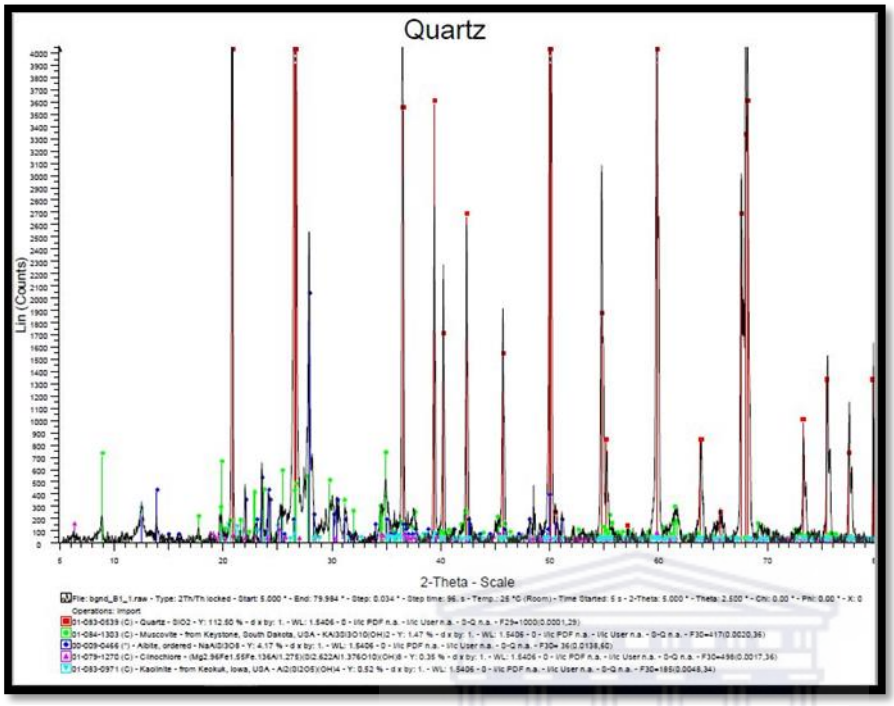

Figure 6.3.1.(A): XRD analysis of sample 1

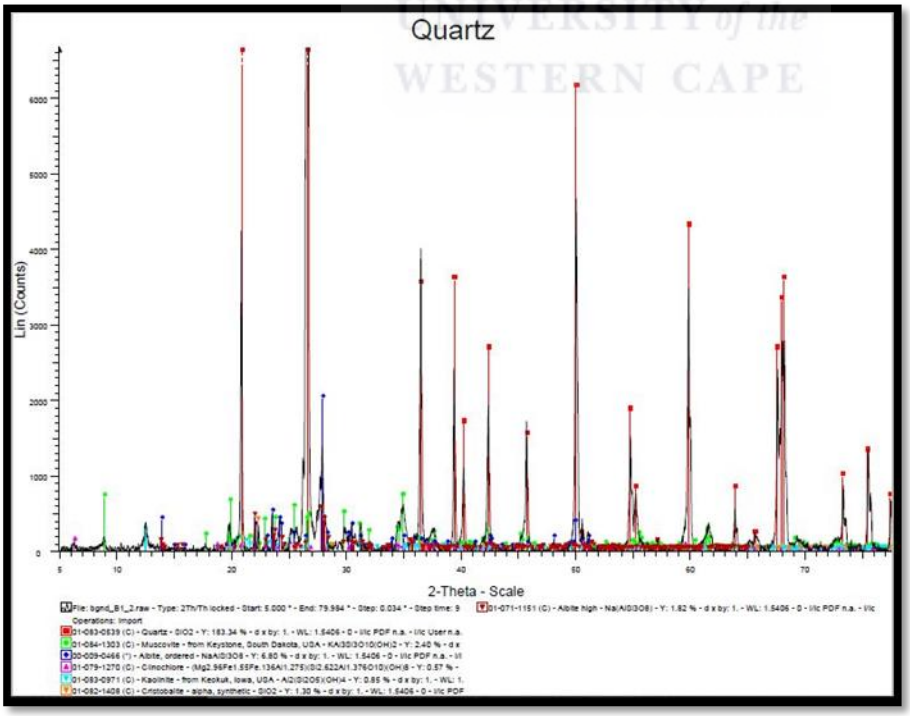

Figure 6.3.1.(B): XRD analysis of sample 2

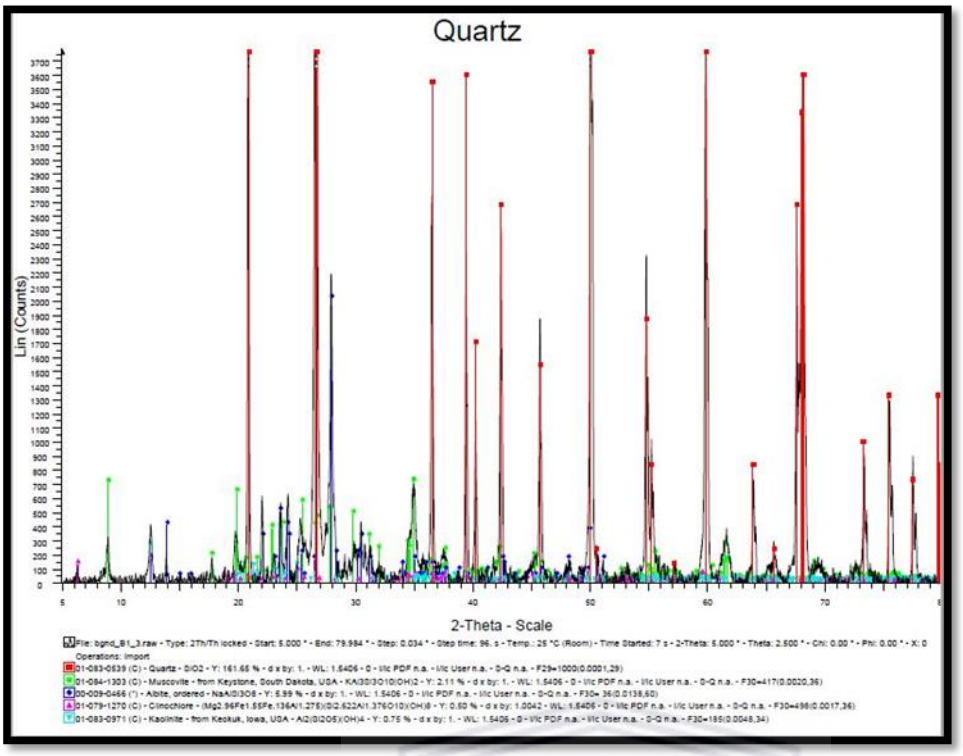

Figure 6.3.1.(C): XRD analysis of sample 3

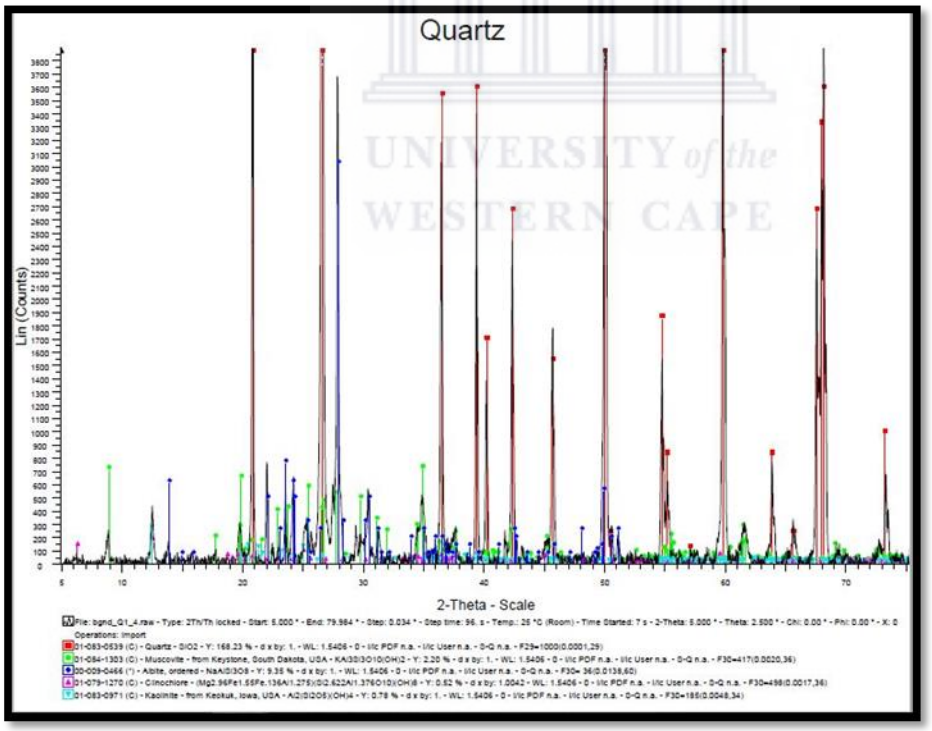

Figure 6.3.1.(D): XRD analysis of sample 4

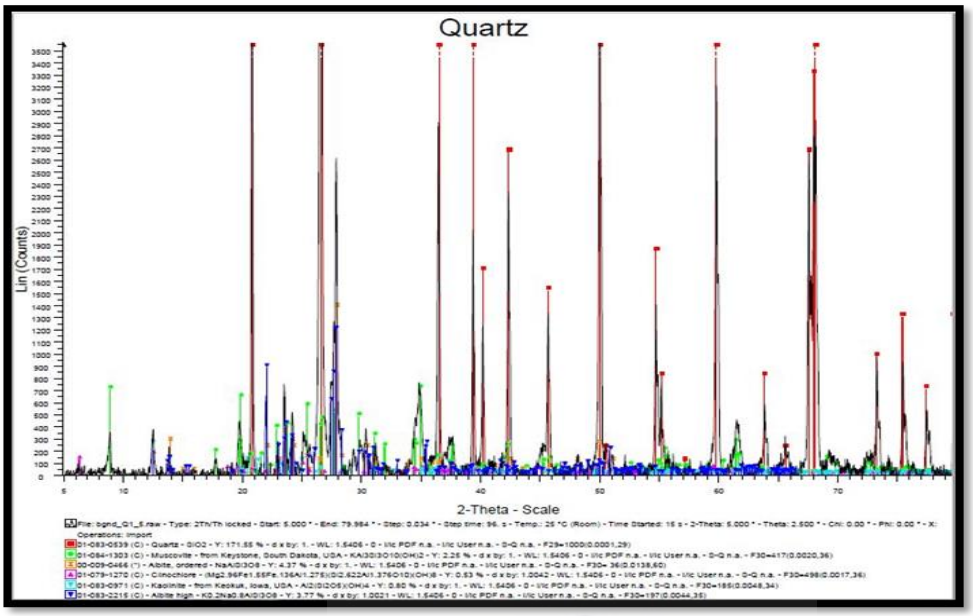

Figure 6.3.1.(E): XRD analysis of sample 5

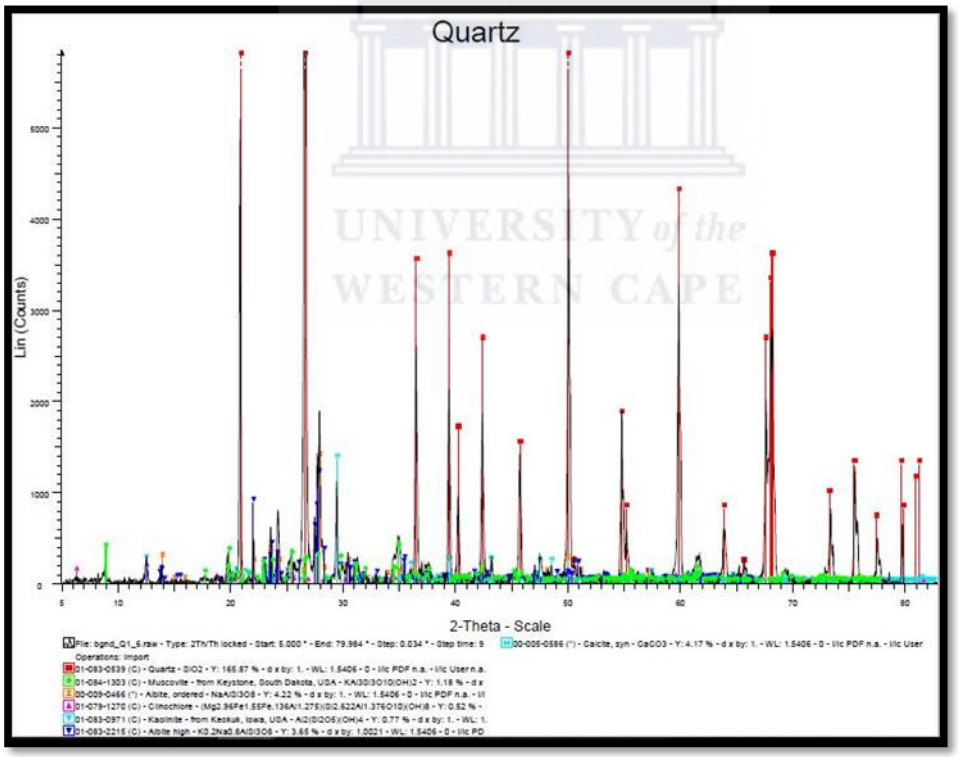

Figure 6.3.1. (F): XRD analysis of sample 6

6.3.2. XRD interpretation of well Ga – S1

The XRD analyses of the six samples show a very consistent mineralogical composition. All six samples from well Ga-S1 are similar in mineralogical composition, the only difference are the concentrations of the minerals per sample (refer to QEMSCAN analysis). Quartz is the dominant mineral. The clay minerals identified are Kaolinite and Clinochlore. The iron rich Illite, Glauconite is not detected by XRD but is detected by QEMSCAN and was observed under the microscope. Other minerals identified are Muscovite, Albite and Cristobalite. The presence of the mineral Calcite as cement is also noticeable.

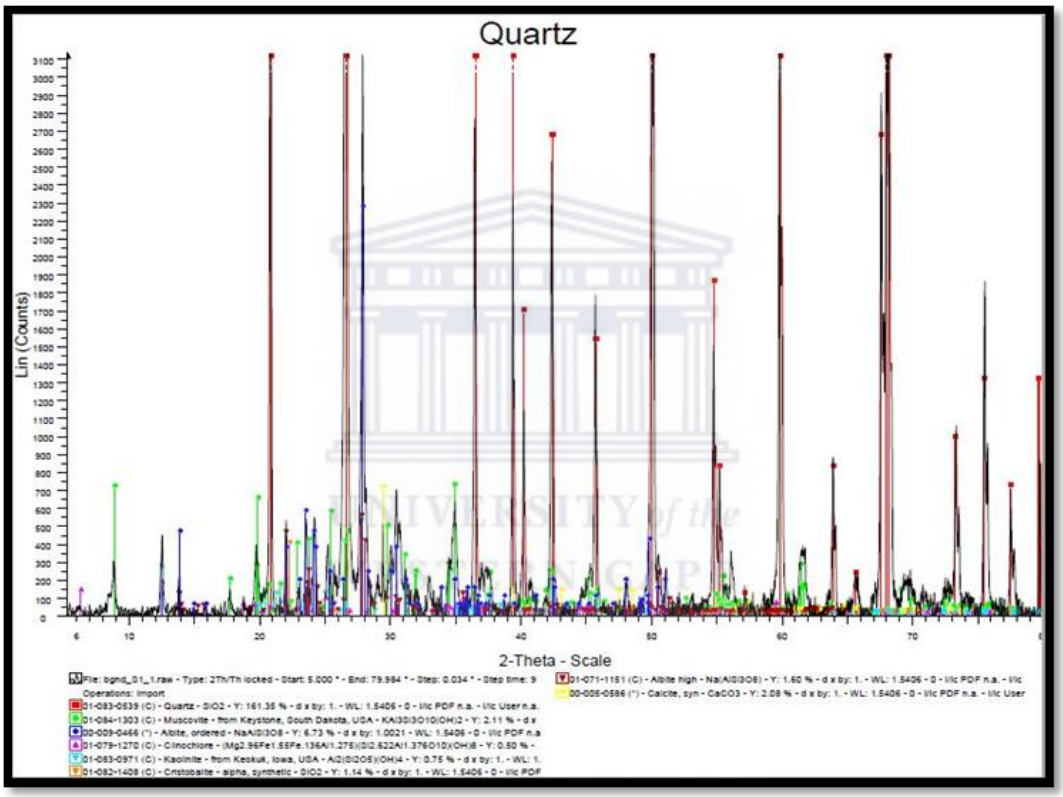

Figure 6.3.2. (A): XRD analysis of sample 1

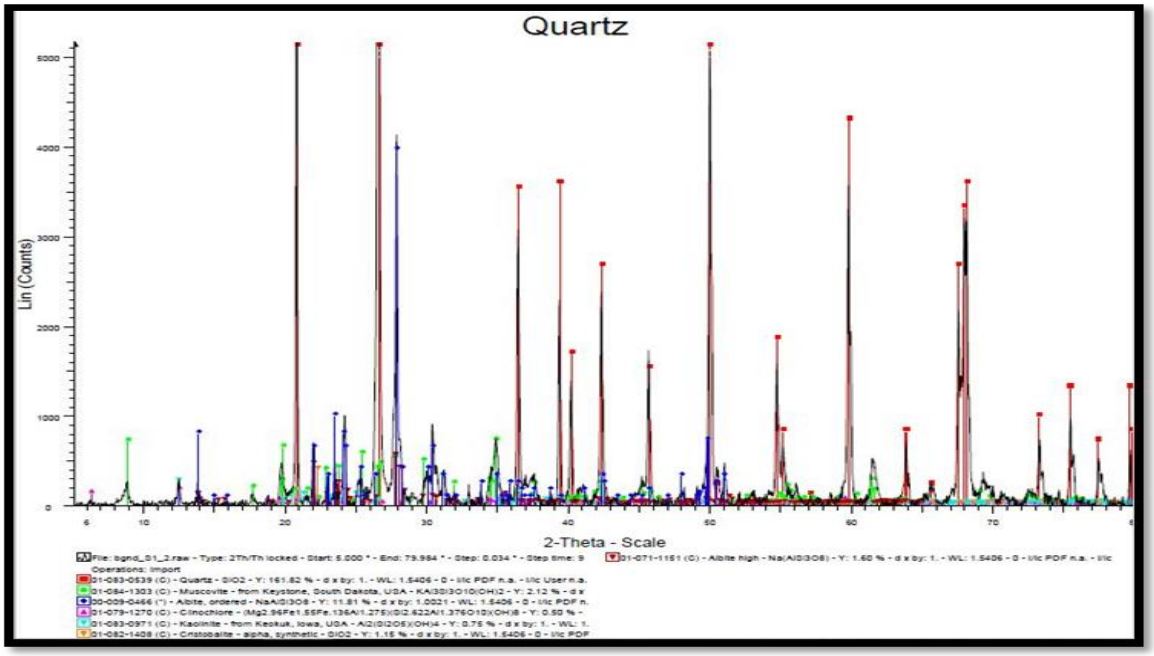

Figure 6.3.2. (B): XRD analysis of sample 2

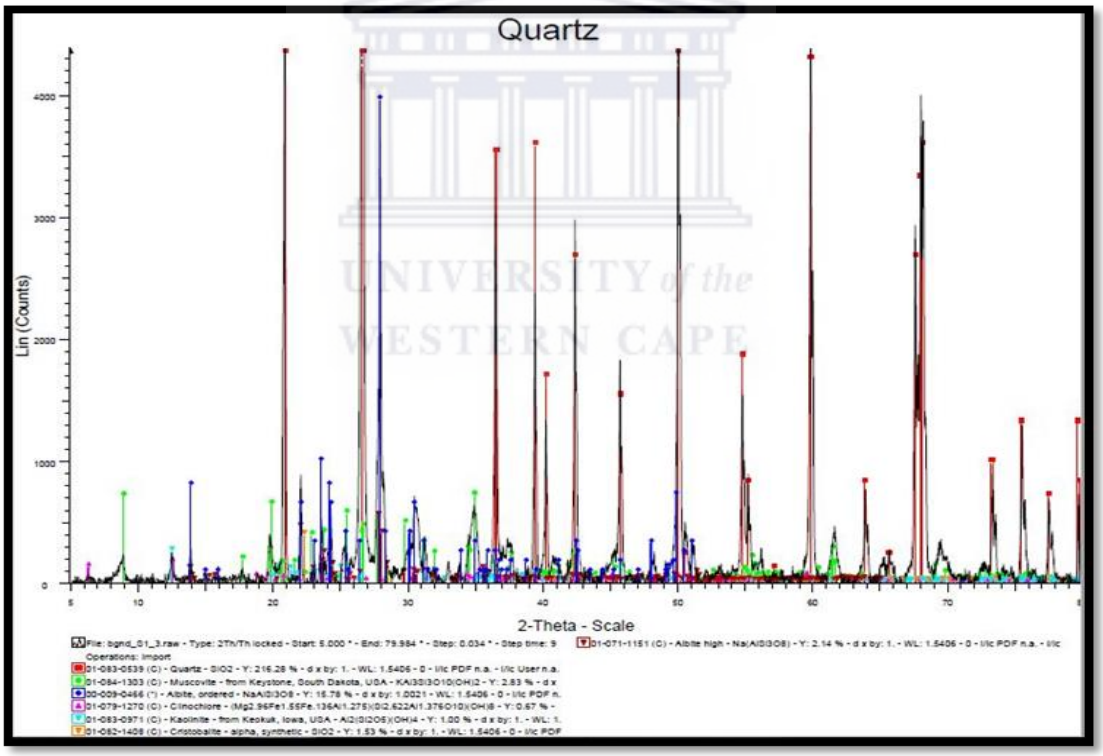

Figure 6.3.2. (C): XRD analysis of sample 3

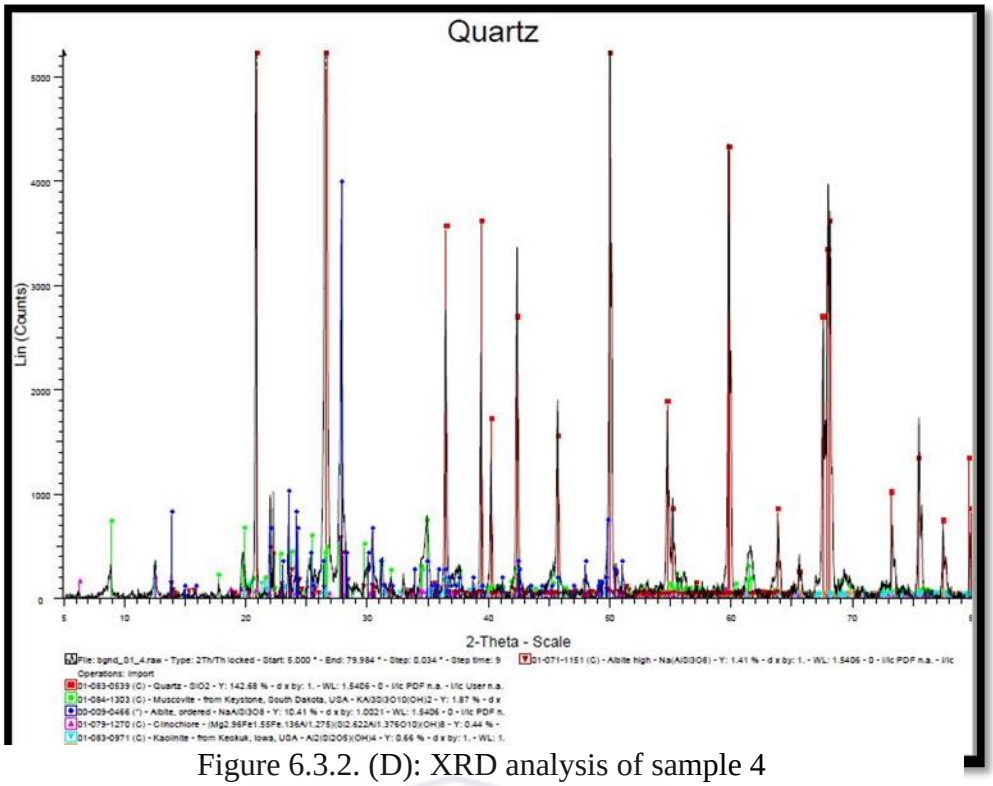

Figure 6.3.2. (D): XRD analysis of sample 4

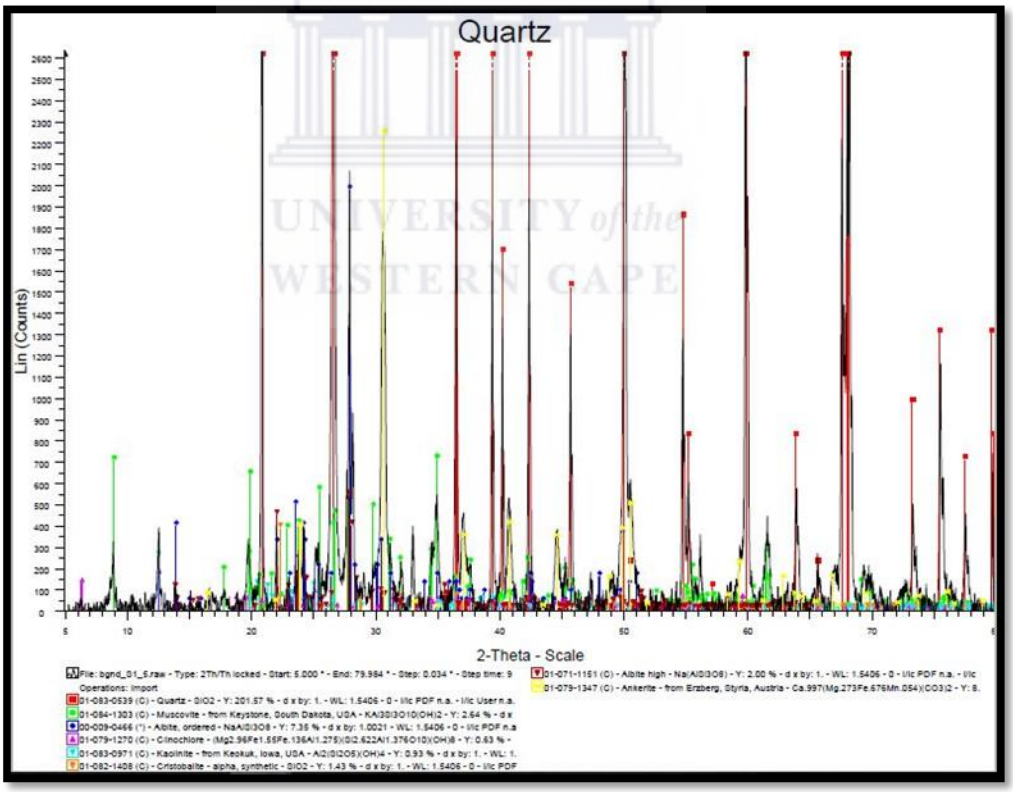

Figure 6.3.2. (E): XRD analysis of sample 5

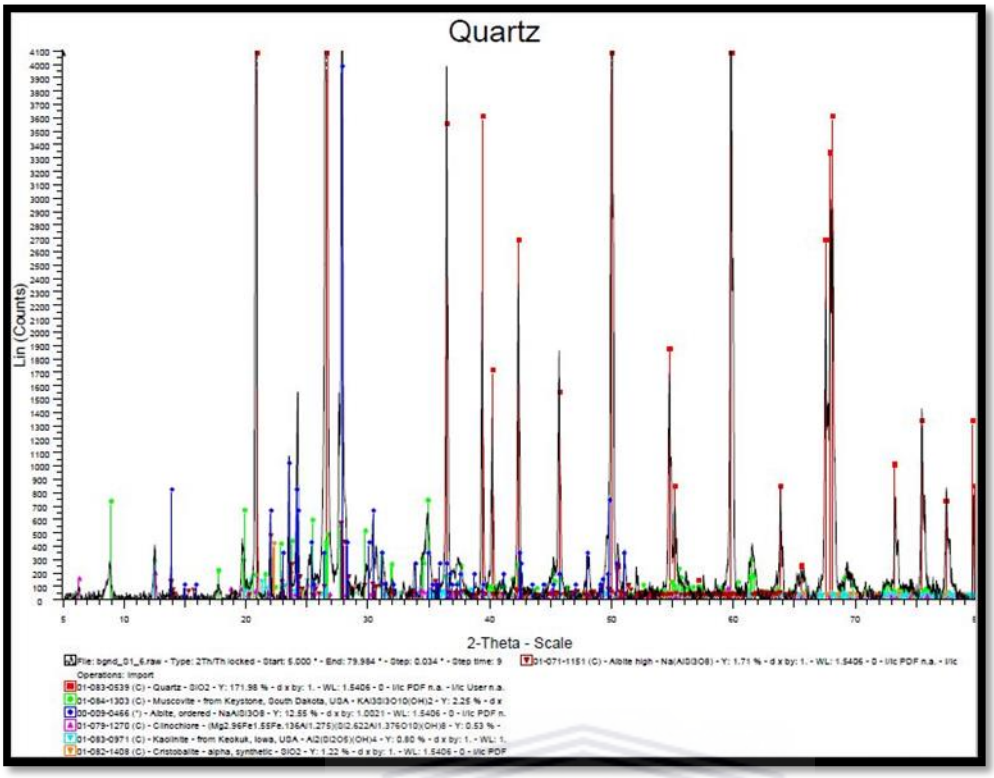

Figure 6.3.2. (F): XRD analysis of sample 6

6.3.3. Summary of XRD interpretations

The XRD analysis results suggest that well Ga-Q1 and Ga-S1 have comparable mineralogical compositions. By analyzing each sample from the two wells we also observe a similar trend. The minerals found in both wells and in all the samples are: Quartz, Albite, Muscovite, Kaolinite, Clinochlore, Cristobalite and Calcite. The study shows that the quartz mineral is dominant. This is also confirmed by QEMSCAN where Quartz generally makes up 90% of the sample. The clay minerals identified by XRD analysis also shows consistent results; Kaolinite and Clinochlore have been identified as the dominant clay minerals. However, Glauconite which is quantified by QEMSCAN and observed under the microscope is not detected by XRD. As a result, the clay minerals present within wells Ga-Q1 and Ga-S1 are Kaolinite, Glauconite and Clinochlore. The reason for Glauconite not being detected by XRD could be due to the presence of Muscovite. Muscovite and Glauconite are both phyllosilicates and both have the same monoclinic crystalline structure. The XRD could easily group Glauconite as Muscovite. When Muscovite mica undergoes chemical alteration it will form Glauconite. Calcite cement precipitation is prominent in both wells (Ga – Q1 and Ga – S1). The presence of calcite is significant because it confirms that the two wells were deposited under shallow marine conditions.

6.4. Pore water chemistry interpretation

Pore water chemistry can be described as the chemistry of the pore fluids occupying the in between grains. Around 30- 80% of the volume of the sediments can be occupied by pore water. Fine grained silty sediment occupies a greater volume of water than sand sediment (Simpson, et al., 2005). Pore water samples selectively taken from wells Ga-S1 and Ga-Q1. The samples were subjected to a centrifugation process. The most accurate method of extraction for chemical elements is centrifugation (Simpson et al., 1995).

The measurement of the pore water chemistry allows for the pH and Ec of the fluids to be determined. These two factors play a crucial role. An increase in pH from acidic to neutral values, from 3-7, the precipitation of aluminosilicates and carbonates are favored (Curtis, 1983). In alkaline systems, where the pH is above 7, carbonate precipitation relative to aluminosilicates and quartz cements are favored (Buyukutku, 2003). Electrical conductivity (Ec) analysis were conducted on samples taken at selected intervals. The underestimation of hydrocarbon saturation is often as a result of ignoring the effects of clay conductivity (de Waal, 1989). Ec is the measurement of the dissolved solids in pore water and its ability to conduct an electrical current. The more dissolved ions present the higher the Ec value. It is measured in milli Siemens per centimeter (mS/cm).

6.4.1. Pore water chemistry interpretation of well Ga- Q1

Six pore water samples were extracted from core samples from well Ga-Q1 and were subjected to Ph and Ec analysis after which the values were plotted as illustrated below (Figure 6.4.1. A and Figure 6.4.1. B). The pH value ranges from 6.63 to 7.50. The pH range reflects a slightly acidic medium to slightly alkaline medium. The electrical conductivity ranges from 200ms/cm to 380ms/cm. In well Ga -Q1 there is a distinctive trend; the electro conductivity (E_c) of the pore fluid increases with depth and pH of the pore fluid decreases with depth.

Table 6.4.1: Pore Water Chemistry Analysis of Well Ga – Q1

Sample Number (Depth)	**pH**	**Ec (micro Siemens/cm)**
Sample 1 **(2330m)**	7.02	200
Sample 2 **(2334m)**	7.23	270
Sample 3 **(2337m)**	7.24	310
Sample 4 **(2339m)**	6.90	240
Sample 5 **(2343,30m)**	7.50	380
Sample 6 **(2347,27m)**	6.63	320

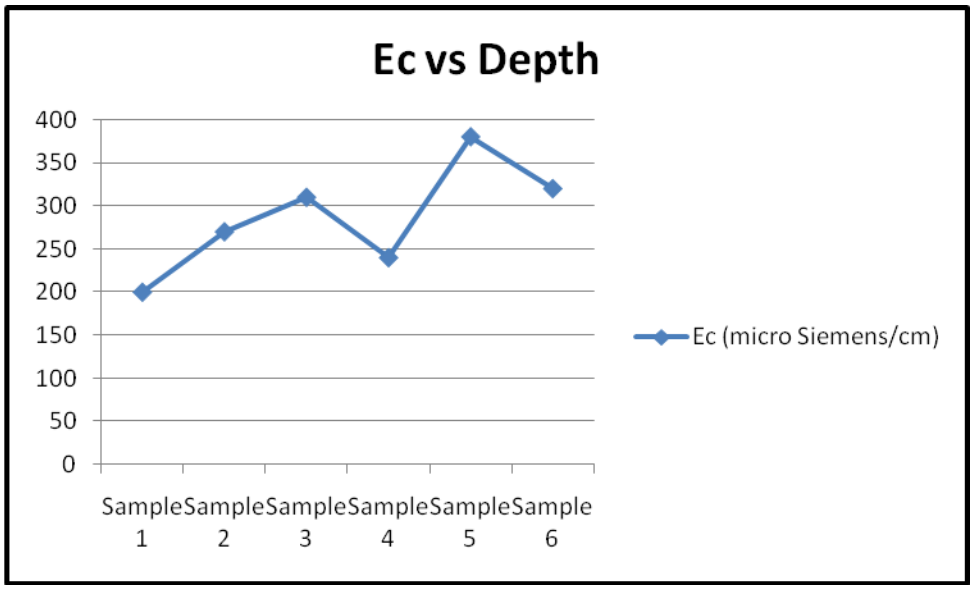

Figure 6.4.1. (A): a graph illustrating the electro conductivity (E_c) against sample number (depth) of well Ga – Q1.

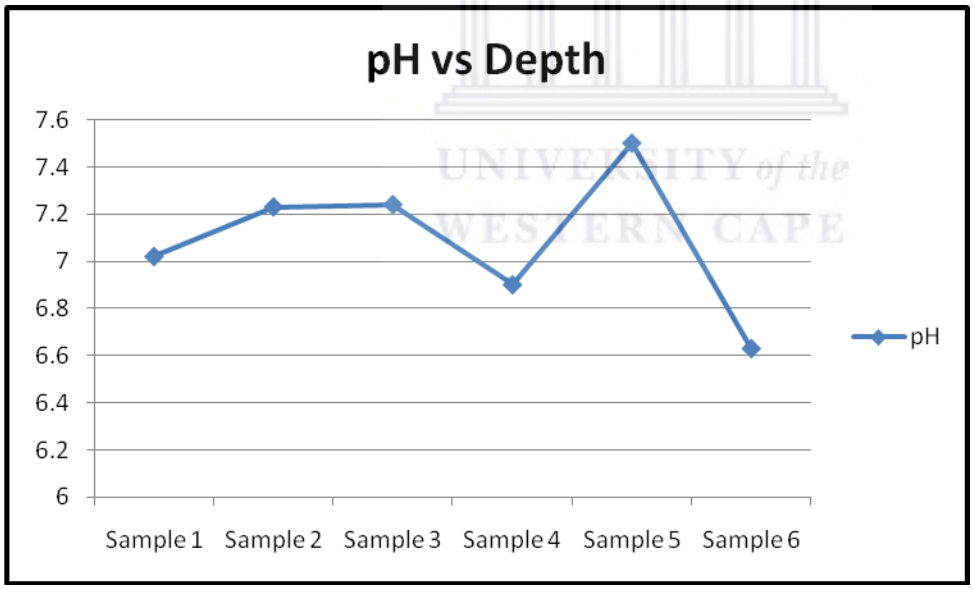

Figure 6.4.1. (B): a graph illustrating the pH against sample number (depth) of well Ga – Q1.

6.4.2. Pore water chemistry interpretation of well Ga- S1

Six pore water samples were extracted from core samples taken from well Ga-S1 and were subjected to pH and Ec analysis after which the values were plotted as illustrated below (Figure 6.4.2. A and Figure 6.4.2. B). The pH values range from 6.76 to 7.63. The pH range reflects a slight acidic medium to alkaline medium. The electrical conductivity (Ec) ranges from 260 ms/ cm to 370 ms/ cm. In well Ga –S1 the distinctive trends observed were: the electro conductivity (E_c) of the pore fluid decreases with depth while the pH of the pore fluid increases with depth.

Table 6.4.2: Pore Water Chemistry Analysis of Well Ga – S1

Sample Number (Depth)	**pH**	**Ec (micro Siemens/cm)**
Sample 1 **(3028,88 m)**	6.76	310
Sample 2 **(3030,45 m)**	7.04	290
Sample 3 **(3033,65 m)**	7.63	310
Sample 4 **(3036,90 m)**	6.96	260
Sample 5 **(3039,82 m)**	7.05	370
Sample 6 **(3044,50m)**	7.25	290

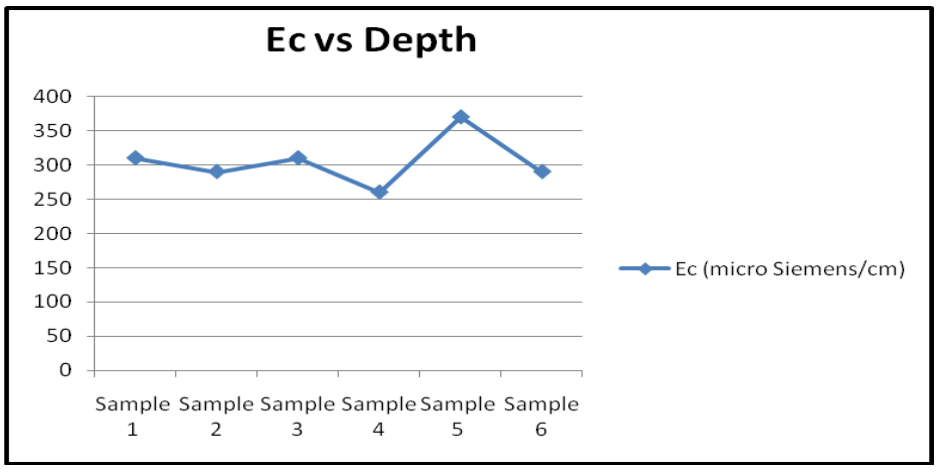

Figure 6.4.2. (A): a graph illustrating the electro conductivity (E_c) against sample number (depth) of well Ga – S1.

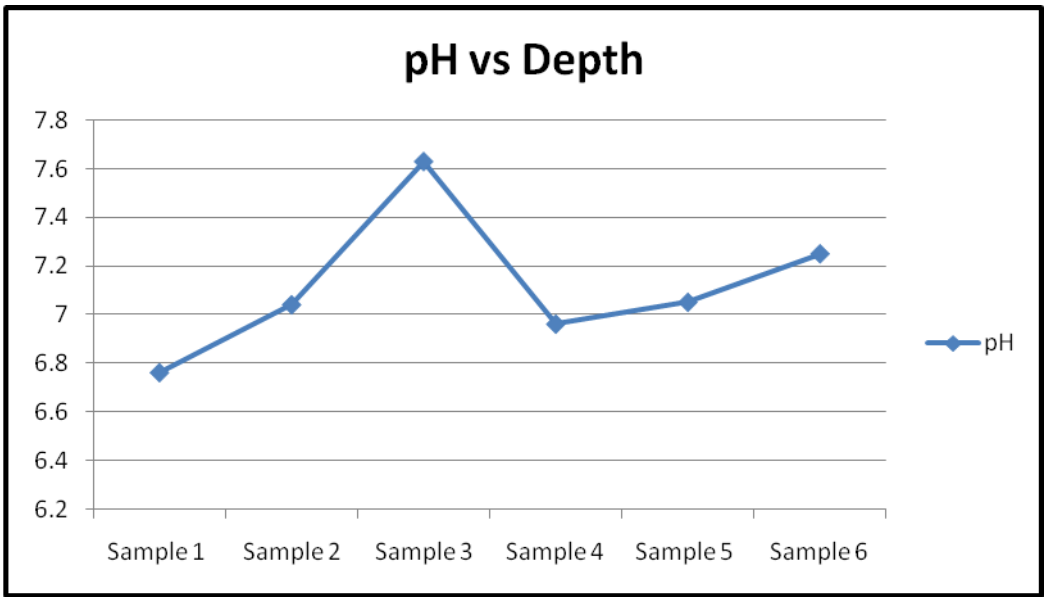

Figure 6.4.2. (B): a graph illustrating pH against sample number (depth) of well Ga – S1.

6.4.3 Summary of Pore Water Chemistry Interpretations

Results derived from the pore water chemistry analysis provide information about the pore fluids present. Well Ga – Q1 pore fluids show a pH range of 6.63 – 7.50 and an E_c range of 200ms/cm – 380 ms/cm. Well Ga-S1 pore fluids show a pH range of 6.76 – 7.63 and an E_c range of 260 ms/cm – 370 ms/cm. The pH range favours formation of a quartz, alumino silicates, clay minerals (Kaolinite, Glauconite and Clinochlore) as well as Calcite cement

Both wells show a distinctive trend, the graphs presented reflect an inverse relationship. In well Ga-Q1, the E_c increases with depth and the pH decreases with depth. In well Ga –S1, the E_c decreases with depth and the pH increases with depth. The pH of the pore fluids for both wells are comparable hence the pH ranges are similar. This could be due to both wells being deposited in a shallow marine environment and was influenced by saltwater.

The electro conductivity (E_c) of a pore fluid is the ability of a solution to conduct an electrical current. Therefore, a solution with dissolved cations and ions is a better conductor of an electrical current. The electro conductivity for both wells shows a distinct difference. Well Ga – Q1 has a greater E_c range while the E_c range of well Ga – S1 is much less. It can be assumed that

the higher the concentration of ions in the pore fluid, the higher the conductivity (E_c) will be. A high E_c is directly related to the total dissolved solids (TDS).

It can be assumed based on information derived from this study, the pore fluids dissolved a variety of cations and ions (Na, K, Ca, Al, Fe, Mg, O, H) together with a slightly acidic to slightly alkaline pH range, conditions were favourable for the formation of minerals detected and observed. Hence, the formation of Quartz, Albite, Kaolinite, Glauconite, Calcite, Muscovite and other minerals are detected.

CHAPTER SEVEN

7.1. Discussion

A range of methods were discussed to assess and understand how different clay minerals affect the petrophysical properties of sandstone reservoirs from the Offshore Pletmos Basin. To carry out this study geochemical methods (XRD and pH and E_c) and petrography (QEMSCAN and thin sections analysis) were studied in combination with core analysis and wireline logs. All these methods were necessary in order to achieve the aim of the study. This study's results were obtained from two wells (well Ga -Q1 and well Ga-S1) from the Offshore Pletmos Basin. The results of the various methods will be discussed below.

7.1.1. Well Ga – Q1

(A) Core analysis and Gamma ray log response

Core descriptions reveal a coarsening upward sequence of very fine to medium grained sandstones. The gamma ray log response confirms the coarsening upward sequence described from the cored interval. The gamma ray log curve defined the GR shapes from the log are: Cylindrical GR shape (shape A), an irregular GR shape (shape B) and a bow/hour glass GR shape (shape C). The sandstones are considered glauconitic to feldspathic. They are moderately compacted in less bioturbated sections and highly compacted in silt/shale sections. Sand – dominated heterolithic bedding known commonly referred to as Flaser bedding, was preserved in the sand sections. Mud and silt laminae which are rippled are observed. The ripples are asymmetrical and preserved in sand sections. Vertical burrowing was also observed. Based on the above mention information, well Ga-Q1 was interpreted to be deposited in a shallow marine environment, but more specifically due to the sedimentary features and mineralogical composition, the cored interval of well Ga – Q1 is assumed to be deposited in the inter – tidal zone of the tidal flat environment.

(B) Petrophysical parameters

Detailed interpretation of wireline logs reveals a 18m thick reservoir interval with a clay volume of 40%. The reservoir interval is classified as a shaly reservoir due to high volume of clay (greater than 35%). A gamma ray average of 78 API is observed which reflects the mixed sediment nature. Sand sections observed in the cored interval have significantly better petrophysical parameters than silt/shale sections. The petrophysical parameters were further enhanced by the vertical burrowing observed. As a result, there is a greater variation in porosity and permeability values vertically (Shallow to deep depths) than horizontally. This could be attributed to the bioturbation observed.

The three identified gamma ray log (GR) shapes can be linked to the clay mineral content and petrophysical values. The following three GR shapes are identified from wireline logs: GR shape A – Cylindrical, GR shape B – Irregular and GR shape C – Bow/hour glass.

From the top well Ga – Q1 we find GR shape C, 'Hour glass shape' (2329m to 2333m), we observe a porosity range of 5% to 17% and a permeability range of 0.1 mD to 0.6Md. We observe a high Glauconite content and low Kaolinite and Calcite content. The 'hour glass' shape reflects the influx of mix sediment hence; we find mud/silt and sand. This section is characterized by Flaser bedding. The extremely low permeability values can be attributed to the high Glauconite content which restricted pore connectivity.

GR shape A is a cylindrical shape (2334m to 2340m and 2346m to 2347m) we observe a porosity range of 11% to 15% from 2334m to 2340m and 12% to 14% from 2346m to 2347m. We observe a permeability range of 0.2 mD to 2.5 mD (from 2334m to 2340m) and 0.2 mD to 0.6 mD. The cylindrical GR shape reflects the relativity uniform sediment hence, the little change in the porosity and low permeability range. The reason for the permeability range peaking at 2.5 mD between 2334m and 2340m is due to vertical burrowing which could promote better permeability values. The Glauconite mineral remains the most dominant and influential affecting the permeability hence, the extremely low permeability values. Kaolinte and Calcite is significantly less (Figure 7.1.3).

GR shape B is an irregular shape occurring between 2340m and 2346m. The irregular shape is characterized by very fine silty to muddy material. We observe a porosity range of 5% and 11%

and a permeability range of 0.1 mD and 0.3 mD. We observe a high Calcite and Glauconite content and low Kaolinite content. The clay mineral influence is reflected in the low porosity range and extremely low permeability range. This section of the reservoir interval has to be consider extremely poor.

The average water saturation as calculated by the Indonesian water saturation model averages at 80% with gas saturation at 20%. The average permeability is 0.2 mD and the average porosity value as calculated by the sonic – derived log is 9%. Sand sections have porosity values ranging from 11% to a high of 17% and permeability values ranging from 0.2mD to 2.5mD. The sand section (GR shape A) has significantly better petrophysical values than the average parameters of the well as well as the highly compacted silt/shale sections. Furthermore, the high concentration of clay minerals observed in shale sections results in the low porosity (avg. 9%) and permeability (avg. 0.2 mD) values.

(C) Clay mineral assemblages

The clay minerals identified by XRD, QEMSCAN and thin sections are: Kaolinite (Kaolinite group), Glauconite (Illite group) and Clinochlore (Chlorite group). The dominant clay mineral as confirmed by the QEMSCAN technique is the clay mineral Glauconite. Glauconite can be seen under the microscope as dark green in colour (plain polarized light and cross polarized light). Glauconite is a significant mineral as it only forms under certain conditions and in shallow marine environments. The presence of Glauconite indicates a marine influence. The presence of the clay minerals, Glauconite and Kaolinite, together with Calcite have a ‘pore - bridging and pore - filling – effect’ and will have an adverse affect on the permeability. The chemical alteration of the mineral Muscovite to Glauconite could explain its presence. The chemical alteration of feldspars (Albite) could explain the presence of Kaolinite. Although Clinochlore is detected by XRD, the quantification of Clinochlore by the QEMSCAN method reveals its values is less than 0.1% and therefore can be considered not to influence the petrophysical parameters of the sandstone reservoir in any way.

(D) Geochemistry and petrography

Thin section petrography shows a compacted thin section dominated by quartz with calcite cement surrounding the grains. The Glauconite mineral is easily distinguished under the microscope under plain polarized light. The Glauconite mineral appears dark green in both plain polarized light and cross polarized light. The presence of Calcite in samples confirms the sediment encountered from the cored interval was shallow marine setting. Calcite is also observed to be the dominant cement in the samples. QEMSCAN and XRD analysis confirms the presence of the clay minerals: Kaolinite, Glauconite and Clinochlore. Glauconite is the dominant clay mineral followed by Kaolinite. On average Glauconite makes up 3, 24 % of the sample compared to Kaolinite that makes up 1, 02% of the sample. Calcite makes up 1, 42% of the sample. The pore waters of well Ga-Q1 displays a pH range of 6, 63 to 7, 50 implying that the pore waters range from slightly acidic to slightly alkaline. The pH range favors the formation and precipitation of the clay minerals and minerals found in this well.

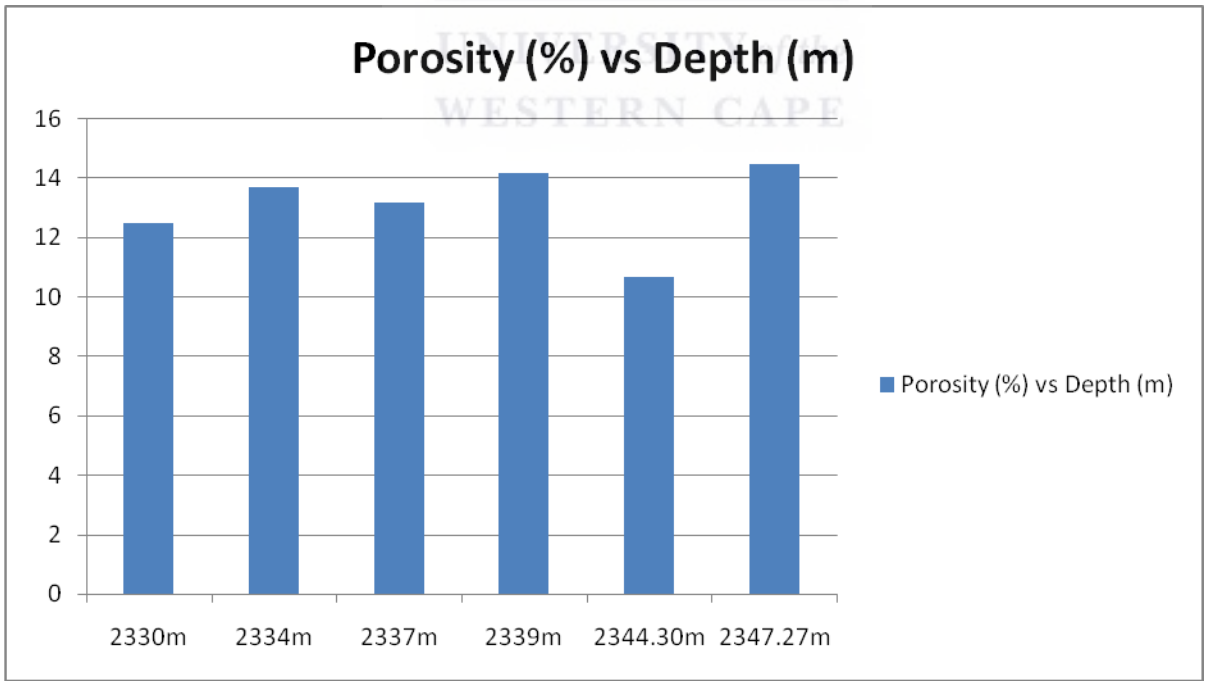

Figure 7.1.1: Well Ga – Q1 showing the porosity variation with depth.

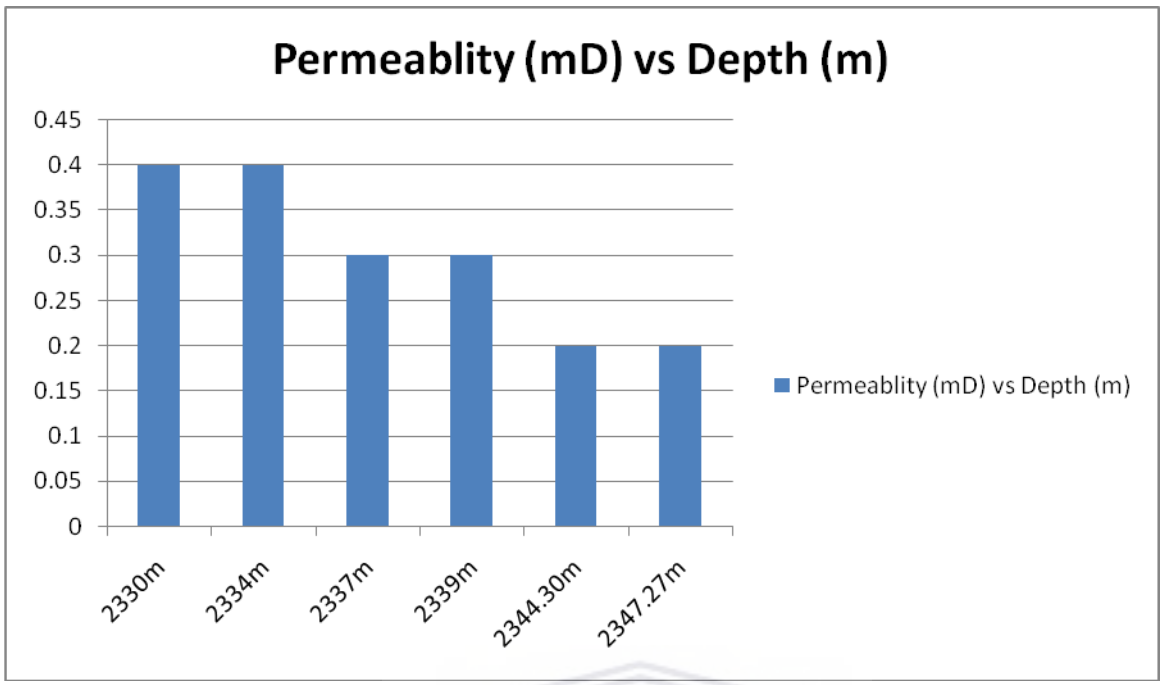

Figure 7.1.2: Well Ga – Q1 showing the variation in permeability with depth.

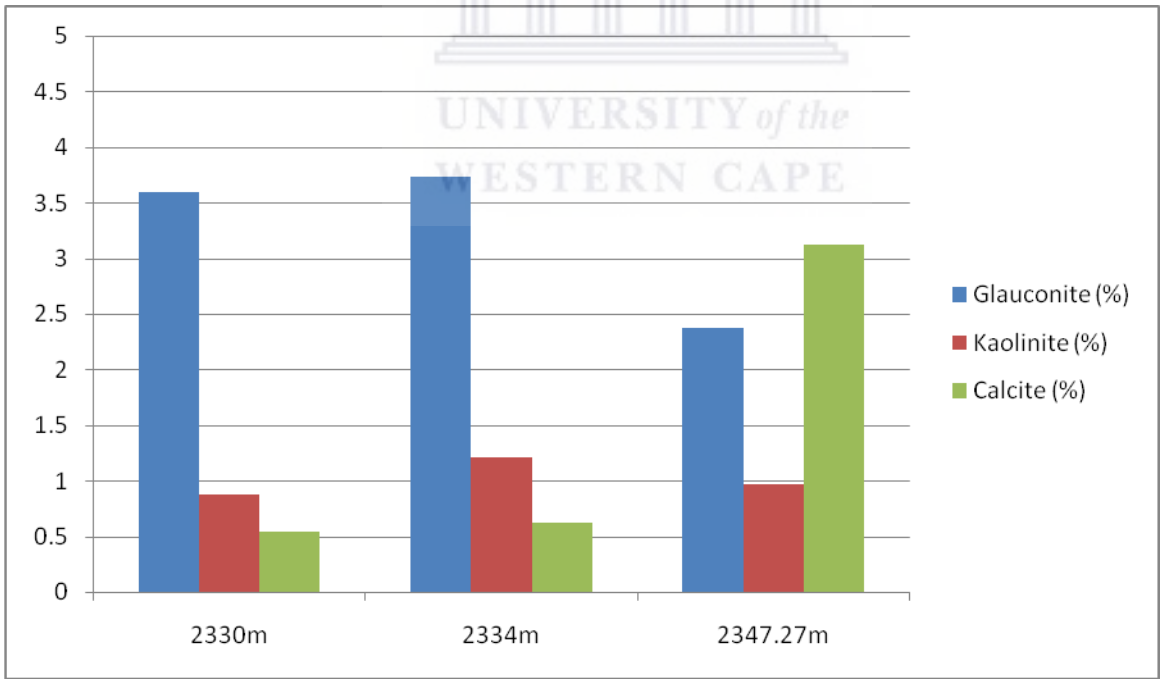

Figure 7.1.3: Well Ga – Q1 showing the variation of identified clay mineral concentration with depth

7.1.2. Well Ga – S1

(A) Core analysis and Gamma ray log response

Core descriptions reveal a light grey, very fine to fine-grained sandstone with medium grained sandstones appearing near the top of the cored section. The sandstones are considered to be Glauconitic to slightly carbonaceous and are moderately compacted. The sandstones are subjected to intense vertical bioturbation and burrowing. The intense bioturbation has obscured sedimentary features but has enhanced the porosity and permeability. The cored interval can be described as an 18m fine-grained sandstone section with insignificant variation in grain size. From the base of the core to the cored interval it medium fine to medium grained sandstone then fines upwards to a point (around 3035m) and then coarsens upwards again. The gamma ray log response displays a bell (shape B) and cylindrical (shape A) shape which confirms the description made from the cored interval. The trace fossils *Helminthoida* and *Ophiomorpha nodosa* are found and are characteristic of the lower shoreface zone. Based on the acquired information the environment which this well was deposited in was a shallow marine environment, more specifically, the lower shoreface zone of the beach environment.

(B) Petrophysical parameters

Detailed interpretation of wireline logs reveals a reservoir interval of 18 thick with an average gamma ray value of 59 API. The volume of clay for the reservoir interval is 21% therefore this cored interval can be classified as a shaly/sand reservoir. The average water saturation as calculated by the Indonesian water saturation model is about 42% and 58% gas saturation. The average permeability (K) for the cored section is 0.3 mD and the average porosity as calculated by the sonic – derived log is 12%.

The reservoir interval is predominantly medium to fine grained sand material that has been intensely bioturbated and fine - grained sands that have not been bioturbated. The intensely bioturbated sections have petrophysical parameters (porosity and permeability values) that have been significantly enhanced. The enhancement of the porosity and permeability values is prominent in a vertical direction (shallow to deep) and not in horizontal direction. This can be attributed to the intense bioturbation observed from depths of 3040m and deeper.

Two gamma ray shapes were identified from the wireline logs (GR shape A – Cylindrical and GR shape B – Bell) and each GR shape can be linked to clay mineral content and petrophysical values.

From the top of well Ga – S1 (3028m to 3034), we find GR shape A which is a cylindrical GR shape occurs at the top of the reservoir interval (3028m to 3034m) and the base of the reservoir interval (3042m to 3046m). The cylindrical shape reflects the uniform sediment nature. For these sections we observe a porosity range of 10% to 16% (top) and 13% to 18% (base). The permeability ranges from 0.3 mD to 1.6 mD (top) and 0.4 mD to 4 mD (base).

Between 3034m and 3042m we find GR shape B which is considered a Bell shape. The Bell shape can be characterized as a fining upward sequence. From the base of the Bell shape at 3042m to the top at 3034m, there is a decrease in reservoir quality (decrease porosity and permeability values). We observe a porosity high of 18% and that decreases to 10% at 3034m. The same is observed for the permeability where we see a high of 4 mD at 3042m and decreases to 0.1 mD at 3034m.

For GR shape A and B, the clay mineral content is fairly consistent. Glauconite is the most abundant and dominant clay mineral and has the most influential role in affecting the petrophysical parameters. Kaolinte and Calcite content is considerably less than Glauconite. Calcite mineral content increases with depth and Kaolinte fluctuates with depth (Figure 7.2.3). Due to Glauconite being the most abundant it affected the permeability more than porosity. That is why we observe good porosity values and extremely low permeability values. However, between a depth of 3041m and 3045m we observe high porosity values of 13% to 18% and high permeability values of 2 mD to 4 mD. These anomalous values can be attributed to the extensively bioturbated sand section which enhanced the permeability values significantly.

Sand - dominated sections that have been intensely bioturbated have porosity values ranging from 10% to 18% and permeability values ranging from 0.2 mD to 4 mD. By doing a simple comparison well Ga – S1 has better porosity and permeability values compared to well Ga – Q1.

(C) Clay mineral assemblages

The clay minerals identified by XRD, QEMSCAN and thin sections are: Kaolinite (Kaolinite group), Glauconite (Illite group) and Clinochlore (Chlorite group). The clay mineral Glauconite is by far the dominant clay mineral this confirmed by QEMSCAN analysis. Glauconite can be seen under the microscope as dark green in colour (plain polarized light and cross polarized light). Glauconite is a significant mineral as it only forms under certain conditions and in shallow marine environments. The presence of the clay minerals (Glauconite, Kaolinite) and Calcite will have a 'pore – bridging and pore - filling effect' and will as result in affecting the permeability values. The chemical alteration of the mineral Muscovite to Glauconite could explain its presence. Glauconite also reflects a marine influence. The chemical alteration of feldspars (Albite) could explain the presence of Kaolinite. Although Clinochlore is detected by XRD, the quantification of Clinochlore by the QEMSCAN method reveals its values is less than 0.1% and therefore can be considered not to influence the petrophysical parameters of the sandstone reservoir in any way.

(D) Geochemistry and petrography

Thin section petrography reveals tightly compacted samples that are dominated by quartz. The quartz mineral makes up about 87-92 % on average. Compared to well Ga- Q1, the mineralogical composition is very similar. Calcite acts as the dominant cement in the samples confirms that the well was deposited in a shallow marine setting. QEMSCAN and XRD analysis confirms the presence of the clay minerals: Kaolinite, Glauconite and Clinochlore. Glauconite is the dominant clay mineral followed by Kaolinite. On average Glauconite makes up 2, 87 % of the sample compared to Kaolinite that makes up 0, 89% of the sample. Calcite makes up 0, 5% of the samples. The pore waters of well Ga–S1 displays a pH range of 6.76 to 7. 63 implying that the pore waters range from slightly acidic to slightly alkaline. The pH range favors the formation and precipitation of the clay minerals and minerals found in this well.

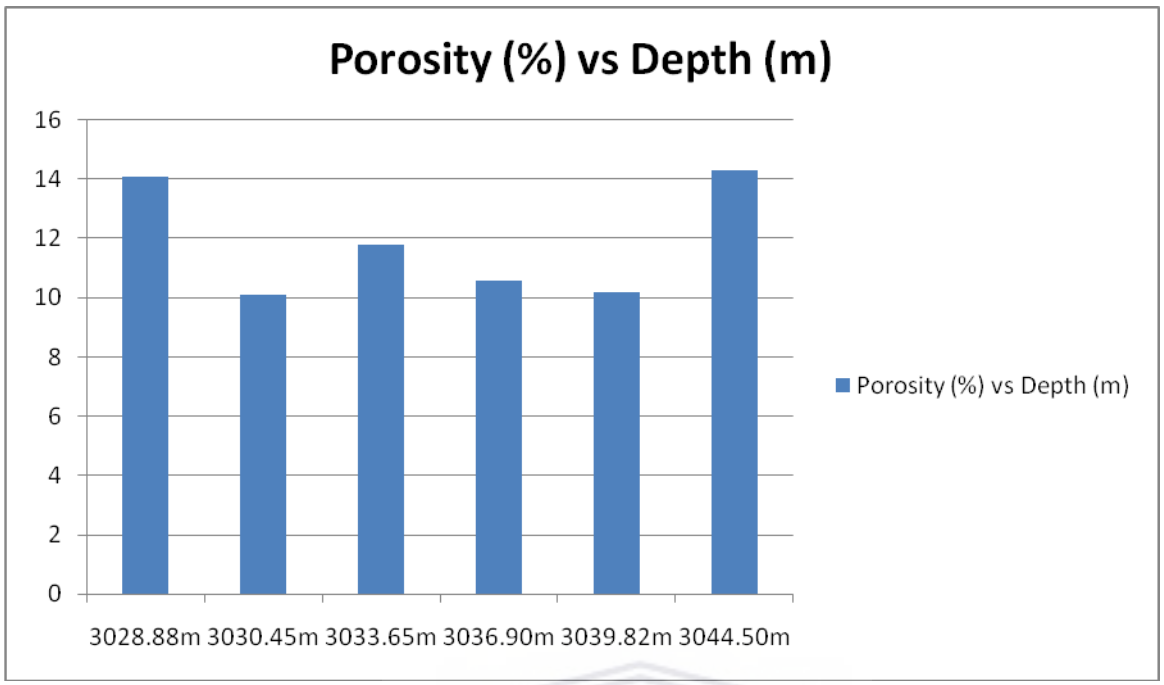

Figure 7.2.1: Well Ga – S1 showing the variation in porosity with depth

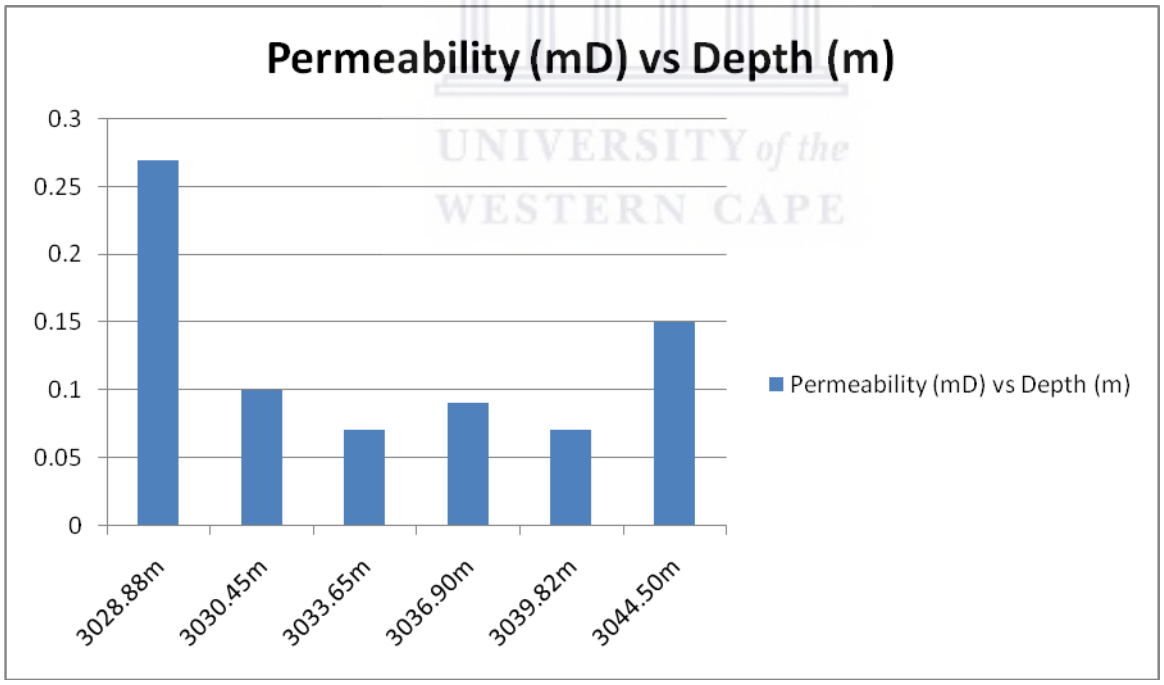

Figure 7.2.2: Well Ga – S1 showing the variation in permeability with depth

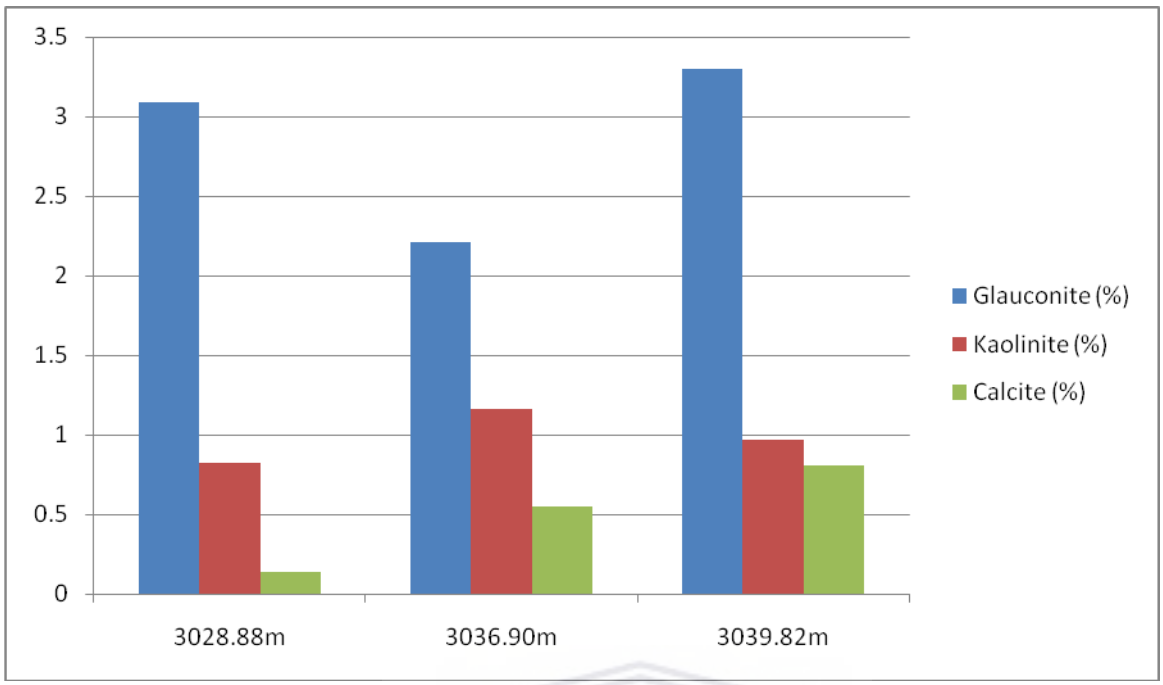

Figure 7.2.3: Well Ga – Q1 showing the variation of identified clay mineral concentration with depth

Table 7.0: The table displays the different calculated petrophysical properties by the Interactive Petrophysics software program.

Well name	Average Porosity (%)	Average Permeability (mD)	Average Water Saturation (%)	Avg. Volume of clay (%)
Ga– Q1	9	0.2	80	40
Ga – S1	12	0.3	42	21

CONCLUSION

This study emphasizes the effects of clay minerals on the petrophysical properties of sandstone reservoirs. The reservoirs encountered in the two wells are comparable in reservoir quality. Information derived from core and geochemical analysis indicates that sediments of the studied intervals were deposited in a shallow marine setting, have similar mineralogy and clay mineral composition.

This study suggests that the source of sediment for these two wells could have been from the same environment. The evidence for this can be taken from the core and mineralogical analysis. We find similar minerals in both wells as well as clay minerals (Glauconite) that are indicative of a shallow marine environment. The consistent presence of Glauconite (as observed in thin sections) indicates a marine influence in both the studied sections. The presence of Calcite in both wells indicates that the wells were deposited under shallow marine condition. As a result, due to the similarity in minerals indicative of a shallow marine setting, both wells are suggested to be deposited in a shallow marine setting. To accurately identify the depositional environments of the two wells, information was derived from core analysis by analyzing sedimentary features and trace fossils. As a result, it was confirmed that well Ga – Q1 was deposited in a tidal flat environment (inter tidal zone) and well Ga – S1 was deposited in a beach environment (lower shoreface zone). The intensely bioturbated nature seen in well Ga – S1 help promote better permeability values. This can be clearly seen from the petrophysical parameters (Table 7.0).

The results derived from the petrophysical study clearly suggest that well Ga-S1 has better reservoirl properties. The occurrence of the pore – bridging Glauconite and pore – filling Kaolinite definitely affected the permeability of the reservoirs. This is evident from the petrophysical parameters that were calculated. The reservoir interval of well Ga-S1 has a clay content of about 21% compared to that of 40% from the reservoir interval from well Ga-Q1. The porosity, permeability and water saturation values are better in well Ga-S1 compared to well Ga-Q1 (Table 7.0). Aside from the dominant quartz cement observed in both wells: Calcite, Glauconite (Illite group), Kaolinite (Kaolinite group) and Clinochlore (Chlorite group) are clays and cements that significantly compromised the petrophysical parameters of the sandstone reservoir. The clay mineral composition is higher in well Ga-Q1 than well Ga- S1 and has a detrimental effect on the petrophysical properties.

To conclude, the presence of Glauconite, Kaolinite and Calcite have negatively affected the pore connectivity (permeability) more than the porosity in both wells .The characteristics of the clays have 'lined' the pores and consequently had a detrimental effect on the pore connectivity. By comparing the two wells the higher clay volume and clay mineral content in well Ga–Q1 has had a detrimental effect on the petrophysical parameters. We therefore see poor reservoir quality in well Ga – Q1 compared to well Ga–S1. .

LIST OF REFERENCES

- **Aargard, P and Helgesson, H.C., (1983).** Activity/composition relations among silicates and aqueous solutions: II. Chemical and thermodynamic consequences of ideal mixing of atoms on homological sites in montmorillontes, illites and mixed-layer clays. Clays Clay Min 31: pp 207 – 217.
- **Archie, G.E., (1942).** The electrical resistivity log as an aid in determining some reservoir characteristics. Transaction of AIME 146; pp54.
- **Archie, G.E., (1950). "**Introduction to petrophysics of reservoir rocks". American Association of Petroleum Geologists Bulletin 34 (5): pp 943 – 961.
- **Bailey, S.W., (1988).** Chlorites: structures and crystal chemistry, pp. 347 – 403 in: Hydrous Phyllosilicates (Exclusive of Micas) (S. W. Bailey, editor). (Reviews in Mineralogy, vol. 19). Mineralogical Society of America, Washington DC, United States.
- **Bain, D. C., (1977).** Geoderma 17, pp. 19.
- **Bayliss, P., (1975).** Nomenclature of the trioctahedral chlorites. Journal of Can. Miner. Vol 13, pp 178 – 188.
- **Beard, D.C and Weyl, P.K., (1973).** Influence of Texture on Porosity and Permeability of Unconsolidated Sand, AAPG Bulletin, February 1973, vol. 57, pp 349 – 369.
- **Beaufort, D., Cassagnabe're, A., Petit, S., Lanson, B., Berger, G., Lacharpagne, J.C and Johansen, H., (1998).** Kaolinite to Dickite conversion series in sandstone reservoirs. Clay Minerals, 33, pp 297 – 316.
- **Berger, A., Gier, S., and Krois, P., (2009).** Porosity preserving chlorite cements in shallow marine colcaniclastic sandstones: Evidence from Cretaceous sandstones of the Sawan gas field, Pakistan AAPG Bulletin, vol. 93, pp. 595 – 615.
- **Berger, G., Lacharpagne, J.C., Velde, B., Beaufort, D. and Lanson, B., (1995).** Me'canisme et contraintes cine'-tiques des re'actions d'illitisation d'argiles se'dimentaires, de'duits de mode'lisations d'interaction eauroche. Bull etin de Cent re de Reche rche s. Exploration et Production, 19, pp. 225 – 234.
- **Bilbey, S.A., Kerns, R.L., and Bowman, J.T., (1974).** Petrology of the Morrison Formation, Dinosaur Quarry Quadrangle, Utah: Utah Geological and Mineral survey special studies 48, pp 15.

- **Bjorlykke, K., (1984).** Formation of secondary porosity: how important is it? [In:] D.A. McDonald and R.C. Surdam (Eds): Clastic Diagenesis, American Assocaition of Petroleum Geologists, Memoir 37, pp. 277 – 286.
- **Bjorlykke, K., (1983).** Diagenic reactions in sandstones. In: Parker, A., Sellwood, B.W. (Eds.). Sediment Diagenesis. Reidel Publishing, Holland, pp. 169-213.
- **Bjorkum, P.A. and Nadeau, P.H., (1998).** Temperature controlled porosity/permeability reduction, fluid migration and petroleum exploration in sedimentary basins. Australian Pet. Prod. & Expl. Assoc. Journal, vol. 38, pp. 453 – 464.
- **Bloch, S., Lander, R.H. and Bonnell, L., (2002).** Anomalously high porosity and permeability in deeply buried sandstone reservoirs: Origin and predictability. AAPG Bulletin, 2002. Vol. 86, pp. 301 – 328.
- **Boles, J.R. and Francks, G.S., (1979).** Clay diagenesis in Wilcox sandstones of Southwest Texas: Implications of Smectite diagenesis on sandstone cementation. Journal of Sedimentary Petrology, vol. 49, pp. 55 – 70.
- **Broad, D.S., Jungslager, E.H.A., McLachlan, I.R. and Roux, J., (2006).** Offshore Mesozoic Basins, Geology of South Africa, pp 553 – 565.
- **Brown, L.F., Benson, J.M., Brink, G.J., Doherty, S., Jollands, A., Jungslager, E.H.A., Keenan, J.H.G., Muntingh, A. and Van Wyk, N.J.S., (1995).** Sequence stratigraphy in offshore South Africa divergent basins. An atlas on exploration for cretaceous lowstand traps by SOEKOR (Pty) Ltd. Am. Ass. Petro. Geol. Stud. In Geology, vol. 41.
- **Burley, S.D., and McQuaker, J.H.S., (1992).** Authigenic clays, diagenetic sequences and conceptual diagenetic models in contrasting basin margin and basin center, North Sea Jurassic sandstones and mudstones, Origin, Diagenesis and Petrophysics shelf, Clay Minerals, vol. 24, pp. 233 – 253.
- **Burst, J.F., (1969).** Diagenesis of Gulf coast clayey sediments and its possible relation to petroleum migration, American Association of Petroleum Geologists Bulletin 53, pp. 73 – 93.
- **Buyukutku, A.G., (2003).** The diagenesis of middle Eocenc sandstones from the Western Thrace Basin, Turkey. Journal pf Geological Society of India, vol. 62, pp. 83 – 90, July 2003.

- **Chamley, H., (1994).** Clay mineral diagenesis In: Quantitative Diagenesis: Recent developments and Applications to Reservoir Geology (Ed. By A. Parker and B.W. Sellwood), Kluwer Academic Dordrecht, pp. 161 – 188.
- **Chamley and Weaver (1989).** Introduction to clay sedimentology. Publisher: Springer-Verlag, Language: English.
- **Clavier, C., Coates, G. and Dumanoir, J., (1984).** Theoretical and Experimental bases for the dual-water model for interpretation of shaly-sands. SPE Journal, vol. 24, no. 2, pp. 153 – 168.
- **Cocker, J., (1986).** The reservoir properties and diagenesis of the Brent Group: a regional perspective Geological Society, London, Special Publications, 1992, vol. 61, pp 289 – 327.
- **Curtis, C., (1983).** Geochemistry of porosity enhancement and reduction in clastic sediments. In: J. Brooks (Ed), Petroleum Geochemistry and Exploration of Europe. Geological Society of London, Special publications, vol. 12, pp. 113 – 125.
- **De Ros, C., (2009).** Integrated Petrographic, Stratigraphic and Statistical Analysis of complex Albian Reservoirs in the Espirito Santos Basin, Eastern Brazil. A paper presented at AAPG international conference and exhibition, Rio de Janeiro, Brazil, 2009.
- **De Waal, J. A., (1989).** Influence of clay distribution on shaly sand conductivity, SPE Formation Evaluation, vol. 4, pp. 377 – 383.
- **De Wit, M.J., Bowring, S., Ashwal, L.D., Randrianasolo, L.G and Morel, V.P.I., (2001).** Age and tectonic evolution of Neoproterozoic ductile shear zones in Southwestern Madagascar, with implications for Gondwana studies. Tectonics, vol. 20, pp. 1-45.
- **Dingle, R., Siesser, W., and Newton, A., (1983).** Mesozoic and Tertiary GeoMesozoic and Tertiary Geology of South Africa: A Global approach to Geology, Rotterdam: Taylor and Francis.
- **Ehrenberg, S.N., (1991).** Kaolinized, potassium-leached zones at the contacts of the Garn Formation, Haltenbanken, mid – Norwegian continental shelf, Marine Petroleum Geology, vol. 8, pp. 250 – 269.
- **Ellis, D.V and Singer, J.M (2007).** 'Clay Quantification', well logging for earth scientist.

- **Emery, D., Myers, K.J. and Young, R., (1990).** Ancient Subaerial exposure and freshwater leaching in sandstones, Geology vol. 18, pp. 1178 – 1181.
- **Esteoule – Choux., (1983).** Kaolinitic weathering profiles in Brittany: genesis and economic importance, In: WILSON RCL (ed), Residual Deposits: surface related weathering process and materials. Geological Society of London special publications, vol. 11, pp. 33 – 38.
- **Garven, G., (1986).** The role of regional fluid flow in the genesis of the Pine Point deposits, Western Canada sedimentary basin, Economic Geology, vol. 81, no. 4, pp. 1015.
- **Grigsby, J.D., (2001).** Origin and growth mechanism of authigenic chlorite in sandstones of the lower Vicksburg formation, South Texas, Journal of Sedimentary Research, vol. 71, no. 1, pp. 27 – 36.
- **Grim, R.E., (1951).** The depositional environment of red and green shales, Journal of Sedimentary Petrology, vol. 21, pp. 226 – 232.
- **Guven, N., (1988).** Smectites. In: Bailey, W (ed). Hydrous phyllosillicates (exclusive of micas). Rev Mineral, vol. 19, pp. 497-559.
- **Guven, N., Hower, W.F. and Davies, D.K., (1980).** Naturenof authigenic illites in sandstone reservoirs, Journal of Sedimentary Petrology, vol. 50, pp. 761 – 766.
- **Hancock, N.J., and Taylor, A.M., (1978).** Clay mineral diagenesis and oil migration in the Middle Jurassic Brent sand formation, Journal of the Geological Society of London, vol. 135, pp. 69 – 72.
- **Hassan, M., Hossi, A., and Combaz, A., (1976).** Fundamentals of the different gamma ray log interpretation technique, SPWLA 17th Ann. Symp., Paper 1976-H, pp. 1 – 18.
- **Huang, H., Bowler, B.F.J., Oldenburg, T.B.P., and Larter, S.R., (2004).** The effect of biodegradation on polycylic aromatic hydrocarbons in reservoired oils from the Liaohe Basin, NE China, Org. Geochem, vol. 35, no. 11-12, pp. 1619-1634.
- **Hurst, A., (1987).** Problem of reservoir characterization in some North Sea sandstone reservoirs solved by the application of micro scale geological data, North Sea Oil and Gas reservoirs, Graham and trot man, pp. 153.
- **Hurst, A., and Irwin, H., (1982).** Geological modeling of clay diagenesis in sandstones, Clay Miner, vol. 17, pp. 5-22.

- **Jinglan, L., Morad, S., and Zhang, X., (2002).** Reconstruction of the diagenesis of the fluvial-lucastrine-deltaic sandstones and its influence on the reservoir quality evolution – Evidence from Jurassic and Triassic sandstones, Yanchang Oil Field, Ordos Basin, Sciences in China (Series D). Vol. 45(7), pp. 616-634.
- **Juhasz, I., (1990).** Core Analysis: Opportunities and challenges in the 1990s, European core analysis symposium, pp 1-15.
- **Krygowski, D.A., (2003).** Guide to petrophysical interpretation. Austin Texas USA. Petroleum prospectivity of the Deepwater Orange Basin, South Africa. Petroleum Agency South Africa.
- **Kupecz, J., Gluyas, J., and Bloch, S., (1997).** Reservoir quality prediction in sandstones and carbonates, AAPG Memoir series, vol. 69.
- **Lanson, B., Beaufort, D., Berger, G., Bauer, A., Cassagnabe, A., and Meumier, A., (2002).** Authigenic kaolin and illite minerals during burial diagenesis of sandstones. Clay and Clay minerals, vol. 37, pp. 1-22.
- **Larsen, R., and Ladd, J., (1973).** Evidence for the Opening of the South Atlantic in the early Cretaceous. Nature. Vol. 246, pp. 209-212.
- **Levorsen, A.L., (1967).** Geology of Petroleum,Second Edition: W.H Freeman and Co; San Francisco, United States.
- **MacLuagling, O.M., Haszeldine, R.S., Fallick, A.E and Rodgers, G., (1994).** The case of the missing clay, aluminium loss and secondary porosity. South Brae oilfield, North Sea. Clay minerals journal. Vol. 29, pp 651 – 663.
- **McMillan, I., (2003)**. Foraminiferally defined biostratigraphy episodes and sedimentation pattern of the Cretaceous drift succession (Early Barremian to Late Maastrichtian) in seven basins on the South African ad southern Namibian continental margin: research article. South African Journal of Science. Vol. 99 (issue 11 and 12). Pp. 537-576.
- **McMillan, I., Brink, G., Broad, D., and Maier, J., (1997)**. Late Mesozoic Sedimentary Basins off the South Coast of South Africa. Sedimentary Basins of the World. Vol. 2 (1874-5997). Pp. 319-376.
- **Muller, G., (1967).** Diagenesis in argillaceous sediments In: G. Larsen and G.V. Chilingar (Editors). Diagenesis in sediments. Elsevier, Amsterdam, pp127-177.

- **Opuwari, M., (2010).** Petrophysical evaluation of the Albian age gas bearing sandstone reservoir of the O-M Field, Orange Basin, South Africa.
- **Owen, D.E., Turner-Peterson, C.E., and Fishman, N.S., (1989).** X-ray diffraction studies of the <0.5mm fraction from the Brushy Basin Member of the Upper Jurassic Morrison Formation, Colorado Plateau. U.S Geological Survey Bulletin, 1808-G, pp. 1-25.
- **Pallatt, N., Wilson, J., and McHardy, B., (1984).** The relationship between permeability and the morphology of diagenetic illite in reservoir rocks. J. Pet. Technology. Vol. 36, pp. 2225-2227.
- **Parnell, J., Baroni, J. and Boyce, A., (2000).** Controls on kaolinite and dickite distribution, Highland Boundary Fault Zone, Scotland and Northern Ireland. Journal of the Geological Society of London. Vol. 157, no. 3, pp 635-640.
- **PASA, 2013.** Petroleum Agency South Africa., History of exploration and production. [Online] Available at: www.petroleumagencysa.com/index.php/petroleum-geology-resources/explration-history (Accessed 1 October 2017).
- **PASA, (2010).** Barremian prospects of the Northern Pletmos Basin. [Online]: Available at: www.petroleumagencysa.com/images/pdfs/Northern_Pletmos_Basin.pdf. [accessed 2 October 2017].
- **Penney, R.K., and Looi, S.Y., (1996).** Understanding effective and total porosity: the key to optimizing mineralogical evaluations. APPEA Journal. Vol. 36, pp.284-292.
- **Pevear, D.R., (1999).** Illite and Hydrocarbon Exploration. Proceedings of the National Academy of Sciences of the United States. Vol. 96, pp. 3440-3446.
- **Pittman, E.D., Larese, R.E., and Heald, M.T., (1992).** Clay coats: Occurrence and relevance to preservation of porosity in sandstones. In. D.W. Houseknechtt, and E.D. Pittman (Eds.). Origin, diagenesis and petrophysics of clay minerals in sandstones (pp. 241-264). SEPM Special Publication 47, Society of Economic Paleotologists and Mineralogists.
- **Primmer, T.J., Cade, C.A., Evans, J., Gluyas, J.G., Hopkins, M.S., Oxitoby, N.H., Smalley, P.C., Warren, E.A., and Worden, R.H., (1997).** Global patterns in sandstones diagenesis: their application to reservoir quality prediction for petroleum exploration. American Association of Petroleum Geologists Memoir 69, pp. 61-77.

- **Rahman, S.S., Rahman, M.M., and Khan, F.A., (1995).** Response of low – permeability, illitic sandstone to drilling and completion fluids. J. Pet. Sci. Eng. Vol.12 (4), pp. 309-332.
- **Reedy, G.K., and Pepper, C.F., (1996).** Analysis of finely laminated deep marine turbidites: Integration of core and log data yields a novel interpretation model. Society of Petroleum Engineers Ann. Tech. Conference and Exhibition. Pp.119-127.
- **Reifenstuhl, R.R., (2002).** Reservoir characterization pilot study: Porosity, permeability, petrography and facies analysis of 75 Upper Cretaceous to Mississippian age outcrop samples, East-central Brooks Range foothills and North Slope, Alaska, in Abstracts with programs, American Association of Petroleum Geologists Annual meeting, vol. 11, p146.
- **Rider, M.**, (1996). The Geological Interpretation of Well logs. Second Edition. Ed. Scotland. Caithness: Whittles Publishing.
- **Roux, J., (1997).** Potential outlined in Southern Outeniqua off South Africa. Oil and Gas Journal, volume 95(25).
- **Ruiz Cruz, M.D. (1994).** Diagenetic development of clay and related minerals. Journal of Clay Mineralogy., Vol. 29, pp 93-104.
- **Samakinde, C.A., (2013).** Assessment of the effects of clay diagenesis on the petrophysical properties of Lower Cretaceous sandstones, Block 3A, Offshore Orange Basin, South Africa. Chapter 2 – 4. Pp. 15-58.
- **Schlumberger, (1972).** The essentials of log interpretations, practice, Schlumberger Ltd. Paris, France.
- **Schroeder and Hayes (1968).** Dickite and Kaolinite in Pennsylvanian limestones in Southeastern Kansas. Clays and clay minerals, vol. 16. Pp 41-49.
- **Scotese, C. R. (2002)**. Paleomap. Updated at http://www. scotese. com (accessed October 2018).
- **Serra, O., (1984).** Fundamentals of well log interpretation (volume 1): The Acquiition of logging data. Dev. Pet. Sci. 15A: Amsterdam (Elsevier).
- **Sinclair, G.G., and Duguid, S.J., (1990)**. Laboratory induced damage – A review of the problem'. First SCA European Core Analysis Symposium, London, UK, Gordon and Breach Science Publishers.

- **Shammari, M., Francks, S., and Soliman, O., (2011).** Depositional and facies controls on infiltrated/inherited clay coatins: Unayzah Sandstones, Saudi Arabia. AAPG annual conference and exhibition: Making the next giant leap in Geosciences.
- **Stalder, P., (1973).** Influence of crystallographic habit and aggregate structure of authigenic clay minerals on sandstone permeability. Geologie en miljnbouw, vol. 52(4), pp. 217-220.
- **Sun, Z.L., Huang, S.L., and Zhang, Y.X., (2008).** Origin and diagenesis of authigenic chlorite within the sandstone reservoir of Xujiahe Formation, Sichuan Basin, China. Acta Sedimentological Sinica., vol. 26(3), pp. 459-467.
- **Tardy, Y., (1971)**. Characterization of the principal weathering types by the geochemistry of waters from some European and African crystalline massifs. Chemical Geology, vol. 7.
- **Waxman, M.H., and Smith, L.J., (1968).** Electrical conductivities in oil bearing shaly-sands. Journal of Petroleum Technology, pp.107.
- **Wentworth, C.K., (1922).** 'A scale of grade and class terms for clastic sediments'. Journal of Geology, Vol. 30, pp.377-392.
- **Whitney, E., and Northrop, R., (1987).** Role of water in Smeectite-to-Illite reaction Journal. Clay and Clay minerals. Vol. 38 (4), pp. 343-350.
- **Wilson, H.H., (1977**). 'Frozen-in' Hydrocarbon accumulations or diagenetic traps exploration targets, American Association of petroleum Geologists. Bull. Vol 61. Pp 483-491.
- **Wilson, M.D., and Pittman, E.D., (1977).** Authigenic clays in sandstones: recognition and influence on reservoir and paleoenvironmental analysis. Journal of Sedimenntary Petrology. Vol. 47., pp 3-31.
- **Worthington, P.F., (2008).** The Application of cut-offs in integrated reservoir studies. SPE Reservoir evaluation and engineering (SPE 95428).

APPENDIX A – CONVENTIONAL CORE ANALYSIS WELL GA – Q1

Depth (m)	Porosity (%)		Permeability (mD)
2330	12.5		0.4
2330.25	17.1		2.5
2330.82	9.1		0.2
2331.02	15.1		0.6
2331.26	13.3		0.3
2331.51	13.4		0.3
2331.75	13.1		0.3
2332.5	5.1		0.1
2332.7	4.8		0.1
2332.95	13.7		0.3
2333.7	14.4		0.4
2333.93	13.7		0.4
2334.19	13.7		0.4
2334.62	13.0		0.3
2334.86	13.0		0.2
2335.3	13.9		0.3
2335.55	14.0		0.4
2336.05	14.4		0.4
2336.33	13.3		0.3
2336.58	14.7		0.4
2336.82	14.0		0.4
2337.07	13.2		1.3
2337.32	13.4		0.2
2337.61	13.9		2.5
2337.8	14.2		0.2
2338.06	14.8		0.3
2338.33	15.1		0.4
2338.58	14.5		0.4
2338.83	13.9		0.3
2339.13	14.2		0.3
2339.53	14.3		0.4
2339.78	15.3		0.4
2340.05	14.4		0.4
2340.32	11.8		0.2

2340.54	11.1		0.3
2340.79	5.6		0.1
2341.03	10.2		0.2
2341.27	12.9		0.2
2341.55	10.4		0.2
2341.82	10.7		0.2
2342.05	13.4		0.2
2342.29	11.5		0.2
2342.51	12.6		0.2
2342.79	11.4		0.2
2343.03	11.8		0.2
2343.53	11.7		0.3
2343.79	12.2		0.3
2344.01	10.7		0.2
2344.53	10.3		0.2
2344.78	11.3		0.2
2345.05	11.1		0.2
2345.29	9.3		0.1
2345.54	10.5		0.1
2345.77	5.4		0.1
2346.01	5.3		0.1
2346.28	12.5		0.2
2346.53	13.8		0.2
2346.78	13.4		0.2
2347.14	14.5		0.2

APPENDIX B – CONVENTIONAL CORE ANALYSIS WELL GA – S1

Ga - S1			Gas Sat.	Water Sat.
Depth (m)	Permeability (mD)	Porosity (%)	Sg	Sw
3028.05	1.6	15.8	49	0.51
3028.3	0.33	14.9		
3028.55	0.36	14.5		
3028.8	0.27	14.1		
3029.05	0.21	13.6	58	0.42
3029.35	0.07	11.6		
3029.6	0.11	12.0		
3029.85	0.14	12.3		
3030.14	0.01	09.6	36	0.64
3030.81	0.08	12.7		
3031.03	0.04	11.0	32	0.68
3031.33	0.05	11.7		
3031.58	0.08	12.2		
3031.83	0.04	11.3		
3032.05	0.05	10.8	52	0.48
3032.42	0.05	11.6		
3032.72	0.05	12.0		
3033.01	0.07	11.5	53	0.47
3033.33	0.06	10.7		
3033.56	0.06	11.4		
3033.78	0.07	12.1		
3034.05	0.1	11.7	50	0.5
3034.32	0.08	11.4		
3035.05	0.09	12.1	56	0.44
3036.01	0.08	10.7	35	0.65
3037.02	0.09	10.6	53	0.47
3038.01	0.08	11.4	49	0.51
3038.33	0.07	10.9		
3038.58	0.22	12.5		
3038.83	0.11	10.9		
3039.05	0.04	08.2	40	0.6
3039.42	0.61	13.7		
3039.68	0.07	10.2		
3040.05	0.07	10.2	54	0.46

3040.35	0.17	12.8		
3040.58	1.51	17.0		
3040.81	0.51	15.2		
3041.05	0.83	15.2	53	0.47
3041.32	2.35	17.5		
3041.57	2.75	17.3		
3041.83	3.56	17.5		
3042.08	2.98	17.5	55	0.45
3042.33	2.48	18.0		
3042.57	3.77	17.0		
3042.82	1.84	17.1		
3043.02	1.37	18.2	58	0.42
3043.3	0.18	15.2		
3043.55	0.13	14.1		
3043.8	0.4	14.8		
3044.05	2.98	16.5	59	0.41
3044.38	0.13	14.3		
3044.58	0.15	14.3		
3044.87	0.11	13.1	50	0.5
3045.3	0.12	14.2		
3045.55	0.15	14.6		
3045.82	0.08	13.2	58	0.42